Immobilisation of active enzymes on novel GFP protein particles

A thesis submitted in complete fulfilment of the
requirements of the degree of
Master of Science
in
Microbiology
at Massey University, Palmerston North,
New Zealand.

Mark Piers Venning-Slater
2013

ABSTACT

Inclusion bodies were previously thought to be aggregations of inactive, mis-folded proteins. However, there is a growing body of evidence that suggests otherwise. In 2011 Jahns et al demonstrated a self-assembling GFP protein particle (GFP particle) that not only exhibited fluorescence, but was also able to display functional antibody and ligand binding sites. These functional GFP particles exhibited reasonable activity, and in many cases outperformed commercially available particles. The GFP particles consisted of an aggregation of fusion proteins. These fusion proteins in turn consisted of an N-terminally extended enhanced GFP protein which was fused at its C-terminus to an inactive polyester synthase (PhaC(C319A)) from *Ralstonia eutropha*, and a functionality, e.g. antibody/ ligand binding site. In this study, GFP particles were investigated to ascertain whether they could serve as a support for the immobilization and display of active enzymes; and provide a technology that is potentially more efficient and cost-effective than other enzyme immobilization methods. Furthermore, their inherent fluorescence would provide an additional advantage. The enzymes used for functionality tests were: a thermostable α-amylase from *Bacillus licheniformis* that lacked its signal sequence (Bla(-ss)); *N*-acetyl-D-neuraminic acid aldolase (NanA) from *Escherichia coli*; and organophosphohydrolase (OpdA) from *Agrobacterium radiobacter*. These enzymes were chosen for their differing quaternary structure- monomer, tetramer, and dimer, respectively- and were fused to the C-termini of GFP fusion proteins. The results of this investigation showed that it is possible to generate fluorescent GFP particles inside recombinant *E. coli* BL21(DE3) cells which are also able to display active enzyme. These enzyme-bearing GFP particles exhibited considerable stability across a range of temperature, pH, and storage conditions, and could also be reused. The activity of the particles was also compared to a similar technology- functionalized PHA beads; however, the PHA beads consistently exhibited stronger enzyme activity under all conditions tested. GFP protein particles represent a novel method for the immobilization and display of enzymes. Their ability to immobilise and display active enzymes of different quaternary structure under a range of conditions makes GFP particles particularly attractive to industrial biocatalysis processes. Potential applications include diagnostic assays, food production, pharmaceutical production, and bioremediation.

ACKNOWLEDGEMENTS

Where do I start? As I'm sure every post-grad can appreciate, undertaking a Master's degree is not to be considered lightly. All those who have gone before can tell you how much work is required: the long days; the lack of sleep; the repetition of assays that fail for unforeseen reasons (or foreseen reasons). My project was no exception, and there are many people I'd like to thank for their words of encouragement and advice for which I'm deeply grateful. First, I'd like to thank my supervisor Professor Bernd Rehm for giving me the opportunity of studying under him. Considering that he did not know me beforehand, he took a chance on an eccentric guy from Wellington, and gave me advice and direction that not only helped me with this study, but will also be of great use in my future career. Next, I'd like to thank David Hooks for his endless support and technical knowhow. I was very much a novice in molecular biology when I started, but thanks to David, and his patience, I finish my Master's with a wealth of knowledge- and some fancy squash techniques. A thank you must also go out to Jason Lee for making the weekend work and breaks a lot more enjoyable, and Iain Hay for having the answer I need no matter how obscure the question. A special thanks to the whole Rehm lab and Polybatics for being a great bunch of people to work beside; Trevor Loo for his HPLC expertise; and Rosie Bradshaw's lab for letting me steal their equipment. A big thanks to my flatties Bex Smith for being a whirlwind of energy and laughs; Bob Stewart for helping me get in touch with my Upper Hutt gangsta roots; and Kim Green for the fly-by hugs. As always I'm indebted to my family for their support and encouragement, and financial assistance. I don't want to think how much money they've given me over the years, but I promise it's been worth it.

TABLE OF CONTENTS

	Page
Abstract	ii
Acknowledgements	iii
Contents	iv
Abbreviations	ix
List of Figures	xiii
List of Tables	xvi
Chapter One: Introduction	1
1.1 Enzymes and their Industrial Applications	1
1.2 Enzyme Isolation and Purification	2
1.3 Enzyme Immobilisation	2
1.4 Enzyme Fusion Proteins for Enzyme Isolation, Purification, and Self-immobilisation	3
1.5 Functionalised PHA Granules	4
1.6 Inclusion Bodies	5
1.6.1 Inclusion Body Formation and Structure	6
1.6.2 Inclusion Body Stability	7
1.6.3 Industrial Applications of Inclusion Bodies	8
1.7 Green Fluorescent Protein	8
1.8 GFP particles	11
1.8.1 The Effect of an N-terminal Extension of GFP	12
1.8.2 The Effect of the C-terminal fusion of PhaC on Particle Formation	13
1.8.3 Engineering GFP Particles to Display Foreign Proteins	13
1.8.4 The Effect of Exchanging PhaC as the Fusion Partner	15
1.8.5 The Effect of the Type of N-terminal Extension of GFP on Particle Formation	15
1.8.6 Fluorescent Particle Formation Using Other Types of Fluorescent Protein	17
1.8.7 Characterisation of GFP Particles	18
1.9 Study Aims and Objectives	19
Objectives	23

Chapter Two: Materials and Methods 24
2.1 Strains and Plasmids 24
2.1.1 Strains 24
2.1.2 Plasmids 24
2.2 Primers 26
2.3 Liquid Media 27
2.3.1 Luria-Bertani (LB) Medium 27
2.3.2 25% Glucose Medium 27
2.4 Buffers and Miscellaneous Solutions 28
2.4.1 Potassium phosphate buffer 28
2.4.2 20% (v/v) Ethanol in Potassium phosphate buffer 28
2.4.3 Glycerol in Potassium phosphate buffer 28
2.4.4 Sodium phosphate buffer plus Sodium chloride 28
2.4.5 HEPES buffer 28
2.4.6 20% (v/v) Methanol in HEPES buffer 29
2.4.7 α-Amylase Colour Reagent Solution 29
2.4.8 1.0% (w/v) Soluble Starch Solution 29
2.5 Antibiotics 30
2.6 Stains 30
2.7 SDS-PAGE Solutions 31
2.8 Miscellaneous Solutions 32
2.9 Solid Media 33
2.9.1 X-gal Medium 33
2.10 Liquid Cultivation Conditions 33
2.10.1 PHA Bead Production Conditions 33
2.10.2 GFP Particle Production Conditions 34
2.11 Solid Media Cultivation Conditions 34
2.11.1 Antibiotic Selection 35
2.11.2 Blue/ White Selection 35
2.12 Long-term Storage and Revival of Bacterial Strains 35
2.12.1 Strain Revival 36
2.13 Preparation of Competent *E. coli* Cells 36

2.14 Transformation of Recombinant Plasmids into *E. coli* 38
2.15 Cloning Methodology 38
2.15.1 Plasmid Isolation and Determination of DNA Concentration 38
2.15.2 DNA Restriction Digests 39
2.15.3 Agarose Gel Electrophoresis (AGE) 39
2.15.4 Agarose Gel DNA Extraction 40
2.15.5 Polymerase Chain Reaction 41
2.15.6 DNA A-tailing 42
2.15.7 pGEM-T Easy Ligation 42
2.15.8 DNA Ligation using T4 DNA Ligase 43
2.15.9 DNA Sequencing 43
2.16 PHA Bead and GFP Particle Extraction 43
2.16.1 Bacterial Cell Harvesting 43
2.16.2 Cell disruption 44
2.16.3 Separation of PHA Beads and GFP Particles 44
2.17 Methods for visualising PHA Beads and GFP particles 46
2.17.1 Fluorescent Microscopy 46
2.17.2 Nile Red Staining 46
2.18 Methods for Fusion Protein Analysis 47
2.18.1 Sodium dodecylsulfate Polyacrylamide Gel Electrophoresis (SDS-PAGE) 47
2.18.2 Densitometry 49
2.18.3 MALDI-TOF/MS 51
2.19 HPLC 51
2.20 Enzyme Activity Assay Protocols 51
2.20.1 Quantification of *N*-acetyl-D-neuraminic acid aldolase (NanA) Activity 51
2.20.2 Quantification of α-Amylase (Bla(-ss)) Activity 52
2.20.3 Quantification of Organophosphohydrolase (OpdA) Activity 53
2.21 Enzyme Stability and Reusability Assay Protocols 55
2.21.1 Time Course Assessment of Enzyme Activity 55

2.21.2 Temperature Stability of PHA beads/ GFP Particles displaying Enzyme 55
2.21.3 pH Stability of PHA beads/ GFP Particles displaying Enzyme 55
2.21.4 Reusability of GFP Particles displaying Enzyme 56
2.21.5 Long-term Storage Condition Assay 56

Chapter Three: Results 57
3.1 Formation of GFP particles that display functional enzymes 57
3.1.1 Creation of pET14b-ext(AVTS)gfp-phaC(C319A)-1inker-nanA (pET14b-GiCLN) and pET14b-ext(AVTS)gfp-nanA-1inker-nanA (pET14b-GNLN) and associated GFP particles 58
3.1.2 Assessment of *N*-acetyl-D-neuraminic acid (Neu5Ac) production ability of GiCLN, GNLZ, and GNLN GFP particles 65
3.1.3 Creation of pET14b-ext(AVTS)gfp-phaC(C319A)-1inker-opdA (pET14b-GiCLO) and pET14b-ext(AVTS)gfp-phaC(C319A)-1inker-bla(-ss) (pET14b-GiCLB) 67
3.1.4 Enzyme Activity of GFP particles over time 72
3.2 Characterisation of enzyme-bearing GFP particles 75
3.2.1 Temperature Stability 75
3.2.2 pH Stability 82
3.2.3 Reusability 88
3.2.4 Long-term Storage Stability 91

Chapter Four: Discussion 100
4.1 GFP fusion proteins containing enzymes are capable of forming GFP particles 100
4.2 GFP particles are capable of displaying active enzyme 102
4.3 Consistency of GFP particle activity with change in temperature depends on the enzyme displayed 106
4.4 GFP particles exhibit similar patterns of activity throughout a range of pH 108
4.5 GFP particles exhibit different patterns of activity when recycled 112
4.6 Long-term storage of GFP particles is affected by temperature 114
4.7 Limitations of Study 118

Chapter Five: Conclusion 121

Chapter Six: References 123

ABBREVIATIONS

AGE	Agarose Gel Electrophoresis
Ap^r	Ampicillin resistance gene
AVTS	Amino acids Alanine-Valine-Threonine-Serine that constitute a short N-terminal extension of GFP in GFP fusion proteins
BLA	α-amylase from *Bacillus licheniformis*
Bla(-ss)	α-amylase from *Bacillus licheniformis* that lacks the signal sequence required for extra-cellular export
Bla(-ss)-PhaC	α-amylase/ PHA synthase fusion protein
BSA	Bovine Serum Albumin
bp	Base pair
˚C	Degrees Celsius
CFP	Enhanced cyan-fluorescent protein
CLEA	Cross-linked enzyme aggregate
CLEC	Cross-linked enzyme crystal
Cm^r	Chloramphenicol resistance gene
dATP	Deoxyadenosine triphosphate
DMSO	Dimethyl sulphoxide
DNA	Deoxyribonucleic acid
dNTP	Deoxyribonucleotide triphosphate
dTTP	Deoxythymidine triphosphate
EDTA	Ethylenediaminetetraacetic acid
EGFP	Enhanced green fluorescent protein
ELISA	Enzyme-linked immunoabsorbant assay
extGFP	N-terminally extended green fluorescent protein
FHKP	Amino acids Phenylalanine-Histidine-Lysine-Proline that constitute a short N-terminal extension of GFP in GFP fusion proteins
GB1	IgG binding domain of Protein G from *Streptococcus* Group G
[GB1]3	Triple-repeat of GB1
GFP	Green fluorescent protein
GFP particle	GFP fusion protein particle

GiCL	Fusion protein consisting of ext(AVTS)GFP-inactive PHA synthase-pentaglycine linker.
GiCLB	Fusion protein consisting of ext(AVTS)GFP-inactive PHA synthase-pentaglycine linker-α-amylase. Also denotes resultant GFP particle.
GiCLN	Fusion protein consisting of ext(AVTS)GFP-inactive PHA synthase-pentaglycine linker-[*N*-acetyl-D-neuraminic acid aldolase]. Also denotes resultant GFP particle.
GiCLO	Fusion protein consisting of ext(AVTS)GFP-inactive PHA synthase-pentaglycine linker-organophosphohydrolase. Also denotes resultant GFP particle.
GiCLZ	Fusion protein consisting of ext(AVTS)GFP-inactive PHA synthase-pentaglycine linker-ZZ domain. Also denotes resultant GFP particle.
GNL	Fusion protein consisting of ext(AVTS)GFP-[*N*-acetyl-D-neuraminic acid aldolase]-pentaglycine linker.
GNLN	Fusion protein consisting of ext(AVTS)GFP-[*N*-acetyl-D-neuraminic acid aldolase]-pentaglycine linker-[*N*-acetyl-D-neuraminic acid aldolase]. Also denotes resultant GFP particle.
GNLZ	Fusion protein consisting of ext(AVTS)GFP-[*N*-acetyl-D-neuraminic acid aldolase]-pentaglycine linker-ZZ domain. Also denotes resultant GFP particle.
h	Hour
HcR	Far red protein HcRed
HEPES	4-(2-hydroxyethyl)-1-piperazineethanesulfonic acid
HPLC	High Performance Liquid Chromatography
IB	Inclusion body
IgG	Immunoglobulin G
IPTG	Isopropyl β-D-1-thiogalactopyranoside
kDa	Kilodalton
LAVG	Amino acids Leucine-Alanine-Valine-Glycine that constitute a short N-terminal extension of GFP in GFP fusion proteins
LB	Luria-Bertani
M	mol per litre

µg	Microgram
µl	Microliter
mA	Milliampere
ml	Millilitre
mM	Millimol per litre
MALDI-TOF/MS	Matrix-assisted Laser Desorption/ Ionisation Time-of-Flight Mass Spectrometry
MalE	Maltose binding protein
ManNAc	*N*-acetyl-D-mannosamine
min	Minute
MOPS	3-Morpholinopropanesulfonic acid
MW	Molecular weight
NanA	*N*-acetyl-D-neuraminic acid aldolase from *E. coli*
NanA-PhaC	*N*-acetyl-D-neuraminic acid aldolase/ PHA synthase fusion protein
Neu5Ac	*N*-acetyl-D-neuraminic acid
ng	Nanogram
OpdA	Organophosphohydrolase from *Agrobacterium radiobacter*
PCR	Polymerase Chain Reaction
pET14b-GiCL	pET14b plasmid that encodes the fusion protein GiCL.
pET14b-GiCLB	pET14b plasmid that encodes the fusion protein GiCLB.
pET14b-GiCLN	pET14b plasmid that encodes the fusion protein GiCLN.
pET14b-GiCLO	pET14b plasmid that encodes the fusion protein GiCLO.
pET14b-GiCLZ	pET14b plasmid that encodes the fusion protein GiCLZ.
pET14b-GNL	pET14b plasmid that encodes the fusion protein GNL.
pET14b-GNLN	pET14b plasmid that encodes the fusion protein GNLN.
pET14b-GNLZ	pET14b plasmid that encodes the fusion protein GNLZ.
PHA	Polyhydroxyalkanoate
PhaC	PHA synthase
PhaC (C319A)	Inactive PHA synthase
PhaC-OpdA	PHA synthase/ Organophosphohydrolase fusion protein
PHB	Polyhydroxybutyrate
rpm	Revolutions per minute
R.T.	Room temperature (22 ˚C- 25 ˚C)

SDS	Sodium dodecylsulfate
SDS-PAGE	Sodium dodecylsulfate Polyacrylamide Gel Electrophoresis
SEM	Scanning Electron Microscopy
TEM	Transmission Electron Microscopy
U	Enzyme units
V	Volts
x g	Unit denoting centrifugal force as a multiple of standard gravity on Earth
YFP	Enhanced yellow fluorescent protein
ZZ	IgG binding domain of Protein A from *Staphylococcus aureus*

LIST OF FIGURES

		Page
Figure 1.	Inclusion body formation inside bacterial cells	7
Figure 2.	Three-dimensional structure of green fluorescent protein (GFP)	10
Figure 3.	Types of GFP fusion protein investigated by Jahns *et al.* 2013	12
Figure 4.	Diagram of glycerol gradient for PHA bead/ GFP particle separation before and after centrifugation	45
Figure 5.	Diagram detailing the production of Neu5Ac from the condensation of Pyruvate and ManNAc catalysed by NanA	51
Figure 6.	Diagram detailing the production of maltose from the hydrolysis of starch by Bla(-ss)	52
Figure 7.	Diagram detailing the hydrolysis of methyl parathion by OpdA to *para*-nitrophenol and Dimethyl phosphorothioic acid	54
Figure 8.	Construction of plasmids pET14b-ext(AVTS)gfp-phaC(C319A)-1inker-nanA, and pET14b-ext(AVTS)gfp-nanA-1inker-nanA	59
Figure 9.	Digest of GiCLZ, GNLZ, GiCLN, and GNLN plasmids with *Bam*HI and *Xho*I	61
Figure 10.	Fluorescent images of *E.coli* BL21 (DE3) cells containing GFP particles and GFP particles post-extraction	63
Figure 11.	SDS-PAGE analysis of PHA beads and GFP particles to be used in NanA enzyme activity assays	65
Figure 12.	Neu5Ac production by PHA beads and GFP particles after 16 h and 48 h incubation	66
Figure 13.	Construction of the plasmid pET14b-ext(AVTS)gfp-phaC(C319A)-1inker-opdA	68
Figure 14.	Construction of the plasmid pET14b-ext(AVTS)gfp-phaC(C319A)-1inker-bla(-ss)	69
Figure 15.	Digest of pET14b-GiCLB and pET14b-GiCLO plasmids with *Bam*HI and *Xho*I	70

Figure 16.	Fluorescent images of *E.coli* BL21 (DE3) cells containing GiCLB and GiCLO particles, and GiCLB and GiCLO particles post-extraction	71
Figure 17.	Production of maltose via Bla(-ss)-PhaC PHA bead and GFP particle biocatalysis over a 72 h incubation	72
Figure 18.	Production of Neu5Ac via NanA-PhaC PHA bead and GiCLN particle biocatalysis over a 72 h incubation	73
Figure 19.	Production of *para*-nitrophenol via PhaC-OpdA PHA bead and GFP particle biocatalysis over a 72 h incubation	74
Figure 20.	Production of maltose via Bla(-ss)-PhaC PHA bead and GiCLB particle biocatalysis after heat-treatment	76
Figure 21.	Production of Neu5Ac via NanA-PhaC PHA bead and GiCLN particle biocatalysis after heat-treatment	78
Figure 22.	Production of *para*-nitrophenol via PhaC-OpdA PHA bead and GiCLO particle biocatalysis after heat-treatment	78
Figure 23.	Fluorescent images of GiCLB particles after heat-treatment	79
Figure 24.	Fluorescent images of GiCLN particles after heat-treatment	80
Figure 25.	Fluorescent and Phase contrast images of GiCLO particles after heat-treatment	81
Figure 26.	Production of maltose via Bla(-ss)-PhaC PHA bead and GiCLB particle biocatalysis after pH-treatment	82
Figure 27.	Production of Neu5Ac via NanA-PhaC PHA bead and GiCLN particle biocatalysis after pH-treatment	83
Figure 28.	Production of *para*-nitrophenol via PhaC-OpdA PHA bead and GiCLO particle biocatalysis after pH-treatment	84
Figure 29.	Fluorescent images of GiCLB particles after pH-treatment	85
Figure 30.	Fluorescent images of GiCLN particles after pH-treatment	86
Figure 31.	Fluorescent images of GiCLO particles after pH-treatment	87
Figure 32.	Production of maltose via GiCLB particle biocatalysis over four consecutive cycles	89
Figure 33.	Production of Neu5Ac via GiCLN particle biocatalysis over four consecutive cycles	90

Figure 34.	Production of *para*-nitrophenol via GiCLO particle biocatalysis over four consecutive cycles	91
Figure 35.	Production of maltose via Bla(-ss)-PhaC PHA bead and GiCLB particle biocatalysis after long-term storage at 4 ˚C, room temperature (22 ˚C-25 ˚C) (R.T.), and -80 ˚C	92
Figure 36.	Production of Neu5Ac via NanA-PhaC PHA bead and GiCLN particle biocatalysis after long-term storage at 4 ˚C, room temperature (22 ˚C- 25 ˚C) (R.T.), and -80 ˚C	93
Figure 37.	Production of *para*-nitrophenol via PhaC-OpdA PHA bead and GiCLO particle biocatalysis after long-term storage at 4 ˚C, room temperature (22 ˚C- 25 ˚C) (R.T.), and -80 ˚C	94
Figure 38.	Fluorescent images of GiCLB particles after long-term storage at 4 ˚C, room temperature (22 ˚C- 25 ˚C) (R.T.), and -80 ˚C	96
Figure 39.	Fluorescent images of GiCLN particles after long-term storage at 4 ˚C, room temperature (22 ˚C- 25 ˚C) (R.T.), and -80 ˚C	97
Figure 40.	Fluorescent images of GiCLO particles after long-term storage at 4 ˚C, room temperature (22 ˚C- 25 ˚C) (R.T.), and -80 ˚C	98

LIST OF TABLES

		Page
Table 1.	Bacterial Strains used in this study	24
Table 2.	Plasmids used in this study	24-26
Table 3.	Primers used in this study	26-27
Table 4.	Antibiotic types, stock solution concentrations, and working solution concentrations	30
Table 5.	Stain types, amounts used, solvents used, and final concentration of dissolved stain	31
Table 6.	SDS-PAGE solutions	31-32
Table 7.	Miscellaneous Solutions	32
Table 8.	λ/ *Pst*I DNA Ladder Standard	40
Table 9.	Mark 12^{TM} Unstained Standard protein ladder	50
Table 10.	The duration of incubation required for enzyme-bearing PHA beads and GFP particles to catalyse reactions to their end-points	105

CHAPTER ONE: INTRODUCTION

1.1 Enzymes and their Industrial Applications

Enzymes are protein catalysts. Over millions of years enzymes have evolved to increase the rate of chemical reactions within cells without undergoing permanent change due to the reaction (Price & Stevens, 1999). Furthermore, enzymes have also evolved to facilitate reactions that would not happen under physiological conditions, thus allowing life as we know it to exist (Price & Stevens, 1999; Soetan, Aiyelaagbe, & Olaiya, 2010). Enzymes have been used for thousands of years in fermentation processes and cheesemaking (Price & Stevens, 1999). However, until recently, identification of individual enzymes and their mechanisms of action were not understood (Price & Stevens, 1999). Progress in isolation and purification techniques, structural investigations, and activity assays have allowed scientists to elucidate the biochemical properties of enzymes (Price & Stevens, 1999). This information has increased understanding of how enzymes function in cellular processes, and allowed the application of enzymes to a variety of industrial uses.

The qualities of enzymes that make them attractive to industry include: increased rate of reaction in comparison to non-enzyme catalysts; high substrate specificity; and excellent product enatio- and stereo-selectivity (Lutz, 2010; Price & Stevens, 1999; Steinmann, Christmann, Heiseler, Fritz, & Kolmar, 2010). Furthermore, enzymes also allow reactions to be conducted under more gentle conditions by removing the need for toxic heavy metal catalysts, and harsh treatments with pressure, temperature, or pH (Savile et al., 2010). Industries that currently use enzymes in their processes include: food production; detergent manufacture; agriculture; chemical and pharmaceutical manufacture; textiles; leather; paper; diagnostics; medicine; and bioremediation (Sanchez & Demain, 2011; Scott et al., 2008). The number of industrial processes able to utilise enzymes can be expected to grow, and with the advent of recombinant DNA technologies, mutagenesis harnessing protocols, and computer simulated evolution novel enzymes unseen in nature are now available (Chen & Arnold, 1993; Savile et al., 2010; Siegel et al., 2010). In 2009 the industrial enzyme market was valued at US$5.1 billion (Sanchez & Demain, 2011), and if current trends continue this valuation will

increase. However, although the demand for enzymes can be expected to increase, the equipment and reagents required for their isolation and purification are expensive.

1.2 Enzyme Isolation and Purification

Enzymes can be isolated from all forms of life, although the majority of enzymes used in industry are sourced from bacteria and fungi (Sanchez & Demain, 2011). As most reactions within cells are catalysed by enzymes (Price & Stevens, 1999) it is understandable that isolating and purifying a particular enzyme from a myriad of proteins is difficult. However, various methods have been devised and employed in the purification of enzymes including: centrifugation; gel filtration; dialysis; electrophoresis; isoelectric focusing; influencing solubility; immunoadsorption; and various types of chromatography such as ion-exchange chromatography, hydrophobic chromatography, affinity chromatography, immobilised metal ion chromatography, dye-ligand chromatography, and covalent chromatography (Price & Stevens, 1999). Not every type of protein can be purified by any one technique, and often a combination of techniques will be required to obtain protein of a sufficient quality (Price & Stevens, 1999). Combining techniques compounds the cost of purifying enzyme not only in terms of the equipment and reagents required, but also in terms of the level of expertise necessary (Price & Stevens, 1999). Furthermore, once the enzyme has been used in a reaction it cannot be used again unless it is repurified or new enzyme is obtained, further increasing costs (Price & Stevens, 1999). To this end, various immobilisation methods have been developed which allow enzyme to be reused.

1.3 Enzyme Immobilisation

Enzyme immobilisation involves attaching an enzyme to a solid support. The most frequently used immobilisation techniques can be broadly grouped into five categories: non-covalent adsorption and deposition; immobilisation via ionic interactions; covalent attachment; cross-linking of an enzyme; and entrapment in a polymeric gel or capsule (Hanefeld, Gardossi, & Magner, 2009). Using these methods enzyme can be displayed on the surface of particles or within pores. Immobilisation has been shown to enhance the stability of enzymes in a wider range of environments, including non-aqueous media, as well as improve enzyme performance via increased stability, conformation,

and re-use (Brady & Jordaan, 2009; R. A. Sheldon, 2007). Furthermore, immobilisation can also improve the creation of multi-enzyme systems. However, a common feature that most immobilisation techniques share is the need for multiple steps and reagents in order to produce purified enzyme and its support, and then successfully immobilise the enzyme. These requirements further increase the costs of using enzymes. Various methods exist that allow enzymes to self-immobilise into insoluble particles. These include methods that govern the formation of cross-linked enzyme aggregates (CLEAs), cross-linked enzyme crystals (CLECs), and Spherezymes (Brady et al., 2008; R. A. Sheldon, Schoevaart, & Van Langen, 2005; St. Clair & Navia, 1992). In these processes enzyme aggregates, crystals, or water-in-oil emulsions of dissolved enzyme are permanently stabilised by a bifunctional cross-linker such as glutaraldehyde. This treatment yields insoluble enzyme particles consisting almost entirely of enzyme. There are also methods that allow the purification and immobilisation of enzymes and other proteins in a single step. Pessela *et al.* developed a system where poly-His-tagged-β-galactosidase from *Thermus* sp. strain T2 was produced in *Escherichia coli* (Pessela et al., 2003). The enzyme was then purified and immobilised from extracts using heterofunctional chelate-epoxy sepabeads and the principles of immobilised metal-chelate affinity chromatography and covalent bonding. These self-immobilisation methods reduce the complexity and labour-intensity of producing immobilised enzyme. They have also been shown to allow high catalytic activity, and impart the ability for enzymes to function in both aqueous and organic solvents. However, recent developments using recombinant DNA technology have made it possible to produce, purify and immobilise enzyme to solid supports in a single step.

1.4 Enzyme Fusion Proteins for Enzyme Isolation, Purification, and Self-immobilisation

A number of enzyme immobilisation technologies are based upon gene fusions. In these scenarios the gene of the enzyme of interest is fused to another gene which facilitates the formation of the solid support. In this manner the enzyme is strongly bound to the support by covalent bonds, and enzyme production, purification, and immobilisation occurs in one step inside a host cell. For example, Heyman *et al.* fused a gene that encodes glucose oxidase in frame with that of the ring-like protein SP1 from the aspen poplar *Populus tremula* (Heyman, Levy, Altman, & Shoseyov, 2007). The resultant

fusion protein was able to self-assemble into nanotube particles that displayed active enzyme molecules. A further example involves the creation of fibrils that demonstrated enzyme activity (Guglielmi et al., 2009). In this study a bifunctional chimeric fusion protein consisting of the fibrillogenic domain of Apolipoprotein A-I was fused with the enzyme glutathione S-transferase. After expression, isolation, and three weeks of incubation it was observed that the fusion protein self-assembled into insoluble fibrillar structures which were often found to be organised into larger fibre networks. Another example involves the use of polyhydroxyalkanoate (PHA) granules (Grage et al., 2009). The GFP particles used in this study were produced using protocols that are similar to those used by Rehm *et al.* to produce functionalised PHA granules. Therefore, a brief description of PHA granules and how the natural process of their formation has been exploited is provided below.

1.5 Functionalised PHA Granules

PHA granules are naturally occurring polyesters that are synthesised by most bacteria and some Archaea when essential nutrients are limited and carbon is available in excess quantities (Grage et al., 2009). They serve as carbon and energy storage for bacteria, and can be synthesised from hydroxyl fatty acids of varying chain length. The granules can be observed as insoluble spherical inclusions in the cytoplasm of cells, and are degraded when carbon sources are scarce. PHA granules are composed of a polyester core surrounded by a phospholipid layer that contains proteins such as PHA synthase, phasins, depolymerases, and regulatory proteins. It is the PHA synthase (PhaC) that is integral to granule formation, and this has been the focus of many gene fusions to produce functionalised PHA granules. During granule formation PhaC remains covalently attached to the granule surface and, therefore, any proteins fused to the PhaC are also attached. PHA granules have been functionalised with a variety of different ligands including: a single chain variable fragment (scFv) of an antibody (Grage & Rehm, 2008); genetically engineered proteins for inorganics (GEPIs) that could bind gold and silica (Jahns, Haverkamp, & Rehm, 2008); and the hepatitis C virus core (HCc) antigen for use as a vaccine delivery system (Parlane et al., 2011). PHA granules have also been used as the solid supports for the enzymes α-amylase, β-galactosidase, and organophosphohydrolase (Blatchford, Scott, French, & Rehm, 2012; Peters & Rehm, 2006; Rasiah & Rehm, 2009). Through these studies it has been shown that

different types of functionalities can be fused to either the N- or C-terminus of PhaC without compromising PHA granule formation. This makes PhaC a versatile anchor for functionalities, with the potential to display multiple functions (Jahns et al., 2008). It should be noted that phasins have also been used as fusion partners in order to functionalise PHA beads (Grage et al., 2009). As stated above, the GFP particles used in this study were produced using similar protocols to those that produce functionalised PHA granules. This includes the choice of production host and culture conditions, but also the manner in which DNA is manipulated and the types of fusion protein produced. The feature that separates GFP particles from PHA granules is the effect that the GFP protein has on GFP particle formation, and the types of inclusion bodies produced. PHA granules consist almost entirely of the polyhydroxyalkanoate polyester. Whereas, in the absence of a natural process for particle formation, it is assumed that GFP particles consist entirely of GFP fusion protein. This would make GFP particles similar to inclusion bodies formed in bacteria through the production of recombinant proteins, a process that is beginning to be explained.

1.6 Inclusion Bodies

Inclusion bodies (IBs) are protein aggregates that have been commonly observed in bacteria that have been used to produce recombinant proteins (Garcia-Fruitos et al., 2012). Until recently is was assumed that inclusion bodies consisted of unfolded or misfolded proteins (Baneyx & Mujacic, 2004), and were considered to be waste products. The focus was to either extract recombinant protein from inclusion bodies, and refold the protein into the correct conformation using *in vitro* techniques, or to minimise the formation of inclusion bodies (Garcia-Fruitos et al., 2012). However, recently it has been recognised that, in contrast to previous assumptions, inclusion bodies do in fact contain active protein (Garcia-Fruitos et al., 2005). This realisation has led to further studies that have investigated how inclusion bodies form inside bacteria, and how they might be used for research and industrial processes (M. Carrio, Gonzalez-Montalban, Vera, Villaverde, & Ventura, 2005; Garcia-Fruitos, Aris, & Villaverde, 2007; Garcia-Fruitos et al., 2009; Nahalka, Mislovicova, & Kavcova, 2009; Peternel & Komel, 2011).

1.6.1 Inclusion Body Formation and Structure

The formation of inclusion bodies from protein aggregates is a self-assembled process inside bacterial host cells, as illustrated in Figure 1 (Peternel & Komel, 2011). First, mRNA and target proteins are overexpressed, which saturates protein synthesis machinery and activates quality control mechanisms within the host cells (Peternel & Komel, 2011). This leads to the production of correctly folded soluble recombinant protein, and also an abundance of aggregation-prone misfolded protein that act as seeding nuclei for the formation of soluble proto-aggregates (Garcia-Fruitos, Sabate, de Groot, Villaverde, & Ventura, 2011). During this aggregation correctly folded protein is incorporated into the proto-aggregates by cross-molecular stereospecific interactions (Peternel & Komel, 2011). Interestingly, non-homologous cellular and recombinant proteins are mostly excluded from the nucleation event (Garcia-Fruitos et al., 2011). It has been shown that inclusion bodies contain high levels of pure protein due to protein intermediates aggregating only with themselves (Morell et al., 2008; Speed, Wang, & King, 1996). This is because stereospecific cross-molecular contacts require aggregating proteins to have a native-like secondary structure (Garcia-Fruitos et al., 2012), and this native-like conformation of proteins in inclusion bodies has been confirmed by infra-red spectroscopy (Doglia, Ami, Natalello, Gatti-Lafranconi, & Lotti, 2008). Finally, the proto-aggregates incorporate more protein into themselves, and aggregate together to form mature inclusion bodies (Garcia-Fruitos et al., 2011; Peternel & Komel, 2011). The inclusion body grows as a sphere until it reaches the bacterial cell wall (Peternel & Komel, 2011). At this point the cell wall shapes the inclusion body into a cylinder-like structure as the inclusion body continues to grow (Peternel & Komel, 2011). In general, only one inclusion body is observed per cell (Peternel & Komel, 2011). During cell division the inclusion body is retained in one cell and continues to grow, while protein production and inclusion body formation begin *de novo* in the other cell (Peternel & Komel, 2011). Presumably, this is the reason why in a population of bacterial cells producing recombinant protein there will be inclusion bodies of different sizes. Inclusion bodies formed earlier in the culture will be larger, while those formed later will be smaller (Peternel & Komel, 2011). The size of inclusion bodies is also dependent on the particular protein species produced, and the genetic characteristics of the host cell (Garcia-Fruitos et al., 2009).

Over-expression of heterologous recombinant protein in microbial hosts has been shown to activate quality control mechanisms involving chaperones (M. M. Carrio & Villaverde, 2005; Peternel & Komel, 2011). Chaperones such as DnaK and GroEL have been shown to be intimately associated with inclusion bodies, being able to aid the correct folding of recombinant proteins, and also to disaggregate inclusion bodies into soluble protein (M. M. Carrio & Villaverde, 2005; García-Fruitós et al., 2007; Garcia-Fruitos et al., 2011; Martinez-Alonso, Garcia-Fruitos, & Villaverde, 2008). This shows that the aggregation and disaggregation of inclusion bodies can happen simultaneously, and that they are incorporated into cellular repair pathways (M. M. Carrio & Villaverde, 2002; Garcia-Fruitos et al., 2011).

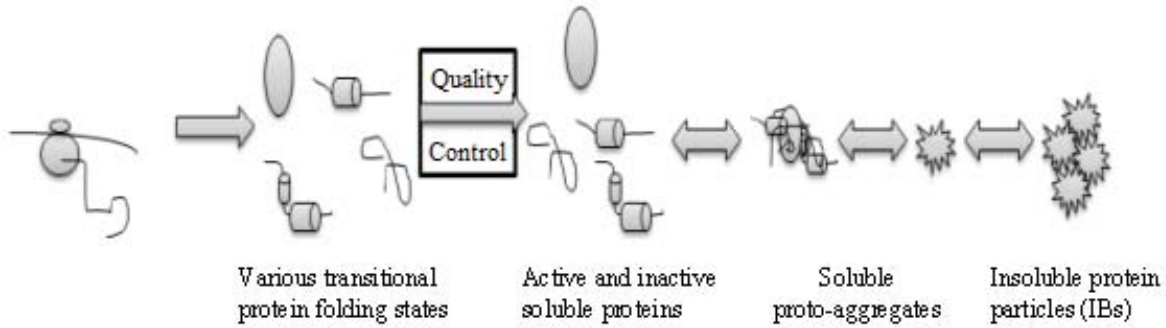

Figure 1. Inclusion body formation inside bacterial cells (Reproduced from Peternel & Komel, 2011)

The inner architecture of inclusion bodies has been examined using a variety of techniques which have yielded interesting structural information. Both native-like secondary structures and amyloid-like cross-molecular β-sheet formations have been identified (M. Carrio et al., 2005; Garcia-Fruitos et al., 2012). Additionally, as the proto-aggregates fuse together the spaces in between are filled by an amorphous matrix (Peternel & Komel, 2011). This amorphous matrix also extends inside the proto-aggregates, and gives inclusion bodies the appearance of a porous surface (Peternel & Komel, 2011).

1.6.2 Inclusion Body Stability

Inclusion bodies are remarkably stable. They have been found to be able to survive ultrasonication, high-pressure, and other physical procedures used to break open cells (Georgiou & Valax, 1999). Furthermore, minimal amounts of protein have been found

to leach from freshly isolated inclusion bodies and only during the first minutes of incubation (Garcia-Fruitos et al., 2007). Following this, inclusion bodies are quite stable under long-term storage conditions and incubation with no observable changes in size, shape, and activity (Garcia-Fruitos et al., 2009). Inclusion bodies can also tolerate lyophilisation and freeze-thawing (Garcia-Fruitos et al., 2012). For proteinaceous particles to exhibit such stability is unexpected, especially in light of previous assumptions concerning their random formation from misfolded proteins. However, inclusion bodies consist of a more complex architecture than previously thought, and possess physical properties that make them attractive to industrial applications.

1.6.3 Industrial Applications of Inclusion Bodies

Due to the recent discoveries concerning inclusion body formation and stability, many studies have explored their potential use in tissue regeneration and biocatalysis (Garcia-Fruitos et al., 2012). Enzymes served as reporter proteins in initial studies on the formation of inclusion bodies which showed that the inclusion bodies consisted, at least to some degree, of active enzyme (Garcia-Fruitos et al., 2005; Tokatlidis, Dhurjati, Millet, Beguin, & J.P., 1991; Worrall & Goss, 1989). The fact that enzyme activity was exhibited by inclusion bodies not only showed how functional protein was incorporated into their structure, but it also highlighted the potential use of inclusion bodies as biocatalysis platforms. Indeed, inclusion bodies consisting of enzyme proteins represent a novel method in the immobilisation of active enzyme. Enzymes that have been incorporated into functional inclusion bodies include oxidases, reductases, phosphatases, kinases, aldolases, glucosidases, phosphorylases, and others (Garcia-Fruitos et al., 2012). The porous nature of inclusion bodies might permit efficient mass transfer of substrate through the inclusion body, and there are potential applications for enzyme-based inclusion bodies in solid phase catalysis (Garcia-Fruitos et al., 2012).

1.7 Green Fluorescent Protein

Green fluorescent protein (GFP) is a protein that is capable of emitting green fluorescence. It is found in numerous bioluminescent organisms; however, the type that is most commonly used for molecular biology was isolated from the jellyfish *Aequorea aequorea* (Zimmer, 2002). This is the type of GFP that will be discussed. GFP has a

unique 11 β-sheet barrel-like structure with a diameter of around 24 Å and a height of 42 Å (Zimmer, 2002). The β-sheets form the sides of the barrel, while an α-helix runs diagonally through it and forms lids on both ends of the barrel (Yang, Moss, & Phillips, 1996; Zimmer, 2002). At the centre of the structure is a cyclised hexapeptide chromophore which is attached to the barrel by the α-helix (Cody, Prasher, Westler, Pendergast, & Ward, 1993; Zimmer, 2002). This structure makes GFP a robust protein. It has been found to be resistant to heat, alkaline pH, detergents, photobleaching, chaotropic salts, organic salts, high pressure, and many proteases (Erhmann, Scheyhing, & Vogel, 2001). With these characteristics GFP has proven itself to be extremely useful in research as is evidenced by the thousands of articles available that describe it or its use in other investigations. The feature of GFP that has made it especially useful is its fluorescence and the manner in which this fluorescence is produced. A three-dimensional representation of GFP is displayed in Figure 2.

The fluorescence exhibited by GFP is produced by the hexapeptide chromophore mentioned above. This chromophore consists of six amino acids (Phe64-Ser65-Tyr66-Gly67-Val68-Gln69), with a post-translational autocatalytic cyclisation occurring in Ser65-Tyr66-Gly67 that does not require any cofactors or substrates (Zimmer, 2002). The only external requirement in order to emit fluorescence is the presence of oxygen and excitation (Chalfie, Tu, Euskirchen, Ward, & Prasher, 1994; Heim, Prasher, & Tsien, 1994; Morise, Shimomura, Johnson, & Winant, 1974). After excitation, green light is emitted from GFP molecules as they return from an excited state to a ground state (Tsuji, 2010). The structure of GFP is very important in its ability to emit fluorescence. The peptide sequence and its resultant three dimensional structure sets up the correct environment for the cyclisation between the Ser65, Tyr66, and Gly67 residues (Zimmer, 2002). Furthermore, deletion experiments have shown that most of the protein is required in order to form the chromophore and achieve fluorescence (Dopf & Horiagon, 1996). However, some specific mutations, rearrangements, or insertions in the structure of GFP can still produce fluorescent GFP (Baird, Zacharias, & Tsien, 1999), and have led to the enhancement of green fluorescence and the creation of fluorescent proteins that emit different coloured light. For example, enhanced green fluorescent protein (EGFP) was created by the mutation S65T, and blue fluorescent protein can be created by the mutations Y66H and Y145H (Heim, Cubitt, & Tsien, 1995; Wachter et al., 1997).

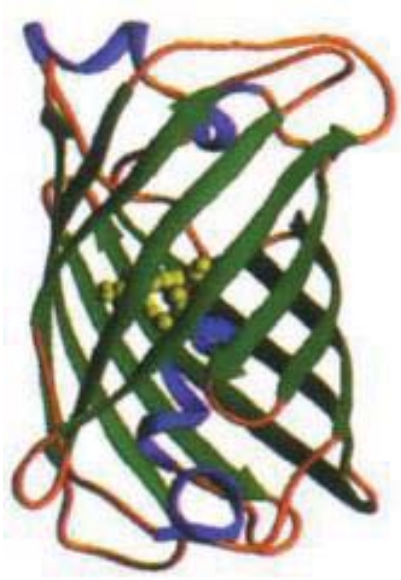

Figure 2. Three-dimensional structure of green fluorescent protein (GFP) (Reproduced from Yang, Moss, & Phillips, 1996).

As stated above, GFP has been used extensively in research. Reasons for this include: it can emit fluorescence without the need of a cofactor or substrate; it rarely affects protein activity or mobility when used as a fusion tag; and in most cases it is non-toxic (Zimmer, 2002). Such qualities have made GFP incredibly useful in elucidating gene expression *in vivo*, protein localisation, and protein-protein interactions. However, besides molecular biology research, GFP has been used in a variety of different applications in medicine and other industries. Such applications include: biosensors (Lumjiaktase, Aguilar, Battin, Riedel, & Eberl, 2010; Raja & Selvam, 2011); tumour tagging to illuminate dissemination (Li et al., 2010); diagnostics (De et al., 2009); drug development (Kepp, Galluzzi, Lipinski, Yuan, & Kroemer, 2011); and monitoring meat fermenting lactobacilli in sausages (Luxananil et al., 2009). GFP was also used as one of the reporter proteins that showed that inclusion bodies do contain correctly folded and active protein. In their 2005 study García-Fruitós *et al.* showed that when GFP is fused to the aggregating polypeptide FMDV VP1 and the recombinant fusion protein is overexpressed inclusion bodies are formed that exhibit fluorescence (Garcia-Fruitos et al., 2005). This result allowed inclusion bodies to be seen not as waste by-products of recombinant protein production, but as aggregates possessing an unforeseen complexity.

Furthermore, in light of the topic of this study, GFP has been helpful in highlighting how GFP fusion proteins behave when aggregated as GFP particles.

1.8 GFP particles

Self-assembling fluorescent protein particles- of the type used in this study- were first observed by Jahns, Maspolim, and Rehm (Jahns et al., 2013). In this study GFP was used to ascertain whether the Class I Polyester synthase (PhaC) from the bacterium *Ralstonia eutropha* could act as a fusion partner that could promote the self-assembly of protein particles. They examined the effect of several features on the formation of green fluorescent protein particles (GFP particles), namely: the effect of extending the N-terminus of GFP; the effect of the type of N-terminal extension of GFP; the effect of PhaC and its replacements; and the effect of fusing different functionalities to the C-terminus of the GFP-PhaC fusion protein. N-terminal fusions of functionalities to GFP were not investigated. A representation of the GFP fusion proteins investigated is provided in Figure 3. Jahns *et al.* also characterised the ensuing particles, and investigated whether fluorescent protein particles could be formed using other types of fluorescent protein- enhanced yellow fluorescent protein (YFP), enhanced cyan fluorescent protein (CFP), and far red protein HcRed (HcR). This study provided a comprehensive foundation from which GFP particles could be reproducibly made, and further tested for other industrial applications.

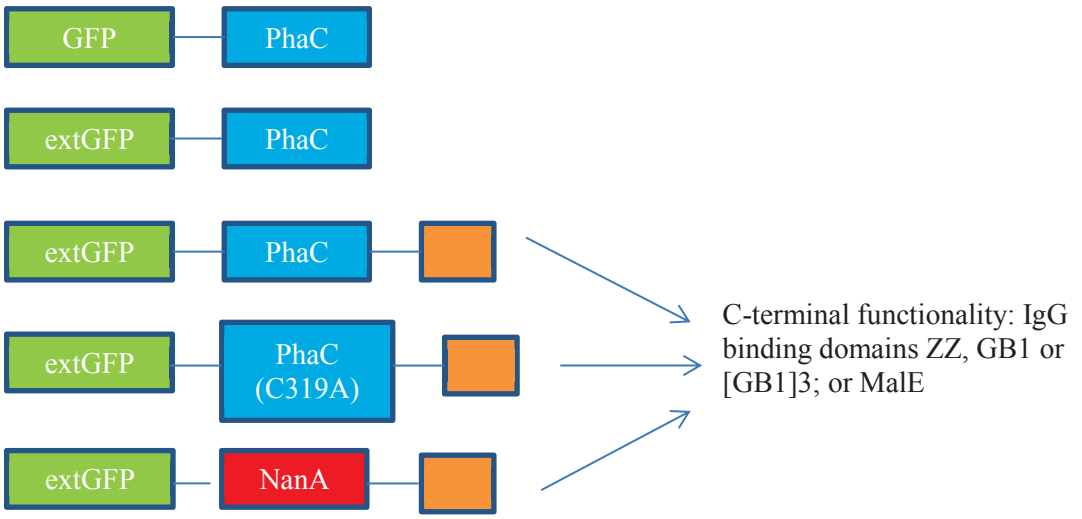

Figure 3. Types of GFP fusion protein investigated by Jahns *et al.* 2013. GFP/ extGFP are situated at the N-terminus of the fusion protein, while the tan boxes denote the C-terminal functionalities which are interchangeable. Abbreviations are as follows: GFP = Green Fluorescent Protein; extGFP = N-terminally extended green fluorescent protein; PhaC = PHA synthase; PhaC(C319A) = PHA synthase that has been mutated to render it inactive; NanA = *N*-acetyl-D-neuraminic acid aldolase; IgG = Immunoglobulin G; ZZ = IgG binding domain of Protein A from *Staphylococcus aureus*; GB1 = IgG binding domain of Protein G from *Streptococcus* Group G; [GB1]3 = Triple repeat of GB1; MalE = Maltose binding protein.

1.8.1 The Effect of an N-terminal Extension of GFP

The first fusion proteins to be produced were GFP with PhaC fused to its C-terminus (GFP-PhaC), and a similar fusion protein that employed an N-terminally extended GFP (extGFP-PhaC). The N-terminal extension was created through the use of an alternative start codon which resulted in the incorporation of four amino acids (AVTS) at the N-terminus of GFP. These residues altered the properties of GFP when fused to PhaC and expressed from the T7 promoter, resulting in the production of protein particles rather than inclusions composed of PHB- polyhydroxybutyrate, a derivative of PHA. Both fusion proteins were encoded in the plasmid pET14b (pET14b-gfp-phaC and pET14b-extgfp-phaC, respectively), and overexpressed using the strong T7 promoter in *E.coli* BL21 (DE3) cells. The bacterial cells also harboured the plasmid pMCS69 which encodes the genes *phaA* and *phaB* which provide the *R*-3-hydroxybutyryl CoA substrate from which PhaC can produce PHB (Amara & Rehm, 2003). *E. coli* BL21 (DE3) cells that were induced to overexpress GFP-PhaC appeared like wild-type cells in regards to colour and PHB content which was approximately 35% (w/w) of cellular dry weight. However, cells that were induced to overexpress extGFP-PhaC appeared to be very

fluorescent, and acquired a PHB content of approximately 8% (w/w) of cellular dry weight. From these observations it appeared that the N-terminal extension of GFP was necessary to produce GFP fusion protein that was able to fluoresce. Furthermore, it appeared that this N-terminal extension was able to override the ability of PhaC to produce PHB, and facilitate the production of GFP protein particles.

1.8.2 The Effect of the C-terminal Fusion of PhaC on Particle Formation

In order to evaluate the role of the C-terminal fusion of PhaC to GFP in particle formation, genes encoding *gfp* and *extgfp* were overexpressed. The genes were encoded on pET14b plasmids, were under the control of T7 promoters, and were overexpressed in two types of *E. coli* BL21 (DE3) cells- cells that harboured pMCS69 and cells that did not. Following overexpression both genes in both types of host produced cells that were fluorescent. Furthermore, it was observed that following cell disruption the fluorescence was found in the soluble supernatant indicating that the proteins had not formed insoluble particles. This was also observed in the overproduction of the fusion proteins GFP-GB1, extGFP-GB1, GFP-L-SG-[GB1]3, extGFP-L-SG-[GB1]3, GFP-ZZ, and extGFP-ZZ, although the cultures of the latter four fusion proteins also produced small amounts of insoluble protein. These results suggest that PhaC is essential in facilitating the aggregation of GFP fusion proteins, and, therefore, the self-assembly of insoluble GFP protein particles.

1.8.3 Engineering GFP Particles to Display Foreign Proteins

The industrial applicability of GFP particles was shown by fusing different functionalities to the C-terminus of the extGFP-PhaC fusion protein. The functionalities investigated were: maltose binding protein (MalE); the IgG binding domain of Protein A from *Staphylococcus aureus* (ZZ); and a single as well as triple repeat of the IgG binding domain of Protein G (GB1 and [GB1]3, respectively) from *Streptococcus* Group G.

Although its activity was never measured, the functionality MalE was used to assess the potential of GFP particles to display protein functions. Hybrid genes encoding the fusion proteins GFP-PhaC-linker-MalE and extGFP-PhaC-linker-MalE were

constructed and carried in pET14b vectors. As with the experiments described above, the fusion proteins were under the control of the T7 promoter, and produced in *E. coli* BL21 (DE3) cells that included the presence of pMCS69. *E. coli* cells that produced GFP-PhaC-linker-MalE in a pMCS69 background produced PHB beads that displayed the fusion protein rather than protein particles. These beads did not exhibit any fluorescence. Cells that produced the fusion protein extGFP-PhaC-linker-MalE did not produce PHB in the presence of pMCS69. Instead, GFP particles were isolated from the cells, and MalE was detected at the particle surface by ELISA using HRP-labelled anti-MalE antibodies. A similar fusion protein, extGFP-PhaC(C319A)-linker-MalE- where the PhaC is mutated to render it inactive- was also produced as described above, and resulted in the production of GFP particles. Again, it appears that the N-terminal extension is essential for GFP particle formation. However, the results from this experiment show that it is possible to fuse a functionality to the C-terminus of GFP fusion proteins and have it displayed on the particle surface without detrimentally affecting the formation of GFP particles.

MalE was replaced by the ZZ, GB1, and [GB1]3 IgG binding domains to yield the fusion proteins extGFP-PhaC-linker-ZZ, extGFP-PhaC-linker-GB1, and extGFP-PhaC-linker-SG-[GB1]3, respectively. Plasmids encoding the active as well as inactive PhaC were constructed, and the fusion proteins produced as described above. All fusion proteins that encoded an active PhaC in the presence of pMCS69 led to the formation of PHB/ GFP fusion protein hybrid particles- with the exception of extGFP-PhaC-linker-SG-[GB1]3 which led to the formation of PHB beads that displayed the fusion protein. All hybrid particles and PHB beads were able to purify IgG from pooled human serum, and the IgG binding domains were detected at the surface of the particles by ELISA. The fusion proteins were also produced in cells that lacked pMCS69. In the absence of pMCS69, all fusion proteins that encoded an active PhaC led to the formation of GFP particles, and PHB could not be detected. All particles could purify IgG from human serum, and the binding domains were detected at the surface of the particles by ELISA. Fusion proteins that encoded an inactive PhaC led to the formation of GFP particles. Once again, all particles could purify IgG from human serum, and the binding domains were detected by ELISA.

From the results of the experiments above it appears that the type of functionality fused to the C-terminus of the GFP fusion protein does impact the formation of GFP particles. MalE appeared to override the activity of PhaC in a pMCS69 background to form GFP particles, whereas the ZZ, GB1, and [GB1]3 functionalities led to the formation of PHB/ GFP fusion protein hybrids, or PHB beads that displayed the fusion protein. It was only in the absence of pMCS69 or when an inactive PhaC was encoded that all types of fusion protein led to the formation of GFP particles. In any case, all types of functionality, immobilised on all types of particle, were shown to be displayed at the surface, and able to perform their designated function (with the exception of MalE that was not assessed). Furthermore, in many cases the hybrid and GFP particles were able to outperform PHB beads and commercial beads displaying the same ZZ and GB1 domains in the purification of IgG from human or goat sera. This highlights the potential for functionalised GFP particles in industrial applications.

1.8.4 The Effect of Exchanging PhaC as the Fusion Partner

To investigate the importance of the presence of PhaC (or PhaC(C319A)) as the central domain in a GFP fusion protein, it was replaced with the enzyme *N*-acetyl-D-neuraminic acid aldolase (NanA) from *E. coli*. The fusion protein extGFP-NanA-linker-ZZ was produced in *E. coli* BL21 (DE3) as described above, and its ability to form functional GFP particles was assessed. Cells that produced extGFP-NanA-linker-ZZ formed GFP particles, and the ZZ domain was detected at the surface of these particles by ELISA. The particles were also capable of purifying IgG from human serum, and the binding capacity of the particles appeared to be 3.5 times higher than a commercial standard. Therefore, PhaC is not essential in GFP particle formation as another enzyme can replace it. Jahns *et al.* suggest that it is the length of the PhaC/ NanA proteins that is essential and not their activity. In essence, they act as a large linker between GFP and the functionality at the C-terminus.

1.8.5 The Effect of the Type of N-terminal Extension of GFP on Particle Formation

In order to evaluate the effectiveness of the N-terminal extension of GFP in facilitating particle formation, three other types of N-terminal extension were investigated. The extensions were FHKP, LAVG, and TS. Each extension was incorporated into a fusion

protein that contained either PhaC/ PhaC(C319A) as the central domain, and either MalE/ ZZ as the C-terminal functionality. All fusion proteins were produced as described above. The different extensions affected particle formation in different ways. A description of some of these effects is provided below.

The extension FHKP had different effects on fusion proteins containing MalE or ZZ. Cells that produced extGFP(MFHKP)-PhaC-linker-MalE in a pMCS69 background exhibited PhaC activity and fluorescence. However, in the absence of pMCS69 the fusion protein formed only fluorescent GFP particles. Cells that produced extGFP(MFHKP)-PhaC(C319A)-linker-MalE, in the absence of pMCS69, formed only GFP particles. MalE was detected on the surface of the particles by ELISA. In a similar fashion, cells that produced extGFP(MFHKP)-PhaC-linker-ZZ in a pMCS69 background exhibited PhaC activity and fluorescence. However, in contrast to the MalE fusion protein, in the absence of pMCS69 protein particles were formed that were not fluorescent. Cells that produced extGFP(MFHKP)-PhaC(C319A)-linker-ZZ, in the absence of pMCS69, also formed particles that were not fluorescent. Interestingly, although non-fluorescent particles were sometimes produced, all types of particle comprised of ZZ fusion protein were able to purify IgG from human serum.

The extension LAVG had a larger range of effects in comparison to FHKP. Cells that produced extGFP(MLAVG)-PhaC-linker-MalE in a pMCS69 background exhibited PhaC activity and fluorescence. However, when analysed by ELISA only a low level of MalE was present. In the absence of pMCS69 the fusion protein formed fluorescent protein particles. Cells that produced extGFP(MLAVG)-PhaC(C319A)-linker-MalE formed GFP particles independent of the presence of pMCS69. Again, MalE was detected on the surface of particles by ELISA. Cells that produced extGFP(MLAVG)-PhaC-linker-ZZ in a pMCS69 background also had PhaC activity and exhibited some fluorescence. The particles were whitish-green in colour, and had low IgG binding activity. In the absence of pMCS69 the fusion protein formed particles; however, these were not fluorescent. Cells that produced extGFP(MLAVG)-PhaC(C319A)-linker-ZZ only formed GFP particles in the presence of pMCS69. However, these particles still exhibited IgG binding activity.

The extension TS also displayed a variety of effects on particle formation. Cells that produced extGFP(MTS)-PhaC-linker-MalE in the presence of pMCS69 exhibited PhaC activity, and produced particles that were not fluorescent. MalE was detected at low levels by ELISA. In the absence of pMCS69 the fusion protein formed GFP particles, and MalE was again detected by ELISA. Cells that produced extGFP(MTS)-PhaC(C319A)-linker-MalE did not form GFP particles in the presence or absence of pMCS69. MalE was weakly detectable. Cells that produced extGFP(MTS)-PhaC-linker-ZZ in a pMCS69 background formed GFP particles which exhibited a high level of IgG binding activity. In the absence of pMCS69 GFP particles were still formed; however, no IgG binding activity was observed. Cells that produced extGFP(MTS)-PhaC(C319A)-linker-ZZ did not form GFP particles in the presence or absence of pMCS69. IgG binding activity was present, but only at low levels.

As can be seen, the type of extension used in constructing GFP fusion proteins affects the formation of GFP particles in a variety of ways. There appears to be a link between the type of extension used and the functionality displayed; however, further research is required to explain this interaction.

1.8.6 Fluorescent Particle Formation Using Other Types of Fluorescent Protein

As mentioned above, the fluorescent proteins YFP, CFP, and HcRed were assessed for their ability to form protein particles. This investigation involved exploring the effect of the N-terminal extension AVTS on fluorescent protein particle formation, and incorporated PhaC(C319A) as the central domain, and [GB1]3 as the C-terminal functionality. Non-extended fusion proteins were also investigated. It was observed that all types of fusion protein formed protein particles independent of the presence of pMCS69, although there were differences in the intensity of fluorescence, and IgG binding ability.

Cells that produced YFP-PhaC(C319A)-linker-[GB1]3 formed protein particles that were white in colour, while those that produced extYFP-PhaC(C319A)-linker-[GB1]3 formed particles that were yellow/ orange in colour. Therefore, it appears that the AVTS extension of YFP enhances the colour and fluorescent intensity of YFP particles. In terms of IgG binding extYFP particles were capable of binding IgG, while YFP

particles were not. Cells that produced extCFP-PhaC(C319A)-linker-[GB1]3 formed particles that displayed greater fluorescence intensity than the non-extended particles, and were greenish in colour. Both non-extended and extended CFP particles displayed IgG binding capability with extCFP particles performing best. Cells that produced extHcR-PhaC(C319A)-linker-[GB1]3 formed particles that displayed greater fluorescent intensity than non-extended HcRed particles, and were pink to purple in colour. In terms of IgG binding capability, both types of particle exhibited equal performance.

As can be seen from these experiments, the N-terminal extension AVTS appears to encourage the formation of protein particles that display greater colour and fluorescent intensity. In combination with PhaC(C319A) and [GB1]3 it also produces protein particles that exhibit consistently high IgG binding capability.

1.8.7 Characterisation of GFP Particles

The physical properties of GFP particles were characterised in terms of size, culture conditions, temperature stability, and resistance to protein degrading agents. First, samples of GFP particles were examined under TEM. The particles were irregular in shape with dimensions of approximately 0.5 μm x 1.5 μm. Second, the incubation temperature was shown to be important in the production of fluorescent particles. Cultures harbouring the fusion protein extGFP-PhaC were incubated at 25 ˚C and 37 ˚C. Both cultures produced protein particles, although those extracted from the 37 ˚C culture were non-fluorescent. Third, under anaerobic cultivation conditions no fluorescence is observed. This is in agreement with other studies that showed oxygen is essential for GFP to fluoresce (Chalfie et al., 1994; Heim et al., 1994). Fourth, GFP particles comprised of extGFP-PhaC-linker-MalE or extGFP-PhaC(C319A)-linker-MalE were heat-treated at 50 ˚C, 60 ˚C, 70 ˚C, and 80 ˚C for 30 min. Visible fluorescence for both types of particle appeared to remain relatively unchanged between 50 ˚C and 70 ˚C. However, the 80 ˚C incubation abolished fluorescence. Finally, in order to verify the proteinaceous nature of GFP particles, samples were treated with Proteinase K and 8 M Urea. Such treatments resulted in the degradation (Proteinase K-treatment) and solubilisation (Urea-treatment) of the particles, as well as a loss of fluorescence.

GFP particles are a novel type of particle, and much research needs to be performed in order to explain the mechanism of their formation, and to optimise particle production and activity. However, Jahns et al. conducted a comprehensive investigation of GFP particles, and have laid the foundations of this study. As mentioned above, the focus of this thesis is to explore the potential for GFP particles to display active enzyme, and to characterise these particles in terms of activity, stability, and reusability. The results of such an investigation will extend current knowledge concerning GFP particles, as well as provide a novel immobilisation method for use in industry.

1.9 Study Aims and Objectives

As described above, the international market for enzymes is large, and methods to immobilise enzymes have been the focus of many studies. Immobilisation reduces the expense in using enzymes in industrial processes by increasing enzyme stability, facilitating reusability, and allowing different enzymes to be in close proximity in order to perform reactions that require more than one step of catalysis. However, current methods of immobilisation are expensive, laborious, and can lead to the production of toxic waste products. Some methods, for example enzyme-bearing PHA beads, are able to produce both the enzyme and support and perform immobilisation in a single step at relatively low cost and without toxic by-products. It is this concept of immobilisation that is sought for GFP particles. GFP particles have already been shown to self-assemble inside bacterial cells in a single step, as well as immobilise proteinaceous functions. If active enzymes can also be displayed on these particles the result will be a particle that can not only perform the required catalysis, but is inherently fluorescent without further modification. Such a particle could allow the design of protocols that capitalise on these qualities. Therefore, the main objective of this study is to produce fluorescent GFP particles that can immobilise active enzyme. Subsequent objectives will then be to assess the enzyme activity, stability, and reusability of these particles. The enzymes chosen for this study are: a modified α-amylase (Bla(-ss)) from *Bacillus licheniformis*; an *N*-acetyl-D-neuraminic acid aldolase (NanA) from *E. coli*; and an organophosphohydrolase (OpdA) from *Agrobacterium radiobacter*.

α-Amylase (EC 3.2.1.1) is one of the most extensively used enzymes in industry with applications in food processing, detergent manufacture, paper processing, textiles, and

potential uses in the pharmaceutical and fine chemical industries (Gupta, Gigras, Mohapatra, Goswami, & Chauhan, 2003; Rasiah & Rehm, 2009). α-Amylase hydrolyses starch by cleaving α-1,4 glycosidic bonds in a random fashion to yield smaller and more soluble compounds (Rodriguez, Alameda, Gallegos, Requena, & Lopez, 2006). They can be found in several sources including plants, animals, and microorganisms; however, α-amylases from microbial sources are the most widely used (Gupta et al., 2003). The secreted α-amylase from *Bacillus licheniformis* (BLA) is the most widely used in the starch industry primarily because of its thermostability (Lee, Oneda, Minoda, Tanaka, & Inouye, 2006). This thermostable α-amylase is a monomeric enzyme with a molecular mass of approximately 55 kDa (Hwang et al., 1997). The polypeptide chain folds into three distinct domains: Domain A, Domain B, and Domain C. Domain A forms a β/α 8-barrel structure; domain B is inserted between the third β-strand and third α-helix of Domain A; and domain C folds into an eight-stranded antiparallel β-barrel (Hwang et al., 1997). The active site is located in a cleft at the interface between domain A and B, and consists of a large number of charged groups, including the three amino acids Asp231, Glu261, and Asp328 which are essential for activity (Lee et al., 2006). In this study an optimised commercially-available BLA variant (Termamyl) was used that lacked the signal sequence required for secretion (Bla(-ss)) (Rasiah & Rehm, 2009).

N-acetyl-D-neuraminic acid aldolase (EC 4.1.3.3; NanA) is derived from *E. coli*. It is used in pathogenic strains such as *E. coli* K1 as part of a biosynthetic network to produce *N*-acetyl-D-neuraminic acid (Neu5Ac) (Ringenberg, Lichtensteiger, & Vimr, 2001). Neu5Ac is incorporated into cell surface glycolipids to produce a polysialic acid (PSA) capsule which is able to inhibit the host innate immune system, and mimic the PSA chains of the neural cell adhesion molecule (NCAM) (Ringenberg et al., 2001; Vimr, Steenbergen, & Cieslewicz, 1995). From a general point of view, Neu5Ac is the most ubiquitous member of a group of neuraminic acids called sialic acids (Maru, Ohnishi, Ohta, & Tsukada, 2002). It has an important role in biological recognition systems, and has been implicated as a receptor for the influenza virus, mycoplasma, and other important proteins (Glasgow & Hill, 1980; Maru et al., 2002; Suzuki et al., 1986). As Neu5Ac is involved in a variety of biological processes there has been increasing industrial demand for its use in therapeutic agents such as those for the treatment of influenza (Maru et al., 2002). However, its traditional preparation by extraction from

natural products and chemical synthesis result in poor yields and unsatisfactory stereoselectivity (Maru et al., 2002; P. Xu et al., 2007). The production of Neu5Ac by NanA biocatalysis has been widely reported. NanA catalyses the aldol condensation of *N*-acetyl-D-mannosamine (ManNAc) and pyruvate to yield Neu5Ac, although the reaction can work in the reverse direction (Maru et al., 2002). The enzyme is available from recombinant sources, therefore, allowing Neu5Ac to be produced in large quantities and at high-purity in a more economical fashion. The structure of NanA has been shown to be tetrameric where each subunit consists of an α/β-barrel domain and a C-terminal extension of three α-helices (Izard, Lawrence, Malby, Lilley, & Colman, 1994).

Organophosphohydrolases (OpdA), also known as phosphotriesterases, are enzymes that can be derived from a variety of bacterial sources, and are capable of hydrolysing and detoxifying organophosphate pesticides. Organophosphate pesticides are intentionally used in farming, particularly in the developing world, and account for approximately 200,000 deaths per year (Jeyaratnam, 1990). Their toxicity lies in their ability to inhibit acetylcholinesterase which is a key enzyme involved in nerve signal transmission in fish, birds, and mammals (Hsieh, Deng, Ger, & Tsai, 2001). Therefore, runoff from farming practices has the potential to contaminate waterways, and cause widespread harm. OpdA derived from *Agrobacterium radiobacter* has been shown to rapidly hydrolyse the phosphotriester bonds in various organophosphates, and has been considered for use in bioremediation and the treatment of organophosphate poisoning (Bird et al., 2008; Scott et al., 2008). The structure of this OpdA can be deduced from an extensively studied homologue from *Brevundimonas diminuta* (also known as *Pseudomonas diminuta*). The structure of this enzyme is dimeric when naturally isolated with each subunit containing a binuclear zinc centre that is situated at the C-terminal of an eight stranded α/β barrel ("TIM" barrel) (Benning, Shim, Raushel, & Holden, 2001).

The enzymes described above were chosen to demonstrate the potential versatility of GFP particles for immobilising and displaying active enzymes. They have significant differences in structure, mechanism of activity, and potential applications, and so will serve as broad representatives of all types of enzyme. If successful, the results of this study will add another function to GFP particles, and deepen current knowledge

concerning their physical properties. Furthermore, GFP particles will demonstrate themselves to be an alternative method of enzyme immobilisation with unique attributes.

Objectives:

Part I – Determine which type of GFP fusion protein leads to the formation of the most enzymatically active GFP particles.

- **Construct plasmids** – Construct plasmids encoding extGFP-PhaC(C319A)-linker-NanA and extGFP-NanA-linker-NanA fusion proteins from plasmids that encode extGFP-PhaC(C319A)-linker-ZZ and extGFP-NanA-linker-ZZ fusion proteins (Jahns *et al.*, 2011).
- **GFP particle production** - Transform plasmids into the production host *E. coli* BL21 (DE3), and produce GFP particles.
- **Assess enzyme activity** - Measure NanA activity of all types of GFP particle over 16 and 48 hours. Determine which type of GFP particle exhibits the greatest enzymatic activity.

Part II - Assess GFP particles displaying α-amylase, *N*-acetyl-D-neuraminic acid aldolase, and organophosphohydrolase for activity, stability, and reusability.

- **Construct plasmids –** Construct plasmids that encode extGFP-PhaC(C319A)-linker-BLA(-ss) and extGFP-PhaC(C319A)-linker-OpdA fusion proteins.
- **GFP particle production –** Transform plasmids into the production host *E. coli* BL21 (DE3), and produce GFP particles.
- **Assess enzyme activity –** Perform a time course assay of enzyme activity over 72 h for all types of enzyme-bearing GFP particle. Determine which length of incubation will generate a measurable signal that can be used to observe increases or decreases in enzyme activity due to stability and reusability studies.
- **Assess GFP particle stability –** Treat all enzyme-bearing GFP particles with a range of temperatures and pH, and conduct activity assays following treatment. Obtain fluorescent microscopy images of all particles after each treatment. In addition, measure enzyme activity of GFP particles after long-term storage at 4 ˚C, room temperature (22˚C-25˚C)(R.T.), and -80˚C. Obtain fluorescent microscopy images.
- **Assess enzyme activity over four cycles –** Test the reusability of enzyme-bearing GFP particles by performing activity assays with the same sample of particles for four cycles.

CHAPTER TWO: MATERIALS AND METHODS

Unless otherwise stated, reagents were purchased from Sigma-Aldrich, Ajax Finechem, and Merck.

2.1 Strains and Plasmids

The tables below list the strains and plasmids used in this study.

2.1.1 Strains

Table 1. Bacterial Strains used in this study.

Strain	Relevant Characteristics	Source or Reference
E. coli		
XL1 Blue	*rec*A1, *end*A1, *gyr*A96, *thi*-1, *hsd*R17 (r_{-k}, $m+_k$), *sup*E44, *rel*A1, *lac* [*F′*, *pro*AB, *lacI*q, *lacZ*ΔM15, *Tn10*(T_C^r)]	Stratagene
BL21 (DE3)	F^-; *ompT*; $hsdS_B$ ($r_B^- m_B^-$); *gal*; *dcm* λ (DE3)	Novagen

2.1.2 Plasmids

Table 2. Plasmids used in this study.

Plasmid Name	Characteristics	Reference
pGEM-T Easy	Ap^r, T7 & SP6 RNA Promoter, *lacZ*	Promega
pGEM-nanA	pGEM-T Easy vector containing *nanA* gene with external *Xho*I and *Bam*HI restriction sites.	David Hooks, pers. communication

pGEM-bla(-ss)	pGEM-T Easy vector containing *Xho*I/ *Bam*HI inserted *bla(-ss)* gene	This study
pET14b	Ap^r; T7 Promoter	Novagen
pET14b-ext(AVTS)gfp-phaC(C319A)-1inker-zz	pET14b vector containing a gene fusion of ext(AVTS)gfp-phaC(C319A)-1inker-zz	(Jahns et al., 2013)
pET14b-ext(AVTS)gfp-phaC(C319A)-1inker-nanA	pET14b-ext(AVTS)gfp-phaC(C319A)-1inker-zz derivative containing NanA fragment from pGEM-NanA at the 3′ end	This study
pET14b-ext(AVTS)gfp-phaC(C319A)-1inker-bla(-ss)	pET14b-ext(AVTS)gfp-phaC(C319A)-1inker-zz derivative containing bla(-ss) fragment from pGEM-bla(-ss) at the 3′ end	This study
pET14b-ext(AVTS)gfp-phaC(C319A)-1inker-opdA	pET14b-ext(AVTS)gfp-phaC(C319A)-1inker-zz derivative containing opdA fragment from pET14b-phaC-linker-opdA at the 3′ end	This study
pET14b-ext(AVTS)gfp-nanA-1inker-zz	pET14b-ext(AVTS)gfp-phaC-1inker-zz derivative containing *nanA* in the *Nde*I site	(Jahns et al., 2013)
pET14b-ext(AVTS)gfp-nanA-1inker-nanA	pET14b-ext(AVTS)gfp-nanA-1inker-zz derivative containing NanA fragment from pGEM-NanA at the 3′ end	This study

pET14b-bla(-ss)-phaC	pET14b vector containing bla(-ss)-phaC without the signal sequence encoding region	(Rasiah & Rehm, 2009)
pET14b-phaC-linker-opdA	pET14b vector containing a gene fusion of phaC-linker-opdA	(Blatchford et al., 2012)
pMCS69	Cm^r; T7 promoter; pBBR1MCS derivative containing genes *phaA* and *phaB* from *C. necator* (codon-optimised)	(Amara & Rehm, 2003)

2.2 Primers

The following primers were used in this study. All primers were synthesised by Integrated DNA Technologies (IDT), or were sourced from the Massey Genome Service.

Table 3. Primers used in this study

Primer Name	**Description/ Sequence 5′ to 3′**	**Reference**
Sequencing Primers		
T7	Forward primer	Massey Genome Service
	TAA TAC GAC TCA CTA TAG GG	
SP6	Reverse primer	Massey Genome Service
	ATT TAG GTG ACA CTA TAG	
BLA420f	Forward primer	This study
	ACT CAC TTT CAC TTC CCG GG	

BLA420r	Reverse primer	This study
	CCG GGA AGT GAA AGT GAG TC	
BLA1034f	Forward primer	This study
	TCA AGC CGC TGG CCT ACG C	
BLA1034r	Reverse primer	This study
	TGC GTA GGC CAG CGG CTT G	
pET14b-bla(-ss)-phaC PCR primers		
Bla(-ss)-Fwd	Forward primer	This study
	ATA ATA CTC GAG ATG GCC GCT AAC CTG AAC GG	
Bla(-ss)-Rev	Reverse primer	This study
	AAT AAT GGA TCC TTA GCC ACC ACC ACC ACC GC	

2.3 Liquid Media/ Supplements

The following is a list of the types of liquid media used in this study. The media were sterilised by autoclaving at 121 °C, 15 psi, for 20-25 min.

2.3.1 Luria-Bertani (LB) Medium

Liquid Luria-Bertani (LB) (Acumedia, USA) medium was prepared at a rate of 20 g per litre of R.O. water.

2.3.2 25% Glucose Solution

25% Glucose Solution was prepared at a rate of 25 g per 100 ml Milli-Q water.

2.4 Buffers and Miscellaneous Solutions

The following buffers and colour reagent were prepared for use in preparation of samples, or assays used to characterise the GFP particles.

2.4.1 Potassium phosphate buffer

500 mM Potassium phosphate buffer was made by first preparing 500 mM of K_2HPO_4 in Milli-Q water, and then decreasing the pH of this solution to 7.50 using 500 mM of KH_2PO_4. A 50 mM working solution of Potassium phosphate buffer was made by preparing a 1:10 dilution of the solution above.

2.4.2 20% (v/v) Ethanol in Potassium phosphate buffer

20% Ethanol (v/v) in Potassium phosphate buffer was prepared by diluting 96% Ethanol to the appropriate concentration using 50 mM Potassium phosphate buffer.

2.4.3 Glycerol in Potassium phosphate buffer

The 25%, 44%, 49.75%, 88%, and 99.5% (v/v) concentrations of Glycerol in Potassium phosphate buffer were prepared by diluting 99.5% Glycerol to the appropriate concentrations using 50 mM Potassium phosphate buffer.

2.4.4 Sodium phosphate buffer plus Sodium chloride (Sigma-Aldrich)

20 mM Sodium phosphate buffer plus 6.7 mM Sodium chloride was prepared by dissolving the appropriate amounts of each compound in Milli-Q water, and then adjusting the pH of the solution to 6.9 using Sodium hydroxide.

2.4.5 HEPES buffer

50 mM 4-(2-hydroxyethyl)-1-piperazineethanesulfonic acid (HEPES) buffer was prepared by dissolving the appropriate amount of HEPES in Milli-Q water, and then adjusting the pH of the solution to 8.00 using Sodium hydroxide.

2.4.6 20% (v/v) Methanol in HEPES buffer

50 mM HEPES buffer plus 20% (v/v) Methanol was prepared in the same manner as 50 mM HEPES buffer with the exception that the HEPES was first dissolved in the appropriate amount of Methanol and then brought to volume with Milli-Q water. The solution was then adjusted to pH 8.00 using Sodium hydroxide.

2.4.7 α-Amylase Colour Reagent Solution (Sigma-Aldrich)

α-Amylase Colour Reagent Solution was prepared for use in the Quantification of α-Amylase (Bla(-ss)) Activity Assay (2.20.2). It was made by mixing solutions of Sodium Potassium Tartrate and 3,5-Dinitrosalicylic Acid. These solutions were prepared as follows:

Sodium Potassium Tartrate:
Dissolved 36.0 g of Sodium Potassium Tartrate in 24.0 ml of 2 M Sodium hydroxide that had been heated to 50 ˚C-70 ˚C. The mixture was maintained at this temperature, and stirred with a magnetic stirrer, until the compound had completely dissolved.

3,5-Dinitrosalicylic Acid:
Dissolved 1.31 g of 3,5-Dinitrosalicylic Acid in 50 ml of Milli-Q water that had been previously heated to 50 ˚C-70 ˚C. The mixture was maintained at this temperature, and stirred with a magnetic stirrer, until the compound had completely dissolved. The solution was then adjusted to its final volume of 60 ml with Milli-Q water.

Once the two solutions above had been prepared they were slowly added to 36 ml of Milli-Q water that had been previously heated to 50 ˚C-70 ˚C. The solutions were added separately: first the Sodium Potassium Tartrate, and then the 3,5-Dinitrosalicylic Acid. The solutions were then mixed to yield the α-Amylase Colour Reagent Solution.

2.4.8 1.0% (w/v) Soluble Starch Solution (Sigma-Aldrich)

1.0% Soluble Starch Solution was prepared by mixing the appropriate amount of starch in 20 mM Sodium phosphate buffer plus 6.7 mM of Sodium chloride, pH 6.90. The

mixture was heated to its boiling point, and maintained at this temperature for 15 min with stirring on a magnetic stirrer. The solution was then allowed to cool to room temperature (22 ˚C- 25 ˚C) with stirring, and then adjusted to its original volume with 20 mM Sodium phosphate buffer plus 6.7 mM of Sodium chloride, pH 6.90. It is acknowledged that the solution should have been adjusted to its original volume using distilled water in order to maintain the concentration of Sodium phosphate and Sodium chloride at 20 mM and 6.7 mM, respectively. However, this error was consistent throughout all experiments using α-amylase. The final concentration of compounds in a solution made in this fashion has been calculated to be 1.0% (w/v) Soluble Starch in approximately 30 mM Sodium phosphate buffer plus 10 mM Sodium chloride, pH 6.90.

2.5 Antibiotics

Antibiotic solutions were prepared as described in Table 4. Generally, a 10 ml stock solution was made and then filtered through a 0.2-µm filter (Sartorius Stedim Biotech, Germany) using a 5-ml syringe (Terumo, Philippines). Aliquots (1 ml) were dispensed into 1.7-ml microcentrifuge tubes (Axygen, USA), and the tubes stored at -20 °C until used. All operations were performed in an Airpure Class II Biological Safety Cabinet.

Table 4. Antibiotic types, and working/ stock solution concentrations.

Antibiotic	**Stock Solution Concentration (mg/ml)**	**Working Solution Concentration (µg/ml)**
Ampicillin Sodium Salt (Applichem, Germany)	75 in Milli-Q water and 95%/ 96% Ethanol at a 1:1 ratio	75
Chloramphenicol	50 in 95% Ethanol	50

2.6 Stains

Stains were prepared as outlined in Table 5.

Table 5. Stain types, amounts used, solvents used, and final concentration of dissolved stain.

Name	**Amount**	**Solvent**	**Final Concentration of Stain**
Coomassie Brilliant Blue R250	200 mg	Acetic Acid (20 ml) (Scharlau, Spain) Ethanol/ Methanol (80 ml) Milli-Q Water (to 200 ml)	0.1%
Ethidium bromide	50 µl	R.O Water (500 ml)	0.01%
Nile Red	0.25 mg	DMSO (1 ml)	0.025%

2.7 SDS-PAGE Solutions

The following solutions were prepared as outlined in Table 6.

Table 6. SDS-PAGE solutions

Name	**Reagent**	**Solvent**
5x High Molecular Weight Running Buffer	3-Morpholinopropanesulfonic acid (MOPS), 250 mM (52 g) (Applichem, Germany) Tris buffer, 250 mM (30 g) (Pure Science, NZ) EDTA, 5 mM (2 g) SDS, 0.5% (5 g) (Promega, USA)	Milli-Q Water to 1 L

200x Reducing Agent	Sodium bisulfite, 1 M (5.305 g)	Milli-Q Water to 50 ml
3.5x Gel Buffer	bis-Tris, 1.25 M (65.3875 g)	Milli-Q Water to 250 ml Adjusted pH to 6.5-6.8 with HCl
5x Loading buffer (Laemelli Buffer)	SDS (1.0 g) Glycerol (2.0 g) Bromophenol blue (0.005 g)	Tris solution, 0.5 M adjusted to pH 6.8 with HCl (4 ml) Milli-Q Water to 10 ml
40% (w/v) Ammonium persulphate (APS)	APS (>98%) (0.4 g)	Milli-Q Water to 1 ml
Methanol-based De-stain		Methanol 660 ml Acetic Acid 200 ml Milli-Q water 1140 ml
Ethanol-based De-stain		Ethanol 600 ml Acetic Acid 200 ml Milli-Q water 1200 ml

2.8 Miscellaneous Solutions

The following solutions were prepared as outlined in Table 7.

Table 7. Miscellaneous Solutions

Name	**Reagents**	**Solvent**
10x TBE buffer	Tris, 450mM (109.06g) Boric Acid, 450mM (55.65g) EDTA, 22.5mM (16.75g)	Milli-Q water to 2L
TE Buffer	Tris-HCl, 10mM (0.121g), pH 7.5 (Fisher Scientific, UK) EDTA, 1mM (0.037g), pH 8.0	To 100ml with Milli-Q water Autoclave

2.9 Solid Media

To prepare solid media, 10 g of Luria-Bertani powder and 8 g of Bacteriological Agar (Acumedia, USA) were dissolved in 500 ml of R.O. water. The solution was then autoclaved at 121 °C, 15 psi, for 20 min. Antibiotics, if required, were added at a 1:1000 ratio, once the molten agar had cooled to an appropriate temperature. The molten agar was poured into petri dishes (Labserv, Thermofisher Scientific), allowed to set (approximately 30 min), and then stored at 4 ˚C.

2.9.1 X-gal Medium

Medium containing 5-bromo-4-chloro-indolyl-β-D-galactopyranoside (X-gal) was prepared by spreading 40 µl each of 0.1 M Isopropyl β-D-1-thiogalactopyranoside (IPTG) (Gold Biotechnology, USA) and 20 mg/ml X-gal (Applichem, Germany) onto sterile LB-Agar plates (containing 50 µg/ml Ampicillin). The plates were then allowed to dry- approximately 30 min. IPTG solution was prepared in Milli-Q water, while X-gal was prepared in Dimethyl sulphoxide (DMSO). Preparation was performed in an Airpure Class II Biological Safety Cabinet.

2.10 Liquid Cultivation Conditions

Liquid cultures of bacterial strains were performed in Erlenmeyer flasks, and were incubated at 37 ˚C. Cultures were incubated under aerobic conditions, and agitated on a Thermoline Orbital Shaker Incubator TLM510 (Thermoline Scientific, Australia) set at 200-250 rpm. The ratio of liquid medium to flask volume was 1:5 in order to maximise aeration. Cultivation of bacterial strains was performed in liquid LB medium containing the appropriate antibiotics and supplements, depending on the purpose.

2.10.1 PHA Bead Production Conditions

PHA beads that displayed the enzymes under investigation in this study were to serve as positive controls. Previous studies have shown that functional enzymes can be displayed on PHA beads (Blatchford et al., 2012; Hooks, Blatchford, & Rehm, 2013; Peters & Rehm, 2006; Rasiah & Rehm, 2009), and so they would be a useful benchmark with

which to compare the enzyme activity of the GFP particles. *E. coli* BL21 (DE3) strains harbouring recombinant pET14b plasmids and pMCS69 plasmids that facilitated the formation of functionalised PHA beads were created during the above studies, and PHA beads were produced for this study using the same methodology. Briefly, 1 L of liquid LB media containing 75 µg/ml Ampicillin, 50 µg/ml Chloramphenicol, and 1% (v/v) Glucose was inoculated with a 1% (v/v) inoculum from a 20 ml overnight liquid culture. Inoculated cultures were incubated at 37 ˚C, under aerobic conditions, on a TR/ Novotron shaker (INFORS HT, Switzerland) set to 200 rpm, until OD_{600} was 0.4-0.6 (approximately 4-6 h). At this point the cultures were induced by the addition of IPTG- to a final concentration of 1 mM- and then incubated at 25 ˚C for 48 h under aerobic conditions on a Lab-Line Orbit Shaker (Labline Instruments Inc., USA) set at 200 rpm.

2.10.2 GFP Particle Production Conditions

Recombinant pET14b plasmids were transformed (2.14) into *E. coli* BL21 (DE3) cells that lacked the pMCS69 plasmid. This ensured that PHA was not incorporated into the GFP particles. Particle production was performed in the same manner as for PHA beads, with the exception that 50 µg/ml Chloramphenicol was excluded, and for GFP particles produced previously (Jahns et al., 2013)

2.11 Solid Media Cultivation Conditions

Bacterial cultures were inoculated onto solid agar media in order to screen and store different strains. Solid agar media was prepared as described above (2.9). In general, LB/Agar plates were inoculated with approximately 20 µl of bacterial cells from 20 ml overnight liquid cultures, and then streaked and allowed to dry. However, if cells were transferred from one LB/ Agar plate to another, a portion of an isolated colony from the donor plate was simply streaked onto another plate. All inoculated plates were incubated at 37 ˚C, under aerobic conditions, for 18-24 h, in an incubator (Model 3166, Forma Scientific Inc., USA).

2.11.1 Antibiotic Selection

For the purposes of antibiotic selection and storage, bacterial strains were inoculated on to LB/Agar plates containing the appropriate antibiotics, and incubated at 37 ˚C under aerobic conditions, for 18-24 h.

2.11.2 Blue/ White Selection

Blue/ White selection was used to determine a successful ligation of blunt-ended PCR products that had been A-tailed (2.15.6) into the pGEM-T Easy vector (2.15.7). Briefly, A-tailed PCR products were ligated into pGEM-T Easy vectors and then transformed into competent *E. coli* XL1-Blue cells. These cells were then spread-plated onto LB/Agar plates (containing 50 µg/ml Ampicillin) that previously had a mixture of X-gal and IPTG spread and dried onto their surfaces (2.9.1). The plates were then incubated at 37 ˚C, under aerobic conditions, for 18-24 h. PCR products that are successfully ligated into the pGEM-T Easy vector disrupt the LacZ operon, thereby disrupting the production of β-galactosidase (Promega, 2010). Cells that do not produce β-galactosidase cannot breakdown the X-Gal that was spread on to the surface of the LB/Agar plates and, therefore, produce white colonies. Cells that produce β-galactosidase form blue colonies. White colonies were selected and spread onto fresh LB/Agar plates containing 75 µg/ml Ampicillin, and re-incubated. Correct insertion of PCR products was confirmed by restriction digest and DNA sequencing.

2.12 Long-term Storage and Revival of Bacterial Strains

Viable recombinant *E. coli* strain stocks were made using the following procedure. First, the *E. coli* strains were inoculated into 20 ml of liquid LB media, containing the appropriate antibiotics, in 100-ml Erlenmeyer flasks. The flasks were then incubated at 37 °C, under aerobic conditions, in a Thermoline Orbital Shaker Incubator TLM510 set at 200-250 rpm, for 18-24 h. Second, 20 µl of DMSO was added to 1.8-ml CryoTube™ Vials (Nunc™, Denmark), after which 980 µl of the overnight culture was also added. This resulted in a final concentration of 2% DMSO. The vials were mixed by inversion and the strains stored at -80 °C in a Revco Ultima II -80°C Freezer ULT2586-9-W38

(Kendro Laboratory Products, USA). All operations were performed in an Airpure Class II Biological Safety Cabinet.

2.12.1 Strain Revival

Revival of frozen recombinant *E. coli* strains was achieved by pipetting approximately 20 µl of partially defrosted cell stocks into 20 ml of liquid LB media containing the appropriate antibiotics. The cultures were then incubated at 37 °C, under aerobic conditions, in a Thermoline Orbital Shaker Incubator TLM510 set at 200-250 rpm, for 18-24 h.

2.13 Preparation of Competent *E. coli* Cells

Competent *E. coli* cells for use in transformation were prepared using protocols devised by Chung *et al* (Chung, Niemela, & Miller, 1989) and Hanahan (Hanahan, 1983).

Chung *et al.*:

50 ml of liquid LB media in 250-ml Erlenmeyer flasks were inoculated with 500 µl of overnight culture, and then incubated at 37 °C, under aerobic conditions, on a Thermoline Orbital Shaker Incubator TLM510 set at 200-250 rpm. Once OD_{600} had reached 0.3-0.4 the culture was centrifuged at 1000 x g for 10 min at 4 °C in a Heraeus Multifuge 1 S-R centrifuge (Kendro Laboratory Products, Germany). The supernatant was removed and the cell pellet resuspended in 5 ml of Transformation and Storage Solution (TSS). The suspension was then split into 200 µl aliquots in sterile 1.7-ml microcentrifuge tubes which were then flash frozen in liquid nitrogen. The frozen tubes were stored at -80 °C until required.

Transformation and Storage Solution

Polyethyleneglycol 8000 (PEG 8000)	(10% w/v)
DMSO	(5% v/v)
$MgCl_2$	(20-50 mM)
Liquid LB Medium	(to 25 ml)

Adjust pH to 6.5 using Sodium hydroxide.

Add DMSO after adjusting the pH and filter sterilisation using a 0.2-µm syringe filter in an Airpure Class II Biological Safety Cabinet.

Hanahan:

50 ml of liquid LB media in 250-ml Erlenmeyer flasks were inoculated with 500 µl of overnight culture, and then incubated at 37 °C, under aerobic conditions, on a Thermoline Orbital Shaker Incubator TLM510 set at 200-250 rpm. Once OD_{600} reached 0.3-0.4 the culture was incubated for 10 min on ice. Following incubation, the culture was centrifuged at 4000 rpm for 15 min at 4 ˚C in a Heraeus Multifuge 1 S-R centrifuge, the supernatant removed, and the cell pellet resuspended in 18 ml RF1 solution. The suspension was then incubated on ice for 30 min. Following incubation, the suspension was centrifuged under the same conditions as described above, the supernatant removed, and the cell pellet resuspended in 4 ml RF2 solution. Aliquots of 200 µl were then dispensed into sterile 1.7-ml microcentrifuge tubes (Axygen, USA), and flash frozen in liquid nitrogen. The cells were then stored at -80 ˚C until required.

RF1 solution:

RbCl	100 mM
$MnCl_2$	50 mM
Potassium acetate	30 mM
$CaCl_2x6H_2O$	10 mM

Adjust pH to 5.8 with acetic acid, and filter sterilise.

RF2 solution:

RbCl	10 mM
MOPS	10 mM
$CaCl_2x6H_2O$	75 mM
Glycerol	15% (v/v)

Adjust pH to 5.8 with Sodium hydroxide, and filter sterilise.

2.14 Transformation of Recombinant Plasmids into *E. coli*

To transform recombinant plasmids into competent *E. coli* cells, 40ng of plasmid DNA, or the entirety of a ligation mixture, was pipetted on to the surface of frozen 200 µl aliquots of competent cells. The cells were then allowed to thaw on ice for 1h. This allows the DNA to be adsorbed at the surface of the cells. After the 1h incubation, the plasmid/ competent cell samples were incubated at 42 °C for 90 s in a Digital Dry Bath (Labnet International Inc., USA) to allow the uptake of the DNA by the cells. The samples were then incubated on ice for a further 5 min. Next, 800 µl of liquid LB media was added to all samples which were then incubated at 37 °C for 1h in an incubator (Model 3166) to allow regeneration of cells and expression of plasmid-encoded antibiotic resistance. At the end of this incubation the samples were centrifuged at 16000 x g for 3 min at room temperature (~22 ˚C- 25 ˚C) in a Heraeus Pico 17 Centrifuge (Thermo Scientific, Germany) to pellet the cells, and the supernatant was removed. The cells were then resuspended in 100 µl of liquid LB media, and 50 µl of this was spread-plated onto LB/Agar plates containing the appropriate antibiotics. The plates were allowed to dry- approximately 30 min- and were then incubated at 37 °C, under aerobic conditions, for 18-24 h.

2.15 Cloning Methodology

2.15.1 Plasmid Isolation and Determination of DNA Concentration

2.15.1.1 High Pure Plasmid Isolation Kit (Roche)

Plasmid isolation was achieved using the High Pure Plasmid Isolation Kit (Roche, Germany) according the manufacturer's instructions.

2.15.1.2 DNA Clean and Concentrator Kit (Zymo Research)

When plasmid isolations were significantly contaminated with protein or RNA they were cleaned and concentrated using the DNA Clean and Concentrator Kit (Zymo Research, USA) according to the manufacturer's instructions.

2.15.1.3 Determination of Plasmid DNA Concentration

To determine the concentration of plasmid DNA one of two techniques were used. First, 2 µl samples were measured using a NanoDrop™ 1000 Spectrophotometer and NanoDrop 1000 v. 3.6.0 software (Thermo Fisher Scientific Inc., USA) according to the manufacturer's instructions. The purity of plasmid samples was quantified by calculating the ratio of sample absorbance when measured using two different wavelengths- 260nm:280nm and 260nm:230nm. The 260nm:280nm ratio was used to determine the purity of DNA and RNA where a ratio of ~1.8 indicates "pure" DNA. The 260nm:230nm ratio was used as a secondary measure of DNA purity against co-purified contaminants, and a ratio of ~2.0 was desired. Second, a Qubit™ fluorometer (Invitrogen, USA) was used alongside the Quant-iT DNA BR kit (Invitrogen, USA) according to the manufacturer's instructions.

2.15.2 DNA Restriction Digests

Plasmid DNA was hydrolysed with restriction endonucleases for the purposes of cloning and analysis of the constituent fragments. The endonucleases used in this study were *Bam*HI and *Xho*I, and were purchased from Roche, Promega, and New England Biolabs. The enzymes were used according to the manufacturer's instructions. A typical 20 µl restriction digest would contain the following reagents: 260 ng plasmid DNA; 0.2 µl 100x Purified Bovine serum albumin (BSA) (New England Biolabs Inc., USA); 2 µl 10x endonuclease buffer (NE Buffer 3, New England Biolabs Inc., USA) ; 0.5 µl *Bam*HI (5 units); 0.5 µl *Xho*I (10 units); and Milli-Q water to 20 µl.

2.15.3 Agarose Gel Electrophoresis (AGE)

DNA fragments produced by restriction digest were separated by Agarose Gel Electrophoresis (AGE) using a horizontal set-up. Digests were mixed with 6x concentrated DNA Loading Dye, which also stopped the digest reaction, and were then loaded into the wells of 1% Agarose (Hydragene, China/ USA) gels. A λ/ *Pst*I DNA ladder standard was also loaded. Electrophoresis was conducted in 1x TBE buffer at 100-120 V, 500 mA, for 45-60min, depending on the size of the electrophoresis chamber. Gels that were to be used for screening were stained for at least 20 min in Ethidium bromide solution, and destained for 5 min in R.O. water. Visualisation of

screening gels was performed by exposing the gels to UV using a GEL-DOC 2000 (Bio-Rad Laboratories Inc., USA). In order to visualise DNA fragments for the purposes of cloning, SYBR Safe DNA gel stain (Invitrogen) was added to molten agarose at a 1:10,000 ratio, and the agarose allowed to set. Electrophoresis was performed as described above, and the DNA fragments visualised using a Safe Imager™ 2.0 Blue-Light Transilluminator (Invitrogen).

6x DNA Loading Dye:

Tris-HCl (Fisher Scientific, UK)	60 mM
EDTA	60 mM
Glycerol	60% (v/v)
Orange G	0.2% (w/v)
Xylen Cyanol FF	0.05% (w/v)

λ/ *Pst*I DNA Ladder Standard

The λ/ *Pst*I DNA Ladder Standard consisted of λ-DNA (Invitrogen) that was digested with *Pst*I restriction endonuclease. This process yielded DNA fragments of different sizes as outlined in the table below (Table 8). After digestion, the DNA was mixed with 6x DNA Loading Dye, and the mixture stored at -20 ˚C.

Table 8. λ/ *Pst*I DNA Ladder Standard

Enzyme	DNA fragment size (bp)
*Pst*I	11501, 5077, 4749, 4749, 2838, 2556, 2443, 2140, 1986, 1700, 1159, 1093, 805, 514, 468, 448, 339, 264, 247

2.15.4 Agarose Gel DNA Extraction

DNA was extracted from agarose gel slices using Zymoclean™ Gel DNA Recovery Kit (Zymo Research, USA), and illustra™ GFX™ PCR DNA and Gel Band Purification Kit (GE Healthcare UK Ltd., UK) according to the manufacturer's instructions.

2.15.5 Polymerase Chain Reaction

Polymerase Chain Reaction (PCR) was used to amplify fragments of interest to be used in cloning. PCR was performed using Platinum® *Pfx* DNA Polymerase (Invitrogen), and the PCR reaction performed according to the manufacturer's instructions. Reagent volumes were doubled for use in a 100 µl reaction. With the exception of DMSO, primers, and template DNA, all reagents were manufactured by Invitrogen. The following is a representative PCR mixture for one reaction:

10x *Pfx* Reaction Buffer	20.0 µl
$MgSO_4$ (50 mM)	2.0 µl
DMSO	5.0 µl
Primer 1 (10 µM)	3.0 µl
Primer 2 (10 µM)	3.0 µl
dNTPs (10 mM of each)	3.0 µl
Template DNA	10 pg-200 ng
Pfx-DNA polymerase (2.5 U/µl)	0.8 µl
Autoclaved Milli-Q water	To 100 µl

PCR was performed in a Biometra T-personal Combi (biomedizinische Analytik, Germany) PCR Machine. Typical reaction conditions were as follows:

1. Initial Denature	94 ˚C for 5 min
2. Denature	94 ˚C for 15 s
3. Anneal	At a temperature midway between the primer melting points for 30 s
4. Extend	68˚C for 60 s per 1 kb of DNA

Steps 2 to 4 of the above conditions were repeated for 30 cycles after which the reaction mixtures were kept at 10 ˚C until used in subsequent processing.

2.15.6 DNA A-tailing

Blunt-ended PCR products were A-tailed in order to ligate them into the intermediate pGEM-T Easy vector system (Promega, USA). A-tailing involves extending the PCR products with a chain of dATPs at both the 5′ and 3′ ends which facilitate bonding with the chain of dTTPs present at the 5′ and 3′ ends of the pGEM-T Easy vector. A-tailing reactions were performed in a Biometra T-personal Combi PCR Machine at 70 ˚C for 30 min. With the exception of the PCR product, all reagents were manufactured by Invitrogen. A-tailing reaction mixtures consisted of the following:

dATP (0.2 mM)	1µl
Taq DNA polymerase	1µl
10x *Taq* Reaction Buffer (without $MgCl_2$)	1µl
$MgCl_2$	1µl
PCR product	6µl

2.15.7 pGEM-T Easy Ligation

Once A-tailed PCR products had been prepared they were then used in a ligation reaction with the pGEM-T Easy vector (Promega, USA). With the exception of the A-tailed PCR product, all reagents were manufactured by Promega. The ligation reaction was prepared as follows:

2x pGEM-T Easy Ligase Buffer	5 µl
pGEM-T Easy vector	0.5 µl
pGEM-T Easy ligase	1 µl
A-tailed PCR product	3.5 µl

Once the ligation reactions had been prepared the tubes were suspended in floats and incubated at 4 ˚C, overnight, in a water bath.

2.15.8 DNA Ligation using T4 DNA Ligase

DNA fragments produced by DNA restriction digests were ligated together using T4 DNA ligase (Invitrogen), according to the manufacturer's instructions. An insert to vector ratio of 6:1 was used to maximise the efficiency of the ligation. Once the ligation reactions were prepared the tubes were suspended in floats and incubated at 4 ˚C, overnight, in a water bath.

2.15.9 DNA Sequencing

DNA sequencing of recombinant plasmids was performed by the Massey Genome Service using a capillary ABI3730 Genetic Analyzer (Applied Biosystems Inc., USA). DNA sequencing reactions were prepared in sterile 0.2 ml thin-walled PCR tubes that contained 450 ng of plasmid DNA, 670 nM of sequencing primers, and autoclaved Milli-Q water in a total reaction volume of 15 µl.

2.16 PHA Bead and GFP Particle Extraction

PHA beads and GFP particles were harvested from the recombinant *E. coli* BL21(DE3) cells using mechanical cell disruption and ultracentrifugation using glycerol gradients as described previously (Jahns et al., 2008). The process and differences between PHA bead and GFP particle isolation are outlined below.

2.16.1 Bacterial Cell Harvesting

In order to collect biomass, *E. coli* BL21(DE3) production cultures were poured into 400-ml centrifuge bottles (Nalgene, USA), and centrifuged at 6000 x g, 4 ˚C, for 20 min in a Sorvall RC5C centrifuge (Dupont, USA). The supernatants were removed and the cell pellets resuspended in 15 ml of 50 mM Potassium phosphate buffer, pH 7.5. Next, the suspensions were transferred to 50-ml Cellstar® tubes (Grenier Bio-one, Germany), centrifuged at 6000 rpm for 20 min in a Heraeus Multifuge 1 S-R centrifuge, and the supernatants removed.

2.16.2 Cell disruption

Once biomass had been collected the cells were resuspended in 1 ml of 10 mg/ml Lysozyme (from chicken egg white), 1ml of 1 mg/ml DNase I (from bovine pancreas), and brought to a final volume of 5 ml with 50 mM Potassium phosphate buffer, pH 7.50. Cell disruption was performed using a Z Plus 1.1 kW Benchtop Cell Disrupter (Constant Cell Disruption Systems, UK). Cells suspensions were subjected to 2 passes of mechanical cell disruption using a pressure of 20 kpsi. The resulting cell lysate was then centrifuged at 8000 x g, 4 ˚C, for 20 min in a Heraeus Multifuge 1 S-R centrifuge. Following centrifugation, the pellets were resuspended in 3 ml of 50 mM Potassium phosphate buffer, pH 7.50.

2.16.3 Separation of PHA Beads and GFP Particles

PHA beads and GFP particles were separated from cellular debris in the lysates using two types of glycerol gradient. PHA beads were separated using a 44% Glycerol/ 88% Glycerol (2.4.3) gradient, while GFP particles were separated using a 49.75% Glycerol/ 99.5% Glycerol (2.4.3) gradient. The glycerol gradients were prepared in 12 ml polypropylene tubes (Kendro Laboratory Products, USA) as shown in Figure 4.
Once the samples had been loaded on top of their glycerol gradients the polypropylene tubes were transferred to metal ultracentrifuge buckets, and balanced with 50 mM Potassium phosphate buffer, pH 7.50. The samples were then centrifuged on either a Sorvall WX Ultra Series Centrifuge, WX Ultra 80 (Thermofisher Scientific, USA/ Germany), or a Sorvall® OTD-Combi Ultracentrifuge (DuPont, USA), at 35000 rpm, 10 °C, for 2 h. After centrifugation a layer of PHA beads/ GFP particles could be observed at the interface between the higher and lower concentrations of glycerol.

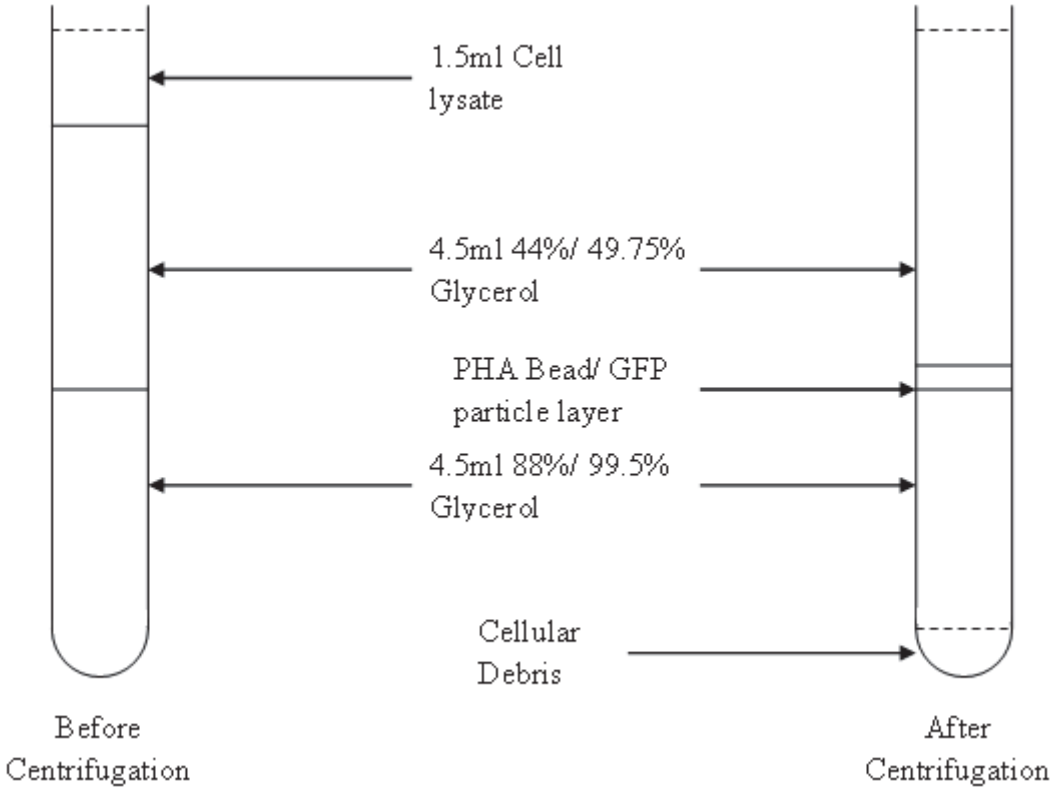

Figure 4. Diagram of glycerol gradient for PHA bead/ GFP particle separation before and after centrifugation.

The PHA bead/ GFP particle layers were harvested from the polypropylene tubes, and resuspended up to a final volume of 40 ml with 50 mM Potassium phosphate buffer, pH 7.50, in 50-ml Cellstar® tubes. The tubes were then centrifuged at 8000 x g, 4 °C, for 20 min in a Heraeus Multifuge 1 S-R centrifuge. The supernatant was removed from the tubes, and the PHA bead/ GFP particle pellets resuspended in either 20% Ethanol in 50 mM Potassium phosphate buffer (2.4.2), or 25% Glycerol in 50 mM Potassium phosphate buffer (2.4.3). The final concentration of PHA bead/ GFP particle slurries was 0.2 g/ml. Aliquots of PHA beads/ GFP particles suspended in 20% Ethanol in 50 mM Potassium phosphate buffer were stored at 4 °C and room temperature (22 °C-25 °C)(R.T.), while PHA beads/ GFP particles suspended in 25% Glycerol in 50 mM Potassium phosphate buffer were stored at -80 °C. Samples stored at 4 °C were used to conduct testing, while samples stored at room temperature and -80 °C were used to assess PHA bead/ GFP particle stability at these storage temperatures.

2.17 Methods for visualising PHA Beads and GFP particles

2.17.1 Fluorescent Microscopy

Images of recombinant *E.coli* BL21 (DE3) cells containing GFP particles, and GFP particles post-extraction, were obtained using an Olympus BX51 Fluorescent Light Microscope (Olympus Optical Co. Ltd., Japan). Images were captured under 100x and 1000x magnification using Filter 3 (U-MWIBA2 Blue excitation (460nm-490nm); Green Emission (510nm-550nm)), an Optronics camera (Optronics, USA), and MagnaFire^{TM} 2.1C Application software (Optronics, USA).

2.17.2 Nile Red Staining (Spiekermann, Rehm, Kalscheuer, Baumeister, & Steinbuchel, 1999)

In order to visualise PHA beads both within recombinant *E. coli* BL21 (DE3) cells and after extraction, cell suspensions and PHA bead extracts were stained with Nile Red. Samples were centrifuged at 16000 x g for 3 min in a Heraeus Pico 17 Centrifuge, the supernatants discarded, and 10 µl of Nile Red (0.25 mg/ml) was then added to the remaining pellets. The stained pellets were resuspended in 1 ml of 50 mM Potassium phosphate buffer, pH 7.50, and incubated in the dark, at room temperature (22 ˚C- 25 ˚C) (R.T.), for 5 min. After incubation, the samples were centrifuged again at 16000 x g for 3 min, the supernatants removed, and the remaining pellets resuspended in 1 ml of 50 mM Potassium phosphate buffer, pH 7.5. The suspensions were then incubated again in the dark, at room temperature (22 ˚C- 25 °C)(R.T.), for 5 min. To prepare samples for microscopy, 5 µl of each sample was pipetted on to a glass slide, covered with a coverslip, and the slides placed in a slide-book to protect them from light. Images were then obtained using an Olympus BX51 Fluorescent Light Microscope (Olympus Optical Co. Ltd., Japan), under 1000x magnification, using Filter 4 (U-MWIG2 Green excitation (520nm-550nm); Red-shifted emission (580nm-Infra Red)). Images were captured using an Optronics camera (Optronics, USA), and MagnaFire^{TM} 2.1C Application software (Optronics, USA).

2.18 Methods for Fusion Protein Analysis

2.18.1 Sodium dodecylsulfate Polyacrylamide Gel Electrophoresis (SDS-PAGE) (Laemmli, 1970)

Fusion proteins associated with PHA beads and GFP particles were analysed using Sodium dodecylsulfate Polyacrylamide Gel Electrophoresis (SDS-PAGE). This method was used to measure the size of fusion proteins, and to calculate the concentration of fusion protein in a PHA bead/ GFP particle slurry via densitometry.

2.18.1.1 Preparation of samples

To prepare PHA bead and GFP particle samples for SDS-PAGE, 20 µl of sample was added to 980 µl of 50 mM Potassium phosphate buffer, pH 7.50. The sample was vortexed to mix, and then centrifuged at 16000 x g for 5 min in a Heraeus Pico 17 Centrifuge. The supernatants were discarded, and the PHA bead/ GFP particle pellets resuspended in 50 mM Potassium phosphate buffer, pH 7.50, to a final volume of 200 µl to yield a 10x dilution. Dilutions of 20x and 40x were also prepared from the 10x dilution. 12 µl of each dilution was then pipetted into separate 1.7-ml microcentrifuge tubes. 3 µl of 5x SDS-PAGE Loading Buffer (2.7) and 1.5 µl of 1.0 M Dithiothreitol (DTT) was then added, and the samples mixed by pipette aspiration. Following mixing, the samples were heated at 95 °C for 1.5 min in a Digital Dry Bath. After heat treatment, the samples were loaded into the wells of a polyacrylamide gel.

2.18.1.2 Polyacrylamide Gel Preparation

The bis-Tris polyacrylamide gels used in this study had an acrylamide concentration of 8% (Resolving Gel) and 4% (Stacking Gel). The size of the fusion proteins investigated were 70 kDa and above, and so effective resolution and separation at this range was required. The preparation of an 8% polyacrylamide resolving gel consisted of the following:

3.5x bis-Tris Gel Buffer	2.9 ml
30% bis-Acrylamide	2.650 ml
Milli-Q water	4.35 ml
40% Ammonium persulphate (APS)	17 µl
Tetramethyl ethylenediamine (TEMED)	19 µl

The 3.5x bis-Tris buffer (2.7), 30% bis-Acrylamide (Bio-Rad Laboratories Inc., China), and Milli-Q water were mixed first, and then the APS and TEMED (Merck, Germany) were added to initiate polymerisation. After all reagents had been mixed the resolving gel was pipetted into pre-constructed Mini PROTEAN® 3 System glass spacer plates (1 mm) (Bio-Rad Laboratories Inc., USA) to a depth of ~2 cm below the edge of the front glass plate. The gel was then covered by isopropanol, and left to set, at a slight angle, for 45-60 min. Once the resolving gel had set, the isopropanol was removed and a stacking gel was poured on top of the resolving gel. The stacking gel consisted of the following reagents:

3.5x bis-Tris Gel Buffer	2.9 ml
30% bis-Acrylamide	1.5 ml
Milli-Q water	5.6 ml
40% Ammonium persulphate (APS)	17 µl
Tetramethyl ethylenediamine (TEMED)	19 µl

Again, the 3.5x bis-Tris buffer, 30% bis-Acrylamide, and Milli-Q water were mixed first and then the APS and TEMED were added to initiate polymerisation. After all reagents had been mixed, the stacking gel was poured on top of the resolving gel to the edge of the front plate, and a gel comb inserted into it. The stacking gel was then left to set, at a slight angle, for 45-60 min.

2.18.1.3 Electrophoresis

Once the polyacrylamide gel had set it was inserted into gel frame, opposite a gel dam, and then placed into a Mini PROTEAN® 3 System SDS-PAGE chamber (Bio-Rad Laboratories, USA). The gap between the gel and the gel dam was filled with High Molecular Weight Running Buffer (2.7), and once it was established that the buffer was

not leaking from this gap more buffer was poured into the chamber to complete the electrical circuit. Before the Running Buffer was added to the chamber 200x Reducing Agent (2.7) was added to it at a 1:200 dilution. Once the gel and electrophoresis chamber were set up, the gel comb was removed from the gel, and samples were loaded into the wells- including the Mark 12™ Unstained Standard protein ladder (Invitrogen, USA). SDS-PAGE was conducted at a constant voltage of 150 V, 1000 mA, for 40-60 min.

2.18.1.4 Staining/ Destaining Polyacrylamide Gels

Polyacrylamide gels were stained with Coomassie Blue Stain (2.6). While a methanol based stain was generally used an ethanol based stain was also used. Gels were stained for at least 20 min, and then de-stained overnight. To de-stain gels, a de-stain solution containing the same alcohol as the stain was used. De-stain solutions were diluted two fold when de-staining overnight. Undiluted de-stain solution was used to complete de-staining when an overnight de-stain was not adequate.

2.18.2 Densitometry

Densitometry was used to calculate the concentration of fusion protein associated with PHA bead and GFP particle extractions. The Bradford assay (Bradford, 1976) was considered; however, inconsistent results were obtained, possibly due to the PHA beads and GFP particles themselves refracting light in unpredictable ways. High-quality computerised images of polyacrylamide gels were obtained using the GEL-DOC 2000 (Bio-Rad Laboratories Inc., USA) and Image Lab Software (Version 3.0 build 11, Bio-Rad Laboratories Inc., USA). The image was then analysed using the Analysis tools provided in Image Lab.

Lanes and Bands- This tool was used to detect the number of lanes and protein bands in a gel. It was also used to tighten parameters so that the analysis area only included that occupied by the protein bands of interest.

MW Analysis Tools- This tool was used to measure the molecular weight of significant bands. The molecular weights of bands present in the Mark 12™ protein ladder (Table

Nine) were previously entered into the program, and a standard curve was created by plotting molecular weight (kDa) of each band versus its relative front. The molecular weight of unknown bands could then be measured by comparison to the bands of the protein ladder to see where they would fit into the standard curve.

Table 9. Mark 12™ Unstained Standard protein ladder (Invitrogen, USA)

Constituent Protein	Molecular Weight (kDa)
Myosin	200
β-galactosidase	116.3
Phosphorylase b	97.4
BSA	66.3
Glutamic dehydrogenase	55.4
Lactate dehydrogenase	36.5
Carbonic anhydrase	31
Trypsin inhibitor	21.5
Lysozyme	14.4
Aprotinin	6
Insulin B chain	3.5
Insulin A chain	2.5

Quantity Tool- This tool was used to calculate the amount of protein present in specific bands. The bands produced by the BSA standards loaded onto the gels were used to generate a standard curve which plotted the relationship between the Absolute Quantity (μg) of protein loaded versus the band volume. The amount of protein present in the BSA standards was 6 μg, 3 μg, 1.5 μg, and 0.75 μg. The standard curve was used to calculate the amount of protein present in fusion protein bands by observing where the measured volume of the bands fell on the trend line. As the entirety of each sample of PHA bead/ GFP particle was loaded into the gels, the amount of protein calculated constituted the amount of fusion protein present in the 12 μl aliquots. The concentration of fusion protein in the original slurries was then obtained by calculating the concentration in the 12 μl aliquot (μg/μl); converting this value to mg/ml; and then multiplying by the dilution factor used to prepare the 12μl aliquot.

2.18.3 MALDI-TOF/MS (Shevchenko et al., 1996)

Fusion proteins of interest, identified by SDS-PAGE, were cut from polyacrylamide gels and examined by Matrix-assisted Laser Desorption/ Ionisation Time-of-Flight Mass Spectrometry (MALDI-TOF/MS). The MALDI-TOF/MS process was conducted by The Centre for Protein Research (University of Otago).

2.19 High Performance Liquid Chromatography (HPLC)

Neu5Ac quantitation was determined by High Performance Liquid Chromatography (HPLC) on a Dionex Ultimate 3000 System (Dionex Softron, Germany) using a Phenomenex Rezex RHM-Monosaccharide H^+ column (300 x 7.80 mm). The flow rate was 0.5 ml/min using a mobile phase of 6mM H_2SO_4. The column was maintained at 60 ˚C; the sample injection volume was 25 µl; and the UV detector was set at 205 nm. The software used was Chromeleon® Chromatography Management system v.6.80 (Dionex, USA).

2.20 Enzyme Activity Assay Protocols

2.20.1 Quantification of *N*-acetyl-D-neuraminic acid aldolase (NanA) Activity

N-acetyl-D-neuraminic acid aldolase (NanA) activity was quantified by measuring the amount of *N*-acetyl-D-neuraminic acid (Neu5Ac) produced by the enzyme from the condensation of Sodium pyruvate and *N*-acetyl-D-mannosamine (ManNAc). The protocol used to quantitate NanA activity was adapted from conditions described by Xu *et al*. (X. Xu et al., 2011).

$$\text{Pyruvate} + \text{ManNAc} \xleftrightarrow{\text{NanA}} \text{Neu5Ac}$$

Figure 5. Diagram detailing the production of Neu5Ac from the condensation of Pyruvate and ManNAc catalysed by NanA. Adapted from Xu et al (P. Xu et al., 2007)

2.20.1.1 General Quantification of Enzyme Activity Protocol (NanA)

Prior to testing, the beads/ particles were stored in 20% Ethanol in 50mM Potassium phosphate buffer which needed to be removed by a wash step prior to testing enzyme activity. Aliquots of PHA bead and GFP particle slurries containing 25 μg of fusion protein were mixed with 50 mM Potassium phosphate buffer, pH 7.50, to a total volume of ~1 ml. The samples were centrifuged at 16000 x g for 5 min in a Heraeus Pico 17 Centrifuge. The supernatant was then removed and the PHA bead/ GFP particle pellets resuspended in their original volume of 50 mM Potassium phosphate buffer, pH 7.50. A substrate solution consisting of 1.0 M Sodium pyruvate and 0.2 M ManNAc in 50 mM Potassium phosphate buffer, pH 7.50, was made, and aliquots of this solution were added to the PHA bead/ GFP particle samples to a final reaction volume of 500 μl. This made the final concentration of fusion protein in the samples to be 0.05 mg/ml per reaction. The samples were then mixed by vortex, and incubated at 50 °C on a Gyrotory Shaker (New Brunswick Scientific Company, USA) set at 200 rpm, under aerobic conditions. Following incubation, the samples were centrifuged at 16000 x g for 10 min in a Heraeus Pico 17 Centrifuge and the supernatants removed. Aliquots of the supernatants were then diluted and assessed by HPLC (2.19). All PHA bead/ GFP particle samples were assayed in triplicate.

2.20.2 Quantification of α-Amylase (Bla(-ss)) Activity

α-Amylase (Bla(-ss)) activity was quantified using a colorimetric assay that measured the amount of maltose liberated by the enzyme through the hydrolysis of starch. This method was adapted from previously described protocols (Sigma-Aldrich; Yamabhai et al., 2008).

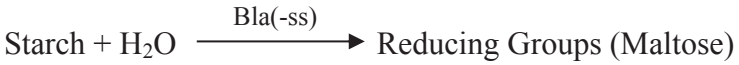

Figure 6. Diagram detailing the production of maltose from the hydrolysis of starch by Bla(-ss). (Sigma-Aldrich)

2.20.2.2 General Quantification of Enzyme Activity Protocol (Bla(-ss))

Aliquots of PHA bead and GFP particle slurries containing 50 µg of fusion protein were mixed with 20 mM Sodium phosphate buffer plus 6.7 mM of Sodium chloride, pH 6.90, to a total volume of ~1000 µl. The samples were centrifuged at 16000 x g for 5 min in a Heraeus Pico 17 Centrifuge, and the supernatants were then removed in order to extract the 20% Ethanol in 50mM Potassium phosphate buffer used for bead/ particle storage. The PHA bead/ GFP particle pellets were resuspended in their original volume of 20 mM Sodium phosphate buffer plus 6.7 mM Sodium chloride, pH 6.90. A 1.0% Soluble Starch solution was prepared as described above (2.4.8). Once the 1.0% Soluble Starch solution was prepared aliquots were dispensed into the PHA bead/ GFP particle tubes to a final volume of 1000 µl. This made the final concentration of fusion protein in the samples to be 0.05 mg/ml per reaction. Aliquots were also dispensed into tubes that did not contain PHA beads or GFP particles, and were to serve as blank controls. All samples were incubated at 25 °C, on a Lab-Line Orbit Shaker (Lab-Line Instruments Inc., USA), at 200 rpm, under aerobic conditions. Following incubation the samples were centrifuged at 16000 x g for 5 min in a Heraeus Pico 17 Centrifuge, and 500 µl of each supernatant was removed to separate glass Kimax tubes (16 x 125 mm, Kimble Glass Inc., Mexico). 500 µl of α-Amylase Colour Reagent Solution (2.4.7) was added, and the tubes mixed by swirling. The tubes were then heated for 15 min at 100 ˚C in a memmert OB 10 oil bath (memmert, Germany). After heating the tubes were placed on ice to cool to room temperature- approximately 3 min. Finally, the tubes were brought to a final volume of 6 ml with Milli-Q water and mixed by inversion. 1 ml of the mixture in each tube was pipetted into separate 2-ml cuvettes, and the absorbance measured at 540 nm using an Ultrospec 2000 spectrophotometer (Pharmacia Biotech, UK). All PHA bead/ GFP particle samples were assayed in triplicate.

2.20.3 Quantification of Organophosphohydrolase (OpdA) Activity

Organophosphohydrolase (OpdA) activity was quantified using a colorimetric assay that measured the amount of *para*-nitrophenol liberated by the enzyme through the hydrolysis of the substrate Methyl parathion. This method was adapted from previously described protocols (Blatchford et al., 2012; Dumas, Caldwell, Wild, & Raushel, 1989).

Figure 7. Diagram detailing the hydrolysis of methyl parathion by OpdA to *para*-nitrophenol and dimethyl phosphorothioic acid. Adapted from Gresham et al. (Gresham, Rosenbaum, Gaspari, Jackson, & Bird, 2010)

2.20.3.1 General Quantification of Enzyme Activity Protocol (OpdA)

Aliquots of PHA bead and GFP particle slurries containing 50 µg of fusion protein were mixed with 20% (v/v) Methanol in 50 mM HEPES Buffer, pH 8.00, to a total volume of ~1000 µl. The samples were then centrifuged at 16000 x g for 5 min in a Heraeus Pico 17 Centrifuge. As described above, the beads/ particles were suspended in 20% Ethanol in 50 mM Potassium phosphate buffer for storage which needed to be removed. The supernatant was removed and the PHA bead/ GFP particle pellets resuspended in their original volume of 20% (v/v) Methanol in 50 mM HEPES Buffer, pH 8.00. A stock solution consisting of 10 mM Methyl parathion was made by dissolving the appropriate amount of Methyl parathion crystals in 20% (v/v) Methanol in 50 mM HEPES Buffer, pH 8.00, that had been heated to 37 °C-45 °C to aid the dissolving process (the melting point of Methyl parathion is 35 ˚C-38 °C). A working solution of 200 µM Methyl parathion was made my diluting from the 10 mM Methyl parathion stock. Aliquots of the 200 µM Methyl parathion solution were added to the PHA bead/ GFP particle samples to a final reaction volume of 1000 µl. This made the final concentration of fusion protein in the samples to be 0.05 mg/ml. Aliquots were also dispensed into tubes that did not contain PHA beads or GFP particles, and were to serve as blank controls. All samples were incubated at 25 °C, on a Lab-Line Orbit Shaker set at 200 rpm, under aerobic conditions. Following incubation the samples were centrifuged at 16000 x g for 5 min in a Heraeus Pico 17 Centrifuge, and the supernatants removed. Absorbance measurements of the supernatants were then conducted using an Ultrospec 2000 spectrophotometer (Pharmacia Biotech, UK) set at 405nm. All PHA bead/ GFP particle samples were assayed in triplicate.

In order to prevent the loss of Methanol during the pre-incubation steps of the stability studies, samples were washed in 50 mM HEPES Buffer, pH 8.00 that lacked the 20% (v/v) Methanol, and then resuspended in their original volume of the same buffer. The

pre-incubation steps of the temperature and pH stability assays were then performed, and the activity of the OpdA enzyme displayed on the PHA beads/ GFP particles assessed as described above.

2.21 Enzyme Stability and Reusability Assay Protocols

2.21.1 Time Course Assessment of Enzyme Activity

To assess the level of enzyme activity over time, samples were incubated for 1 h, 2 h, 3 h, 4 h, 6 h, 12 h, 24 h, 48 h, and 72 h, and samples corresponding to each time point were removed when required. Reaction conditions described in The General Quantification of Enzyme Activity Protocol of the relevant enzyme were employed. All PHA bead/ GFP particle samples were assayed in triplicate.

2.21.2 Temperature Stability of PHA beads/ GFP Particles displaying Enzyme

To assess the temperature stability of enzyme-bearing PHA beads/ GFP particles, samples were suspended in the relevant reaction solvent and pre-incubated at 4 °C, 15 °C, 25 °C, 35 °C, 45 °C, 55 °C, 65 °C, 75 °C, 85 °C, and 95 °C for 10 min in a Digital Dry Bath (Labnet International Inc., USA). Enzyme activity was then assessed using the General Quantification of Enzyme Activity Protocol of the relevant enzyme. All PHA bead/ GFP particle samples were assayed in triplicate.

2.21.3 pH Stability of PHA beads/ GFP Particles displaying Enzyme

To assess the stability of enzyme-bearing PHA beads/ GFP particles at different pH, samples were pre-incubated for 10 min, at room temperature (22 ˚C- 25 ˚C)(R.T.), in the following 20 mM buffers: Potassium chloride (pH 2.00); Sodium citrate (pH 3.00); Sodium acetate (pH 4.00, 5.00 and 6.00); Tris-HCl (pH 7.00 and 8.00); Sodium tetraborate (pH 9.00 and 10.00); and Di-Sodium hydrogen orthophosphate (pH 11.00 and 12.00). After pH treatment, the samples were centrifuged at 16000 x g for 10 min in a Heraeus Pico 17 Centrifuge. The buffer was then removed, and the PHA bead/ GFP particle pellets resuspended in the relevant reaction solvent. Enzyme activity was then

assessed using the General Quantification of Enzyme Activity Protocol of the relevant enzyme. All PHA bead/ GFP particle samples were assayed in triplicate.

2.21.4 Reusability of GFP Particles displaying Enzyme

To assess the reusability of GFP Particles displaying enzyme, samples were prepared and assayed as described in the General Quantification of Enzyme Activity Protocol of the relevant enzyme. At the end of the incubation period, samples were centrifuged at 16000 x g for 5-10 min in a Heraeus Pico 17 Centrifuge, and the supernatant removed and analysed. The GFP particle pellets were then resuspended in fresh substrate solution as described in the relevant General Quantification of Enzyme Activity Protocol, and incubated again. This cycle was repeated four times. All types of GFP particle were assayed in triplicate.

2.21.5 Long-term Storage Condition Assay

To determine the effect of storage conditions on GFP particles, aliquots of each type of enzyme displaying GFP particle were stored at 4 ˚C, room temperature (22 ˚C- 25 ˚C) (R.T.), and -80 ˚C. Samples stored at 4 ˚C and room temperature were suspended in 20% Ethanol in 50 mM Potassium phosphate Buffer, while samples stored at -80 ˚C were suspended in 25% Glycerol in 50 mM Potassium phosphate Buffer (2.11.3). At the end of the storage period the samples were assayed using the General Quantification of Enzyme Activity Protocol of the relevant enzyme, and using the incubation periods used for the Temperature/pH stability and reusability assays. All types of PHA bead/ GFP particle were assayed in triplicate.

CHAPTER THREE: RESULTS

Due to ready availability, initial tests were conducted with GFP particles displaying the enzyme NanA. Three different types of GFP fusion protein containing NanA were constructed and then assessed for their ability to form GFP particles. The resultant particles were then assessed for their ability to exhibit NanA activity, as measured by *N*-acetyl-D-neuraminic acid (Neu5Ac) production. Within these fusion proteins NanA was situated as the central domain (GNLZ), as the C-terminus (GiCLN), and as a central domain/ C-terminus double fusion (GNLN). Strategies to produce these fusion proteins and assess them are described below.

3.1 Formation of enzyme-bearing GFP particles

Enzyme-bearing GFP particles were formed using the same principles first outlined by Jahns et al. (Jahns et al., 2013). In order to replicate the GFP particle formation observed in this study, two plasmids- namely, pET14b-ext(AVTS)gfp-phaC(C319A)-1inker-zz (pET14b-GiCLZ), and pET14b-ext(AVTS)gfp-nanA-1inker-zz (pET14b-GNLZ)- served as vectors into which genes for enzymes from this study could be inserted. It must be noted that the abbreviations pET14b-GiCLZ and pET14b-GNLZ denote the plasmids that encode the GFP fusion proteins, while GiCLZ and GNLZ denote the GFP particles that are produced from the relevant translated fusion proteins. This pattern of nomenclature will also be used to describe plasmids and GFP particles throughout this chapter and the Chapter Four. pET14b-GiCLZ and pET14b-GNLZ were chosen to be acceptor vectors for several reasons. First, GiCLZ particles were able to bind high amounts of IgG in the presence and absence of plasmid pMCS69, and formed only proteinaceous GFP particles. Second, the AVTS N-terminal amino acid extension was shown to be the most effective extension in producing functional GFP particles. Third, using the inactive PhaC (PhaC(C319A)) removed any interference that could occur due to PhaC activity. Finally, NanA was required as the central domain in order to assess its enzymatic activity at this location, and to evaluate the efficacy of a fusion protein containing two copies of the enzyme. Enzyme insertion into the fusion proteins involved removing the ZZ domain gene from the vector, and replacing it with the gene of the enzyme of interest. As the gene for NanA was readily available, it was chosen to be the first enzyme to be investigated. It should also be noted that the particle

production host used in this study was *E. coli* BL21(DE3) (Novagen) that lacked pMCS69. This ensured only GFP protein particles were created.

3.1.1 Creation of pET14b-ext(AVTS)gfp-phaC(C319A)-1inker-nanA (pET14b-GiCLN) and pET14b-ext(AVTS)gfp-nanA-1inker-nanA (pET14b-GNLN) and associated GFP particles

The first GFP fusion proteins created for this study were GiCLN and GNLN, and were encoded by the plasmids pET14b-ext(AVTS)gfp-phaC(C319A)-1inker-nanA, and pET14b-ext(AVTS)gfp-nanA-1inker-nanA, respectively. The formation of GFP particles by these fusion proteins, other than demonstrating the formation of enzyme-bearing GFP particles, would extend information provided by GNLZ. First, it would demonstrate the effect of placing enzymes at different positions in the fusion protein on GFP particle formation; and second, it would highlight the effect of this placement on enzyme activity. The cloning process for the construction of pET14b-ext(AVTS)gfp-phaC(C319A)-1inker-nanA and pET14b-ext(AVTS)gfp-nanA-1inker-nanA is presented in Figure 8.

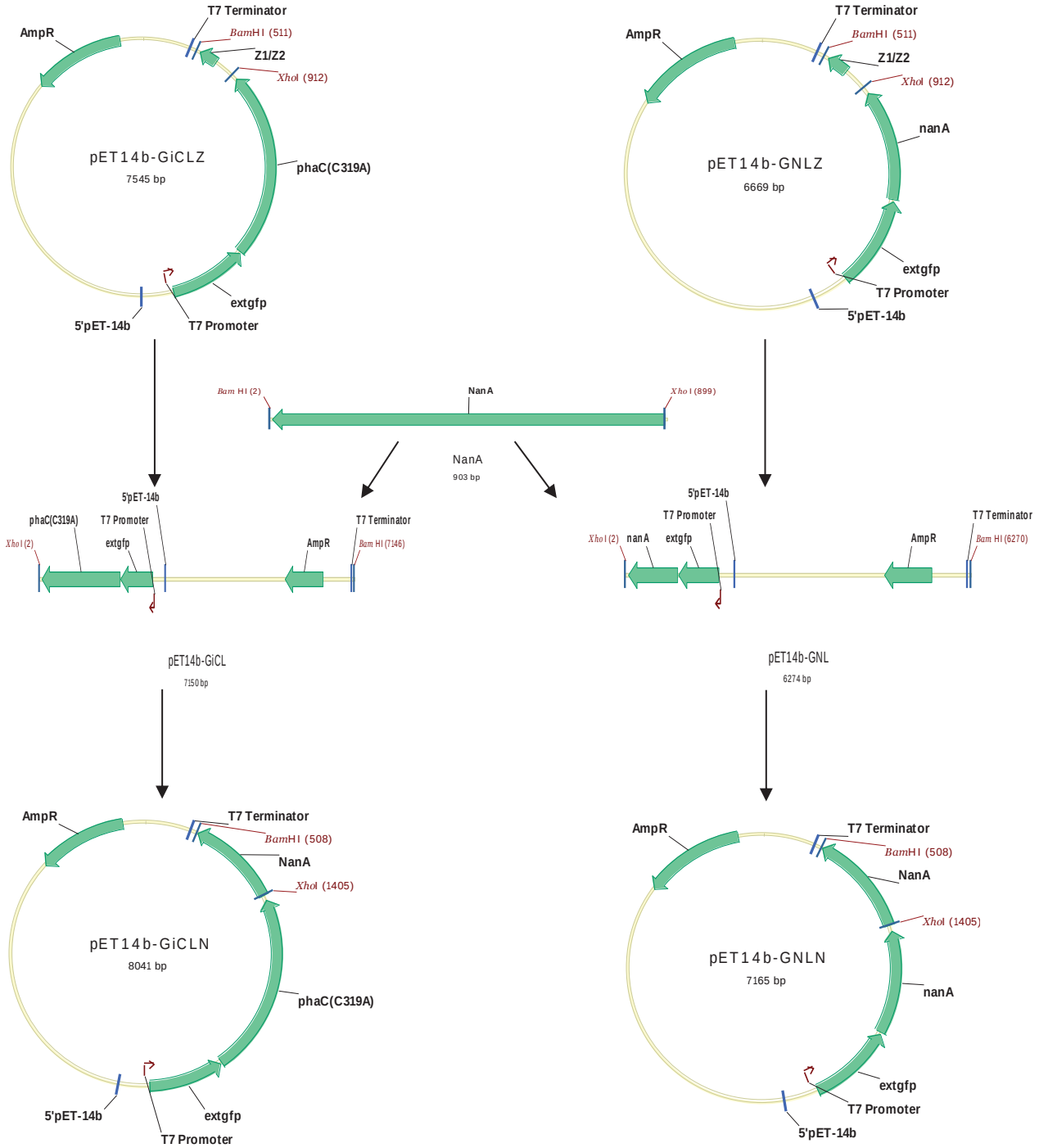

Figure 8. Construction of plasmids pET14b-ext(AVTS)gfp-phaC(C319A)-1inker-nanA, and pET14b-ext(AVTS)gfp-nanA-1inker-nanA. The DNA fragment *nanA* was removed from the plasmid pGEM-nanA by restriction digest using *Bam*HI and *Xho*I (2.15.2), and then isolated using Agarose Gel Electrophoresis (AGE)(2.15.3) and gel DNA extraction (2.15.4) (data not shown). The vectors pET14b-ext(AVTS)gfp-phaC(C319A)-1inker-ZZ (pET14b-GiCLZ), and pET14b-ext(AVTS)gfp-nanA-1inker-ZZ (pET14b-GNLZ) were linearised using the same restriction enzymes, which also removed the ZZ domains, and isolated using AGE and gel DNA extraction. The resulting linearised plasmids were termed pET14b-GiCL and pET14b-GNL. *nanA* was ligated into each linearised vector using T4 DNA ligase (2.15.8) to yield the plasmids pET14b-ext(AVTS)gfp-phaC(C319A)-1inker-nanA (pET14b-GiCLN) and pET14b-ext(AVTS)gfp-nanA-1inker-nanA (pET14b-GNLN).

Once the plasmids were constructed they were transformed into *E. coli* XL1-Blue (Stratagene) for storage. The plasmids were then isolated, and their correct construction confirmed by restriction digest using *Bam*HI and *Xho*I, and Agarose Gel Electrophoresis (AGE). Correct construction was determined by observing DNA bands for the linearised plasmids pET14b-GiCL or pET14b-GNL and *nanA* after restriction digest, indicating that nanA had been successfully ligated into each plasmid. The use of the different *Bam*HI and *Xho*I restriction sites also ensured that *nanA* ligated in the correct orientation. Following confirmation they were then transformed into the production host *E. coli* BL21 (DE3) (Novagen). The plasmids were re-isolated, and their correct construction was again confirmed by restriction digest using *Bam*HI and *Xho*I, and AGE. All transformations, plasmid isolations, restriction digests, and AGE were performed as described above (2.14, 2.15.1, 2.15.2, 2.15.3). Figure 9 presents the results of a restriction digest of plasmid extracted from *E. coli* BL21 (DE3) cells.

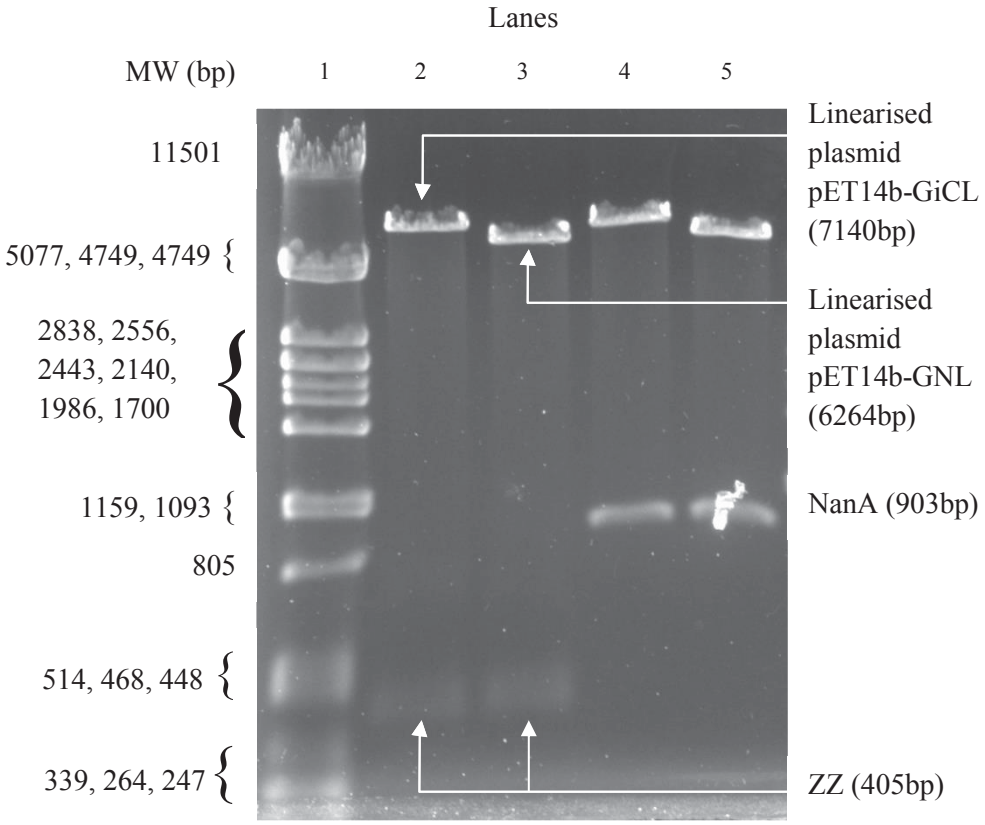

Figure 9. Digest of GiCLZ, GNLZ, GiCLN, and GNLN plasmids with *Bam*HI and *Xho*I. 260 ng of pET14b-GiCLZ (67.61 ng/µl), pET14b-GNLZ (68.27 ng/µl), GiCLN (59.71 ng/µl), and GNLN (61.83 ng/µl) plasmids were digested with *Bam*HI and *Xho*I (2.15.2), and electrophoresed on a 1% Agarose gel in 1xTBE buffer at 100 V, 500 mA, for approximately 1 h (2.15.3). A master mix consisting of 0.5 µl *Bam*HI (5 U), 0.5 µl *Xho*I (10 U), 0.8 µl 100x purified bovine serum albumin (BSA), and 8 µl 10x endonuclease buffer NE Buffer 3 was prepared and 2.45 µl aliquots were added to each digest reaction. Milli-Q water was added to bring the reaction volumes to 20 µl. DNA fragments were visualised by staining the gel in 0.01% Ethidium bromide solution (2.6) and exposing to UV light using a GEL-DOC 2000 (Bio-Rad Laboratories Inc., USA). Lane 1: λ/*Pst*I DNA Ladder; Lane 2: digested GiCLZ plasmid; Lane 3: digested GNLZ plasmid; Lane 4: digested GiCLN plasmid; Lane 5: digested GNLN plasmid.

Once the plasmids were successfully transformed into *E. coli* BL21 (DE3) GFP particles were produced and extracted as described above (2.10.1, 2.10.2, & 2.16). 1 L of Luria-Bertani (LB) medium was supplemented with glucose to a final concentration of 1% (v/v), and ampicillin to a final concentration of 75 µg/ml. Medium that was to support the production of PHB beads was also supplemented with chloramphenicol to a final concentration of 50 µg/ml. Media were then inoculated with a 1% (v/v) inoculum of overnight culture, and incubated at 37 ˚C. When OD_{600} reached 0.4-0.6 gene expression was induced in the cultures using isopropyl β-D-1-thiogalactopyranoside (IPTG), to a final concentration of 1mM, and the cultures were incubated at 25 ˚C for

48 h. After incubation PHB beads and GFP particles were extracted from host cells using a cell disruptor, glycerol gradients, and ultracentrifugation. Fluorescent images of *E.coli* BL21 (DE3) cells harbouring GFP particles, and GFP particles post-extraction were obtained as described above (2.17.1) and are presented in Figure 10. As can be seen, GFP particles could still form when NanA was fused at the C-termini of the GFP fusion proteins. Furthermore, the incorporation of two active NanA enzymes within one GFP fusion protein (GNLN) also leads to the formation of GFP particles. Therefore, as NanA is a tetrameric enzyme, it is predicted GFP fusion proteins consisting of enzymes of the same number or less subunits will also be able to form GFP particles.

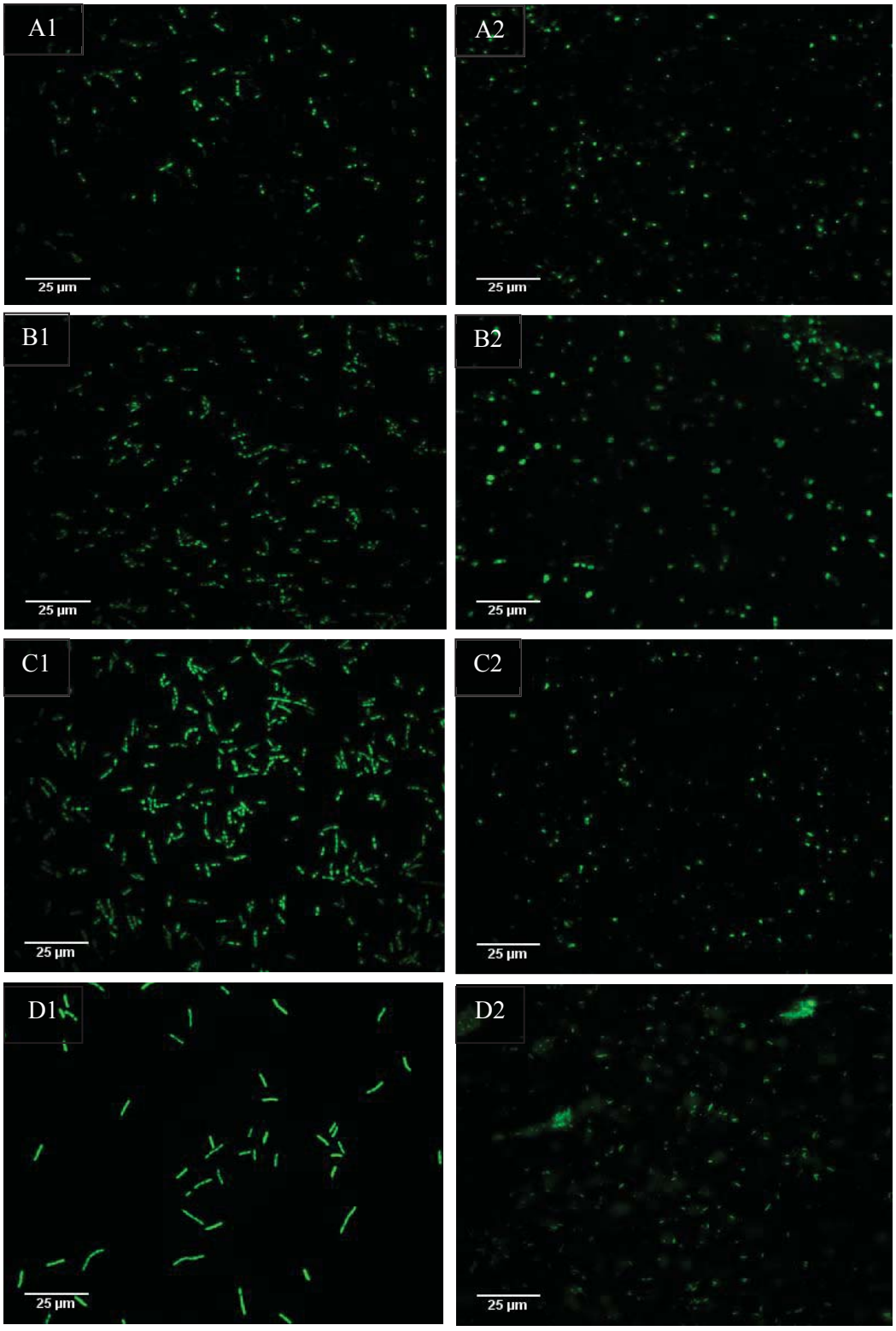

Figure 10. Fluorescent images of *E.coli* BL21 (DE3) cells containing GFP particles and GFP particles post-extraction. Fluorescent images of *E. coli* BL21 cells and GFP particles were obtained at 1000x magnification using a U-MWIBA2 Blue excitation filter cube fitted to an Olympus BX51 Fluorescent Light Microscope (Olympus Optical Co., Japan), an Optronics camera (Optronics, USA), and MagnaFire^{TM} 2.1C Application software (Optronics, USA). A1: GiCLZ cells, A2: GiCLZ particles; B1: GNLZ cells, B2: GNLZ particles; C1: GiCLN cells, C2: GiCLN particles; D1: GNLN cells, D2: GNLN particles.

The GFP particles were analysed by Sodium dodecylsulfate Polyacrylamide Gel Electrophoresis (SDS-PAGE) (2.18.1) in order to confirm that the GiCLN and GNLN fusion proteins had been correctly expressed and isolated. Confirmation was achieved by observing which bands appeared to be over-expressed, and then cutting these bands from the gel and analysing them by MALDI-TOF (2.18.3). MALDI-TOF conducted by the Centre of Protein Research (University of Otago) subsequently confirmed the identification of GiCLN and GNLN fusion proteins (data not shown). GiCLZ and GNLZ fusion proteins were previously confirmed by Jahns *et al.*, and so it was not necessary to repeat a MALDI-TOF analysis. The theoretical molecular weights of the GFP fusion proteins were calculated using Geneious Software, and were as follows: GiCLZ (110.8 kDa), GNLZ (79.1 kDa), GiCLN (126.5 kDa), and GNLN (94.8 kDa). The molecular weights as analysed by SDS-PAGE were as follows: GiCLZ (108.0 kDa), GNLZ (71.5 kDa), GiCLN (116.8 kDa), and GNLN (80.2 kDa).

SDS-PAGE was also employed to calculate the concentration of fusion protein present in the GFP particle samples as well as a NanA-PhaC PHA bead sample using densitometry (2.18.2). The NanA-PhaC bead, where NanA is covalently bound to the N-terminus of the PHA synthase (PhaC), has been previously shown to exhibit high NanA activity (Hooks et al., 2013), and was to serve as the positive control in activity assays involving the GFP particles. To perform densitometry, the band volume of each sample was compared to that exhibited by BSA standards that were loaded on to the same gel. The quantity of protein present in each standard band had been previously calculated, and a standard curve consisting of Absolute Quantity (µg) versus Band Volume was constructed to calculate the quantity of fusion protein present in each PHA bead and GFP particle sample. The fusion protein concentration values were used to standardise the amount of fusion protein from each sample used in the NanA enzyme activity reactions. Fusion protein concentrations were as follows: NanA-PhaC (3.581 mg/ml), GiCLZ (1.725 mg/ml), GNLZ (2.349 mg/ml), GiCLN (3.384 mg/ml), GNLN (2.071 mg/ml).

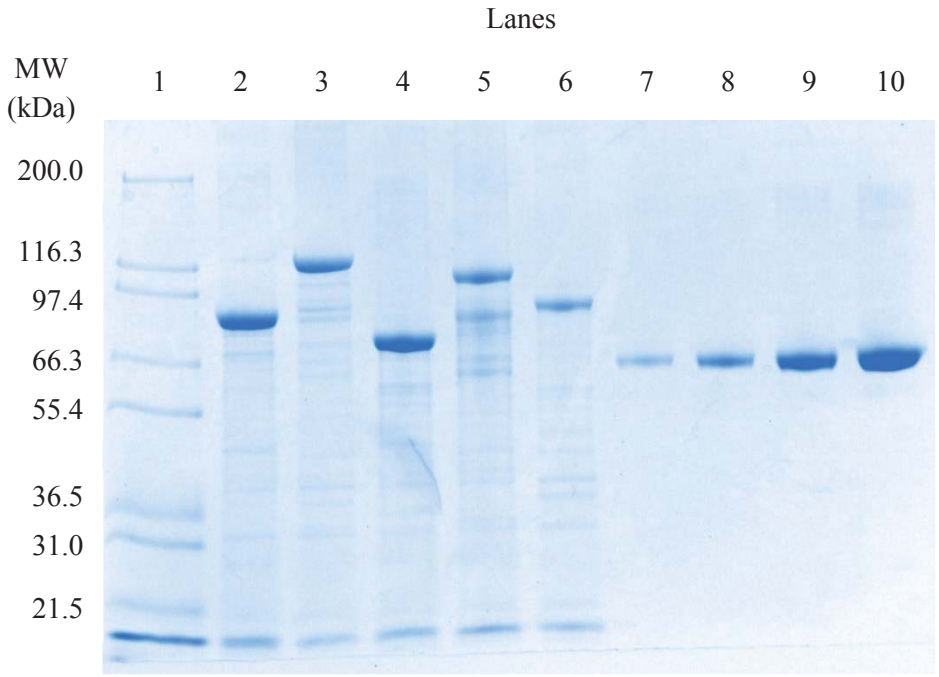

Figure 11. SDS-PAGE analysis of PHA beads and GFP particles to be used in NanA enzyme activity assays. Each sample was washed in 50mM Potassium phosphate buffer, pH 7.50, and diluted 40 fold. 12 µl of each sample was mixed with 3 µl of 5x SDS-PAGE Loading Buffer (2.7), and 1.5 µl of 1.0M Dithiothreitol (DTT), and then heated at 95 ˚C for 1.5 min. The samples were electrophoresed on an 8% bis-Tris Polyacrylamide gel at 150 V, 1000 mA, for 40-60 min, using a Mini PROTEAN® 3 System (Bio-Rad Laboratories Inc., USA). Following electrophoresis the gel was stained with 0.1% (w/v) Coomassie Brilliant Blue R250 for 30min, and destained overnight using a methanol-based destain. The concentration of fusion protein was calculated by comparing band intensities to those exhibited by the BSA standards. Lane 1: Mark 12^{TM} Unstained Standard Protein Ladder (Invitrogen, USA); Lane 2: GNLN; Lane 3: GiCLN; Lane 4: GNLZ; Lane 5: GiCLZ; Lane 6: NanA-PhaC; Lane 7: 0.75 µg BSA; Lane 8: 1.5 µg BSA; Lane 9: 3.0 µg BSA; Lane 10: 6.0 µg BSA.

3.1.2 Assessment of *N*-acetyl-D-neuraminic acid (Neu5Ac) production ability of GiCLN, GNLZ, and GNLN GFP particles

Although the position of NanA within the GFP fusion proteins did not appear to impact GFP particle formation, it was possible that it could affect the strength of enzyme activity and the ability to produce product. To investigate this possibility, NanA-PhaC beads, and GiCLZ, GNLZ, GiCLN, and GNLN GFP particles were tested for the presence of NanA activity. As GiCLZ lacked the NanA enzyme it was to serve as the negative control. The method used to measure NanA activity involved measuring the production of *N*-acetyl-D-neuraminic acid (Neu5Ac) from the aldol condensation of *N*-acetyl-D-mannosamine (ManNAc) and pyruvate, as described above (2.20.1). Although NanA can catalyse this reaction in both directions, the production of Neu5Ac was

investigated in order to explore an alternative means for the production of this compound for use in pharmaceuticals and other industries. The Neu5Ac production assay was conducted for 16 and 48 hours- the results are displayed in Figure 9. The standardised concentration of fusion protein used per sample in this assay was 0.1mg/ml. All the following assays in this study used standardised concentrations of 0.05mg/ml in order to ration the amount of sample.

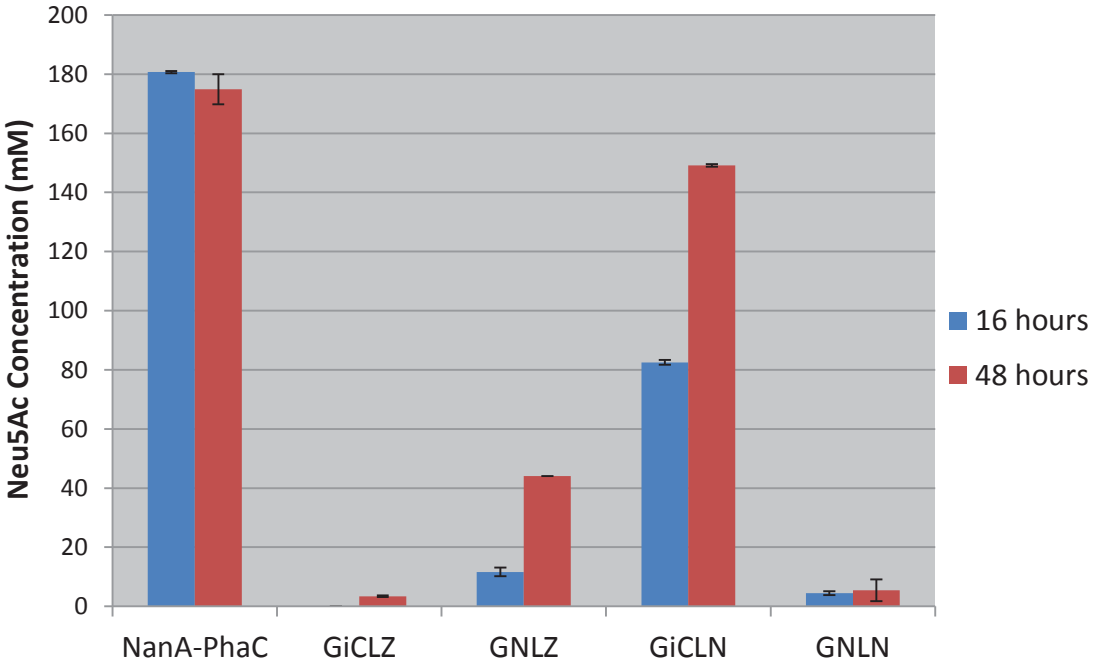

Figure 12. Neu5Ac production by PHA beads and GFP particles after 16 h and 48 h incubation. Aliquots of each sample that contained 50 µg of fusion protein were mixed with a substrate solution, which consisted of 0.2 M *N*-acetyl-D-mannosamine (ManNAc) and 1.0 M Sodium pyruvate, to a final reaction volume of 0.5 ml. The samples were then incubated under aerobic conditions at 50 ˚C, 200rpm, for 16 h and 48 h. Following incubation the samples were centrifuged at 16000 x g for 10min, and the supernatants removed. The supernatants were then diluted and analysed by HPLC (2.14). All samples, at each time point, were assayed in triplicate. Error bars represent ± 1 standard deviation.

The strength of NanA activity varied greatly between the samples. The NanA-PhaC beads produced the largest amount of Neu5Ac in the shortest amount of time, and, therefore, exhibited the strongest enzyme activity overall. The maximum amount of Neu5Ac produced via NanA-PhaC biocatalysis, as seen after 16 h incubation, was 181 mM (3s.f.), which equates to a 90.4% (3s.f.) conversion of ManNAc. The GiCLN particle exhibited the strongest activity in comparison to the other GFP particles, and produced a maximum amount of 149mM (3s.f.) Neu5Ac after 48 h incubation, which

equates to a 74.6% (3s.f.) conversion of ManNAc. The maximum amount of Neu5Ac produced (and associated ManNAc conversions) via GiCLZ, GNLZ, and GNLN biocatalysis after 48 h incubation were 3.42 mM (1.71%), 44.1 mM (22.0%), and 5.45 mM (2.72%) (3s.f.), respectively. It appears that, in the case of the GFP particles, the placement of NanA at the C-terminus of the GFP fusion protein produces GFP particles that exhibit the strongest enzyme activity. Therefore, in order to produce GFP particles that immobilise other enzymes with strong enzyme activity, the C-terminal fusion was chosen as the standard method. As the N-terminal extension of GFP was shown by Jahns *et al.* to be important for GFP particle formation it was retained to encourage the formation of enzyme-bearing GFP particles. Therefore, N-terminal fusions of enzymes to GFP were not investigated.

3.1.3 Creation of pET14b-ext(AVTS)gfp-phaC(C319A)-1inker-opdA (pET14b-GiCLO) and pET14b-ext(AVTS)gfp-phaC(C319A)-1inker-bla(-ss) (pET14b-GiCLB)

The creation of the plasmids pET14b-ext(AVTS)gfp-phaC(C319A)-1inker-opdA (pET14b-GiCLO) and pET14b-ext(AVTS)gfp-phaC(C319A)-1inker-bla(-ss) (pET14b-GiCLB)- which encoded the fusion proteins GiCLO and GiCLB, respectively- utilised two methods of molecular cloning. As the donor plasmid pET14b-phaC-linker-opdA already had *Bam*HI and *Xho*I restriction sites surrounding the *opdA* gene, pET14b-ext(AVTS)gfp-phaC(C319A)-1inker-opdA was constructed in the same manner as outlined in Figure 8. However, the plasmid pET14b-bla(-ss)-phaC did not contain *Bam*HI or *Xho*I restriction sites, and so Polymerase Chain Reaction (PCR) was used to extract the *bla(-ss)* gene. The primers used to amplify *bla(-ss)* were designed to incorporate *Bam*HI and *Xho*I restriction sites (2.2). Diagrams outlining the cloning processes used to produce pET14b-GiCLO and pET14b-GiCLB are presented in Figures 13 and 14.

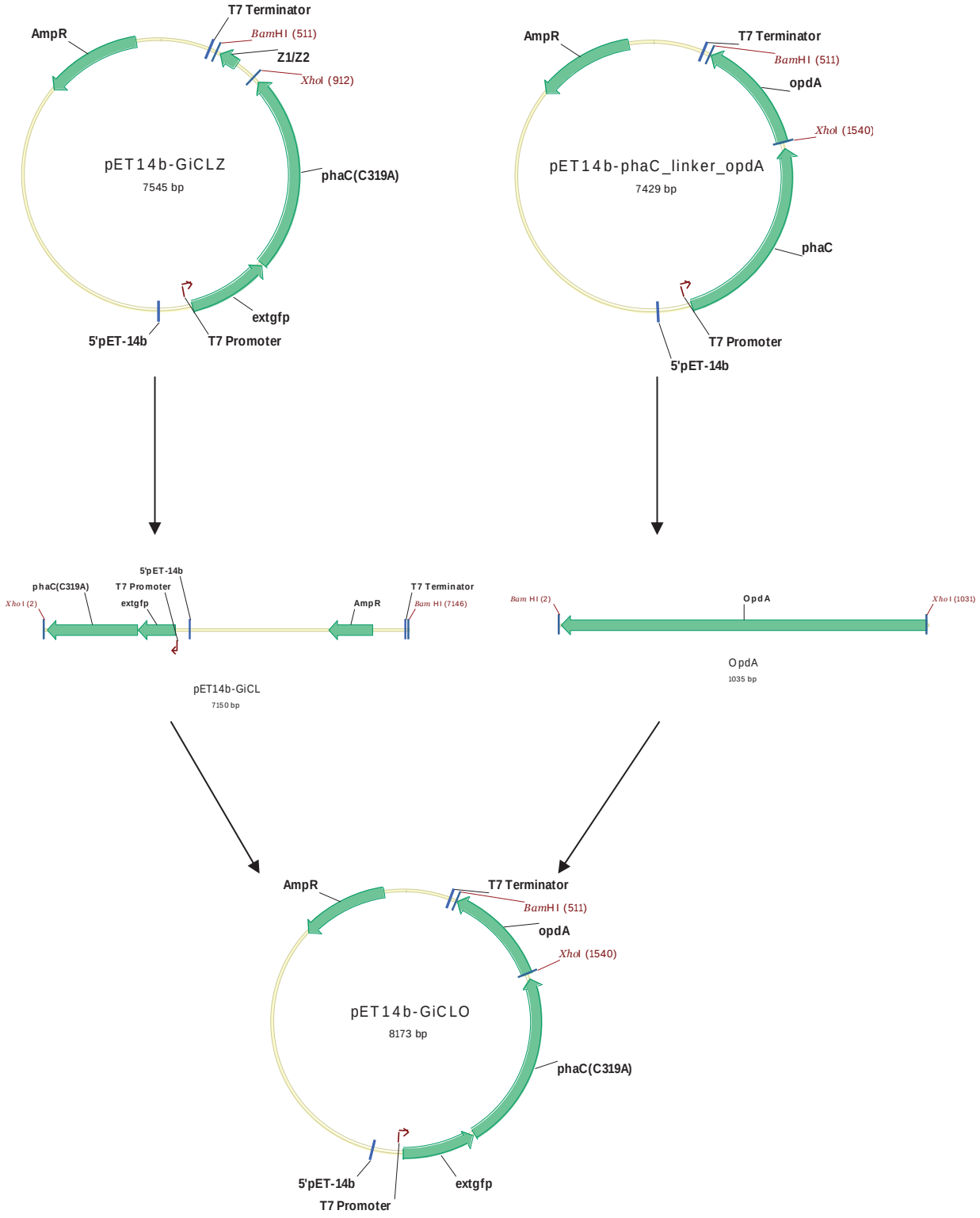

Figure 13. Construction of the plasmid pET14b-GiCLO. The DNA fragment *opdA* was removed from the plasmid pET14b-phaC-linker-opdA by restriction digest using *Bam*HI and *Xho*I (2.15.2), and then isolated using Agarose Gel Electrophoresis (AGE) (2.15.3) and gel DNA extraction (2.15.4). The vector pET14b-ext(AVTS)gfp-phaC(C319A)-1inker-zz (pET14b-GiCLZ) was linearised using the same restriction enzymes, which also removed the ZZ domain, and isolated using AGE and gel DNA extraction. The resultant linearised plasmid was termed pET14b-GiCL. *opdA* was ligated into pET14b-GiCL using T4 DNA ligase (2.15.8) to yield the plasmid pET14b-ext(AVTS)gfp-phaC(C319A)-1inker-opdA (pET14b-GiCLO).

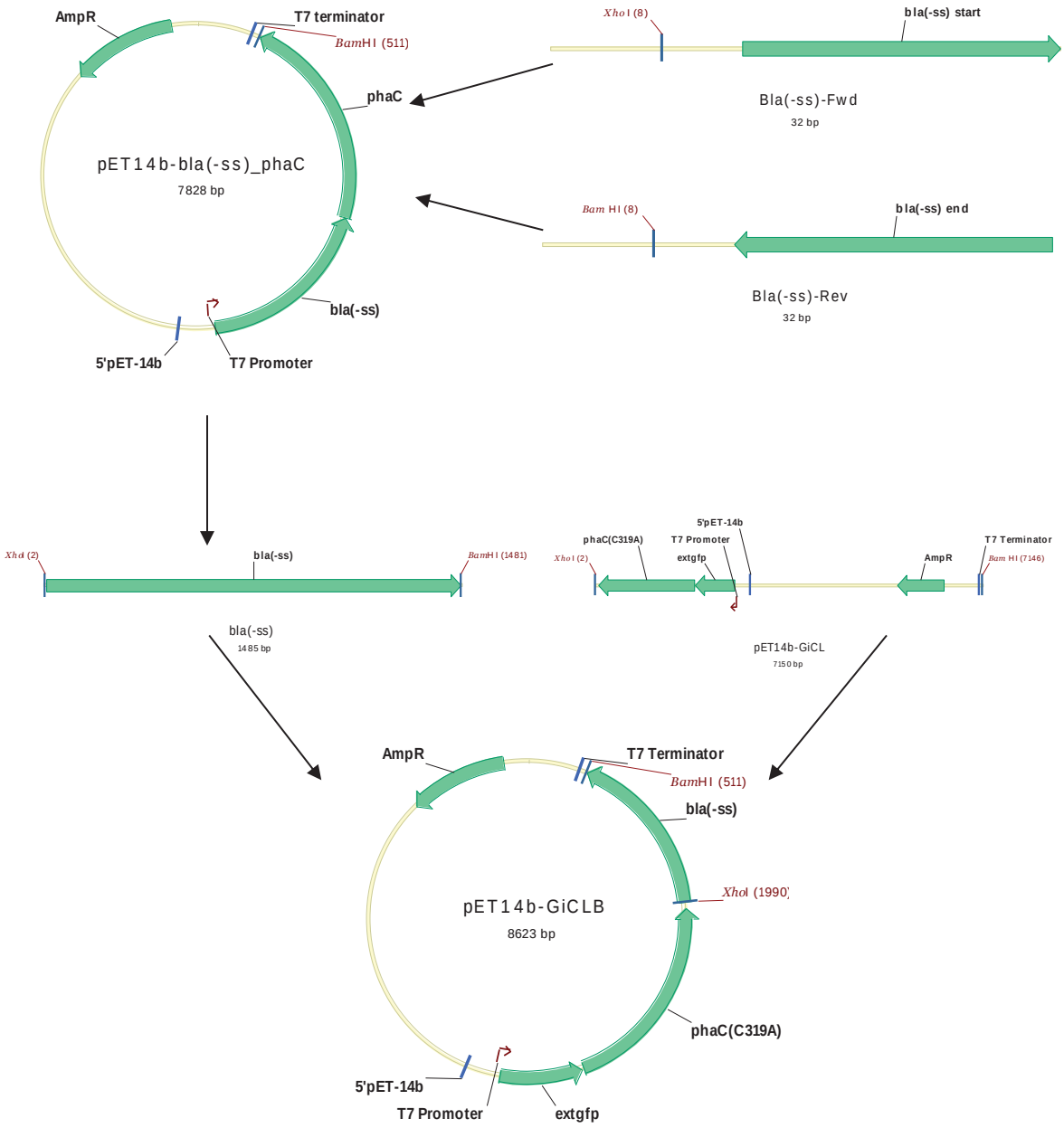

Figure 14. Construction of the plasmid pET14b-GiCLB. The DNA fragment *bla(-ss)* was amplified from the plasmid pET14b-bla(-ss)-phaC using the Polymerase Chain Reaction (PCR) (2.15.5). The forward primer (Bla(-ss)-Fwd) consisted of ATA ATA CTC GAG ATG GCC GCT AAC CTG AAC GG (32 bp), and the reverse primer (Bla(-ss)-Rev) consisted of AAT AAT GGA TCC TTA GCC ACC ACC ACC ACC GC (2.2). PCR conditions were as follows: initial denaturing- 94 ˚C, 5 min; denaturing- 94 ˚C, 15s; annealing- 60 ˚C, 30s; extension- 68 ˚C, 1.5 min; number of cycles = 30. PCR product was isolated by Agarose Gel Electrophoresis (AGE) (2.15.3) and gel DNA extraction (2.15.4). *bla(-ss)* was then A-tailed using PCR (2.15.6), ligated into a pGEM-T Easy vector (Promega, USA) (2.15.7), and the resulting plasmid transformed into *E. coli* XL1-Blue (Stratagene)(2.14)(data not shown). The plasmid was then isolated (2.15.1) and digested with *Bam*HI and *Xho*I to yield the *bla(-ss)* fragment, which was isolated using AGE and Gel DNA Extraction. The vector pET14b-ext(AVTS)gfp-phaC(C319A)-1inker-zz (pET14b-GiCLZ) was linearised using the same restriction enzymes, which also removed the ZZ domain, and isolated using AGE and Gel DNA Extraction. The resultant linearised plasmid was termed pET14b-GiCL. *bla(-ss)* was ligated into the pET14b-GiCL using T4 DNA ligase (2.15.8) to yield the plasmid pET14b-ext(AVTS)gfp-phaC(C319A)-1inker-bla(-ss) (pET14b-GiCLB).

The constructed plasmids were transformed into *E. coli* XL1-Blue (Stratagene), and *E. coli* BL21 (DE3), and their correct construction confirmed as described above (3.1.1). Figure 15 present the results of a restriction digest of plasmid extracted from *E. coli* BL21 (DE3) cells.

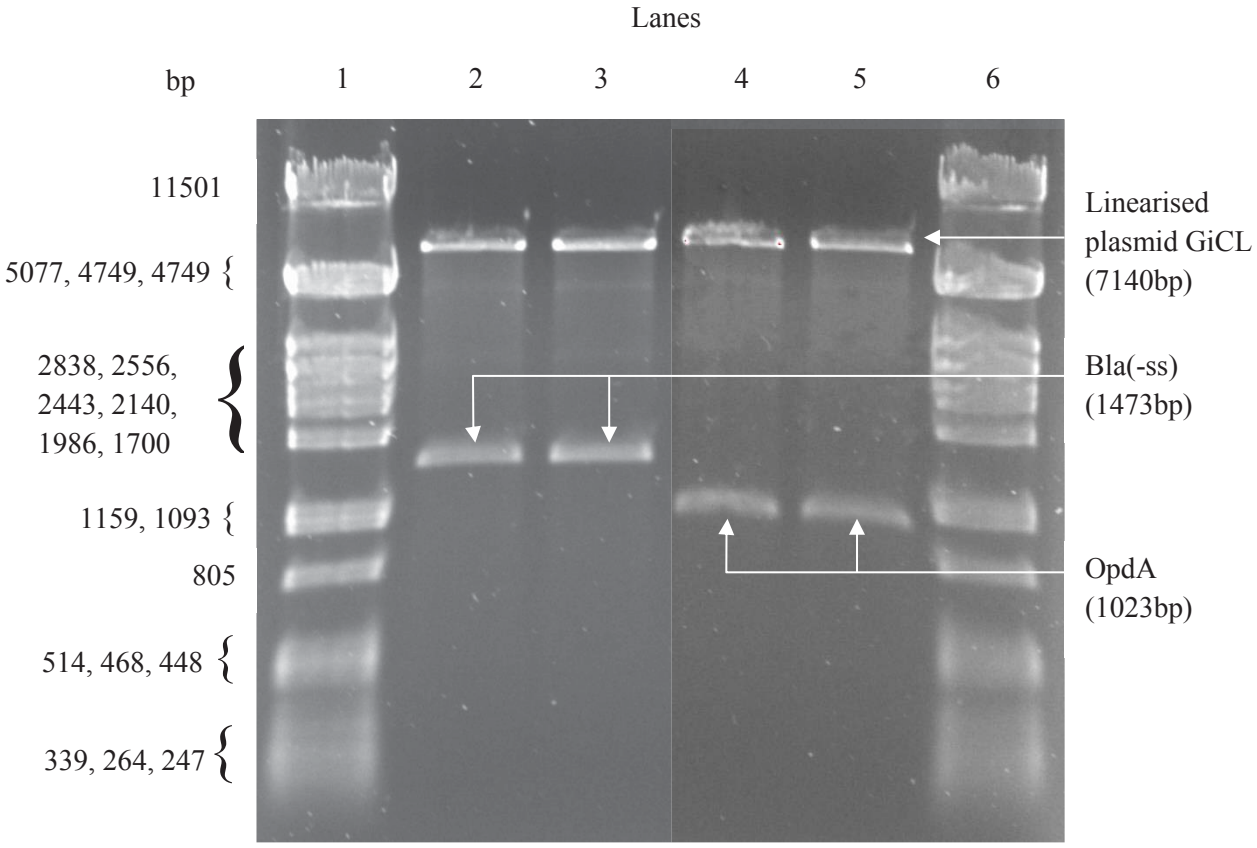

Figure 15. Digest of pET14b-GiCLB and pET14b-GiCLO plasmids with *Bam*HI and *Xho*I. 260 ng of pET14b-GiCLB (29.31 ng/µl and 37.03 ng/µl) and pET14b-GiCLO (41.86 ng/µl and 44.83 ng/µl) plasmids were digested with *Bam*HI and *Xho*I (2.15.2) and electrophoresed on a 1% Agarose gel in 1xTBE buffer at 100 V, 500 mA, for approximately 1 h (2.15.3). A master mix consisting of 0.5 µl *Bam*HI (5 U), 0.5 µl *Xho*I (10 U), 1.2 µl 100x purified bovine serum albumin (BSA), and 12 µl 10x endonuclease buffer NE Buffer 3 was prepared and 2.37 µl aliquots were added to each digest reaction. Milli-Q water was added to bring the volume of each reaction to 20 µl. DNA fragments were visualised by staining the gel in 0.01% Ethidium bromide solution (2.6) and exposing to UV light using a GEL-DOC 2000 (Bio-Rad Laboratories Inc., USA). Lane 1: λ/*Pst*I DNA Ladder; Lane 2: digested pET14b-GiCLB plasmid; Lane 3: digested pET14b-GiCLB plasmid; Lane 4: digested pET14b-GiCLO plasmid; Lane 5: digested pET14b-GiCLO plasmid; Lane 6: λ/*Pst*I DNA Ladder.

Once the plasmids had been confirmed to be correctly constructed in *E. coli* BL21 (DE3) GFP particles were then produced as described above (3.1.1). Correct construction was determined by observing DNA bands for the linearised plasmid pET14b-GiCL and either *bla(-ss)* or *opdA* after restriction digest, indicating that *bla(-ss)* and *opdA* had been successfully ligated into the plasmid. Fluorescent images of *E. coli*

BL21 (DE3) cells containing GiCLB and GiCLO particles, and particles post-extraction, were obtained (2.17.1) and are presented in Figure 16. Bla(-ss)-PhaC and PhaC-OpdA PHA beads were also produced using the same methodology. In the same manner as the NanA-PhaC beads, both have been previously shown to exhibit high enzyme activity, and were to serve as positive controls in subsequent assays. GiCLZ particles were again to serve as the negative control.

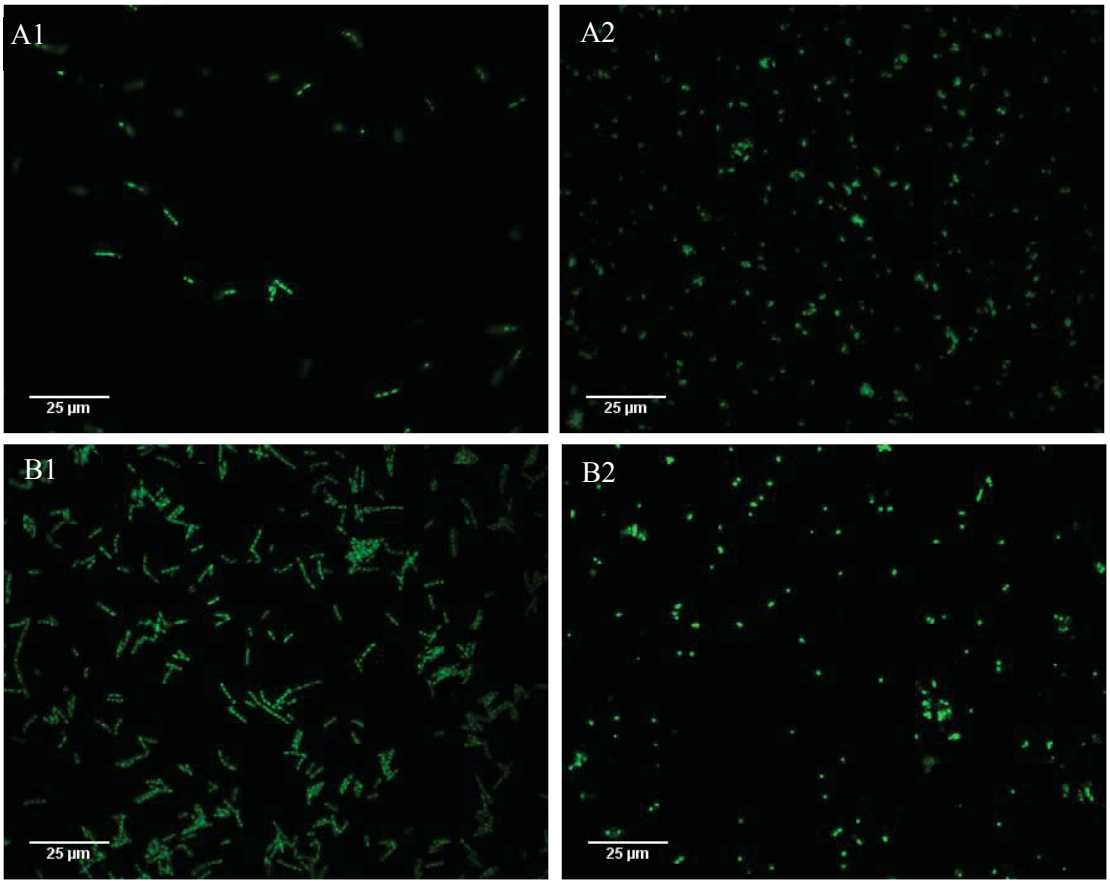

Figure 16. Fluorescent images of *E.coli* BL21 (DE3) cells containing GiCLB and GiCLO particles, and GiCLB and GiCLO particles post-extraction. Fluorescent images of *E. coli* BL21 cells and GFP particles were obtained at 1000x magnification using a U-MWIBA2 Blue excitation filter cube fitted to an Olympus BX51 Fluorescent Light Microscope (Olympus Optical Co., Japan), an Optronics camera (Optronics, USA), and MagnaFire^{TM} 2.1C Application software (Optronics, USA). A1: GiCLB cells, A2: GiCLB particles; B1: GiCLO cells, B2: GiCLO particles.

SDS-PAGE, MALDI-TOF, and densitometry analyses were also conducted on GiCLB and GiCLO particles (2.18.1, 2.18.2, & 2.18.3)(data not shown). SDS-PAGE showed the molecular weights of the constituent fusion proteins to be 134 kDa and 120 kDa, respectively, and MALDI-TOF confirmed their correct identities. The theoretical

molecular weights of GiCLB and GiCLO were 150 kDa and 131 kDa, respectively. Several batches of GiCLB and GiCLO particles were produced and densitometry was used to calculate fusion protein concentration before attempting the activity and stability assays.

3.1.4 Enzyme Activity of GFP particles over time

The enzyme activity of each type of enzyme-bearing GFP particles was charted over a period of 72 hours. The activity assays for each enzyme were performed as described above (2.20 & 2.21.1). The results obtained are presented in Figures 17, 18, and 19.

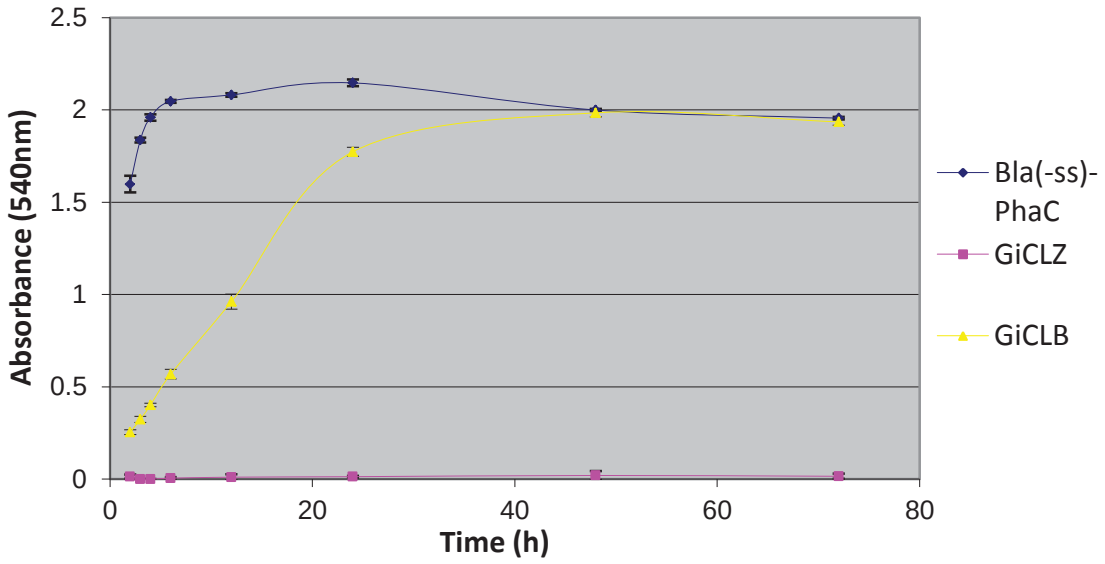

Figure 17. Production of maltose via Bla(-ss)-PhaC PHA bead and GFP particle biocatalysis over a 72 h incubation. Aliquots of each sample that contained 50 µg of fusion protein were mixed with 1.0% (w/v) Soluble Starch substrate solution (2.4.8) to a final volume of 1.0 ml. The samples were then incubated under aerobic conditions at 25 ˚C, 200rpm, for 72 h. Samples were analysed at 1h, 2h, 3 h, 4 h, 6 h, 12 h, 24 h, 48 h, and 72 h incubation. Following incubation the samples were centrifuged at 16000 x g for 5 min, and 0.5 ml of supernatant was removed. The supernatants were then mixed with 0.5 ml of α-Amylase Colour Reagent Solution (2.4.7), and heated at 100 ˚C for 15 min in a memmert OB 10 oil bath (memmert, Germany). After heating the samples were cooled to room temperature (22 ˚C- 25 ˚C), and brought to a final volume of 6.0 ml with Milli-Q water. 1.0 ml of each sample was pipetted into separate 2-ml cuvettes, and the absorbance measured at 540 nm using an Ultrospec 2000 spectrophotometer (Pharmacia Biotech, UK). All samples, at each time point, were assayed in triplicate. Error bars represent ± 1 standard deviation.

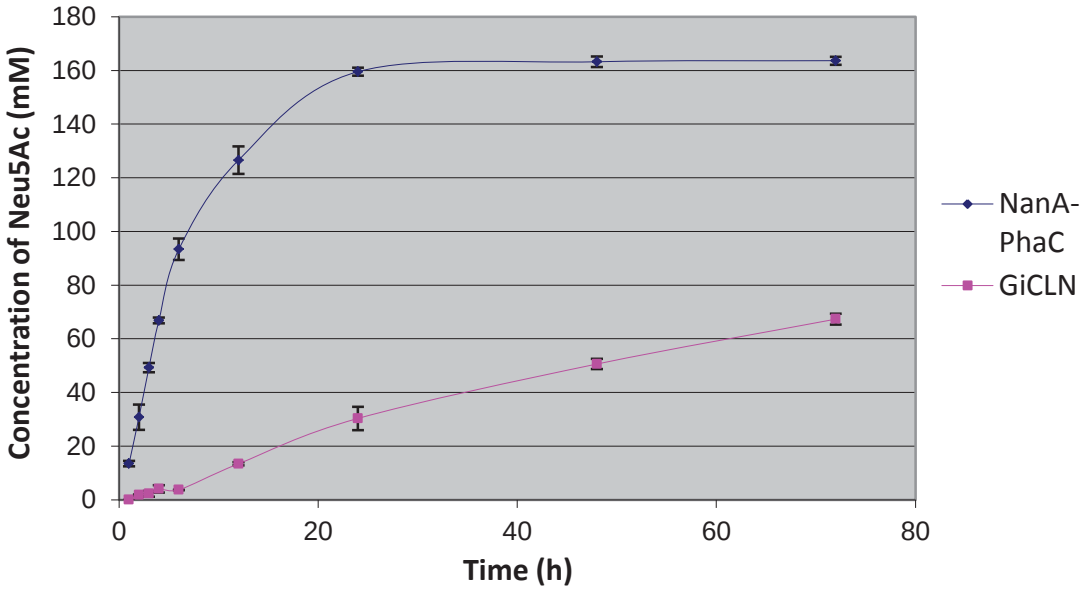

Figure 18. Production of Neu5Ac via NanA-PhaC PHA bead and GiCLN particle biocatalysis over a 72 h incubation. Aliquots of each sample that contained 25 µg of fusion protein were mixed with substrate solution, which consisted of 0.2 M *N*-acetyl-D-mannosamine (ManNAc) and 1.0 M Sodium pyruvate, to a final volume of 0.5 ml. The samples were then incubated under aerobic conditions at 50 ˚C, 200 rpm, for 72 h. Samples were analysed at 1h, 2h, 3 h, 4 h, 6 h, 12 h, 24 h, 48 h, and 72 h incubation. Following incubation the samples were centrifuged at 16000 x g for 10 min, and the supernatants removed. The supernatants were then diluted and analysed by HPLC (2.19). All samples, at each time point, were assayed in triplicate. Error bars represent ± 1 standard deviation.

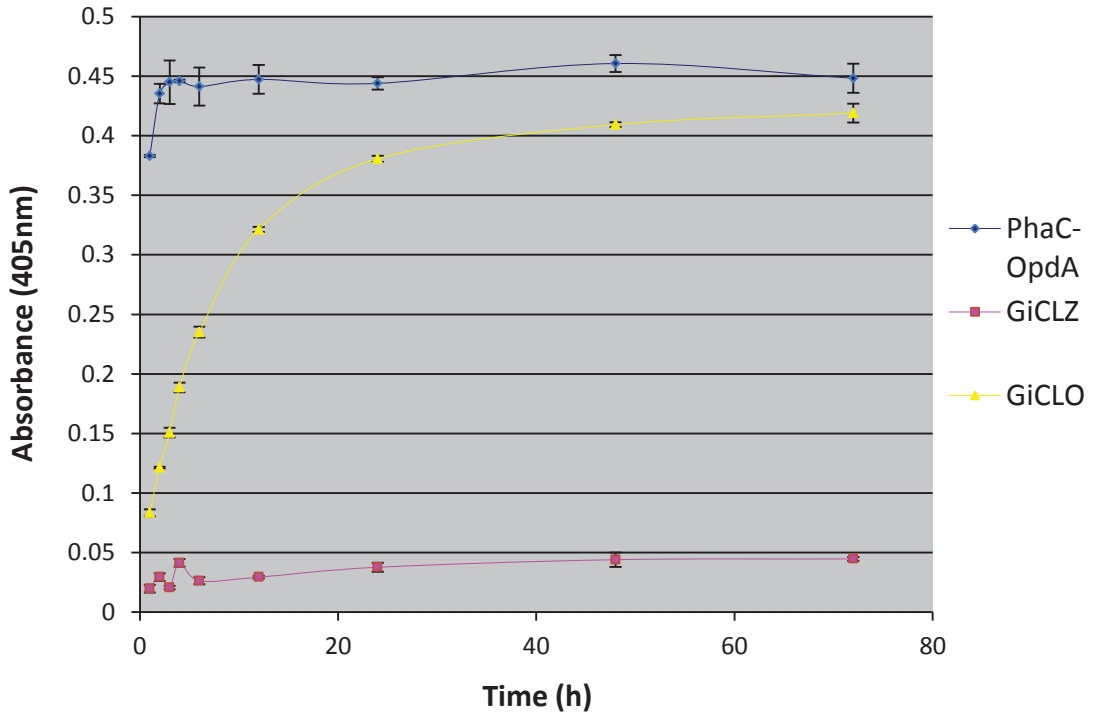

Figure 19. Production of *para*-nitrophenol via PhaC-OpdA PHA bead and GFP particle biocatalysis over a 72 h incubation. Aliquots of each sample that contained 50 µg of fusion protein were mixed with 200 µM Methyl parathion substrate solution to a final volume of 1.0 ml. The samples were then incubated under aerobic conditions at 25 ˚C, 200 rpm, for 72 h. Samples were analysed at 1h, 2h, 3 h, 4 h, 6 h, 12 h, 24 h, 48 h, and 72 h incubation. Following incubation the samples were centrifuged at 16000 x g for 5 min, and the supernatants removed. The supernatants were then pipetted into separate 2-ml cuvettes, and the absorbance measured at 405 nm using an Ultrospec 2000 spectrophotometer (Pharmacia Biotech, UK). All samples, at each time point, were assayed in triplicate. Error bars represent ± 1 standard deviation.

As can be seen from the data presented in Figures 17, 18, and 19, all types of enzyme-bearing GFP particle display active enzyme. GiCLB and GiCLO particles catalysed their respective reactions to their end-points within approximate 48 h and 72 h, respectively. GiCLN particles did not catalyse the Neu5Ac production reaction to its end-point within the timeframe observed. Furthermore, in each assay the enzyme-bearing PHA beads used as positive controls catalysed their respective reactions to their end-points in a shorter period of time in comparison to the GFP particles. This indicates higher enzyme activity in comparison to the GFP particles.

3.2 Characterisation of enzyme-bearing GFP particles

Having shown that GFP particles are capable of immobilising and displaying active enzyme they were then characterised under a variety of conditions. Immobilised enzymes can be expected to be used at a range of temperatures and pH, and be recycled multiple times. Therefore, the GFP particles created in this study were assessed for temperature and pH stability, and reusability. Furthermore, the enzymatic activity of the particles was assessed after long-term storage in order to evaluate shelf-life.

3.2.1 Temperature Stability

To assess temperature stability, the GFP particles were pre-heated at temperatures ranging from 4 ˚C to 95 ˚C, in 10 ˚C increments, and their enzyme activity assessed, as described above (2.21.2). The results are displayed in Figures 20, 21, and 22.

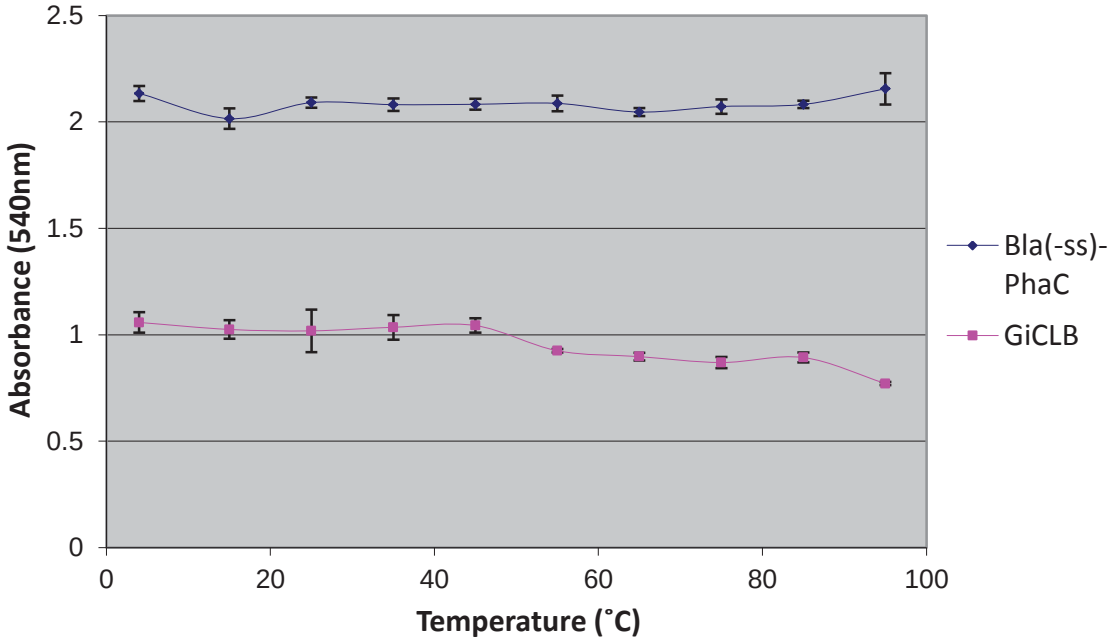

Figure 20. Production of maltose via Bla(-ss)-PhaC PHA bead and GiCLB particle biocatalysis after heat-treatment. Aliquots of Bla(-ss)-PhaC beads and GiCLB particles containing 50 µg of fusion protein were heated for 10 min at the following temperatures: 4°C, 15°C, 25°C, 35°C, 45°C, 55°C, 65°C, 75°C, 85°C, and 95°C. Following heat-treatment the samples were mixed with 1.0% (w/v) Soluble Starch solution (2.4.8) to a final reaction volume of 1.0 ml. The samples were then incubated under aerobic conditions at 25 ˚C, 200 rpm, for 12 h. Following incubation the samples were centrifuged at 16000 x g for 5 min, and 0.5 ml of supernatant was removed. The supernatants were then mixed with 0.5 ml of α-Amylase Colour Reagent Solution (2.4.7), and heated at 100 ˚C for 15 min in a memmert OB 10 oil bath (memmert, Germany). After heating, the samples were cooled to room temperature (22 ˚C- 25 ˚C), and brought to a final volume of 6.0 ml with Milli-Q water. 1.0 ml of each sample was pipetted into separate 2-ml cuvettes, and the absorbance measured at 540 nm using an Ultrospec 2000 spectrophotometer (Pharmacia Biotech, UK). All samples were assayed in triplicate after heat-treatment at each temperature. Error bars represent ± 1 standard deviation.

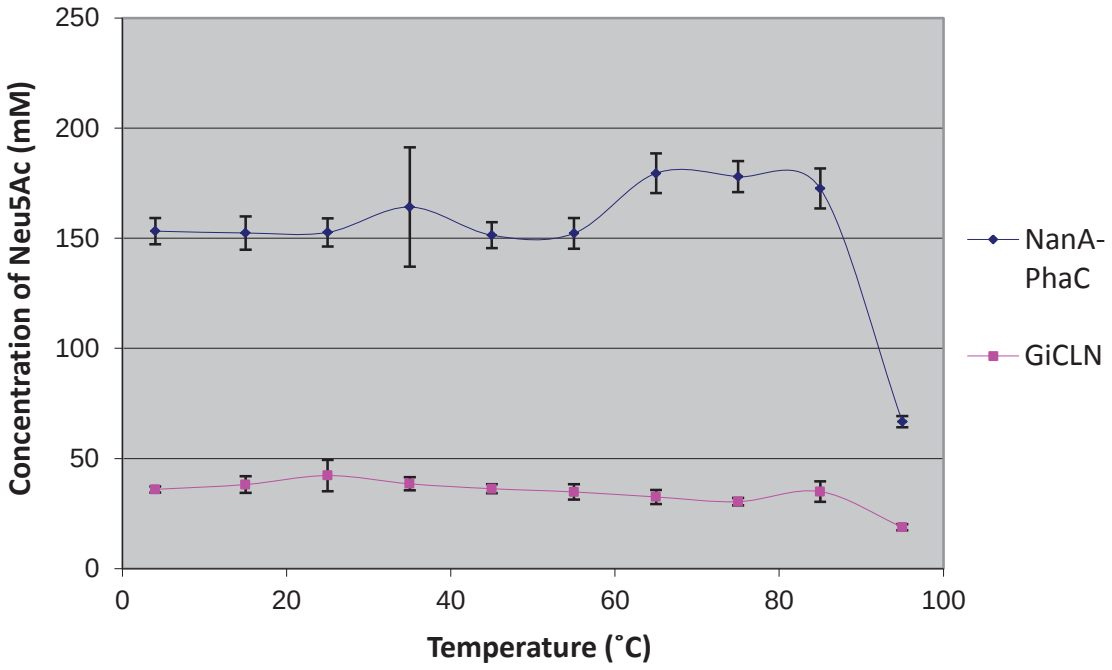

Figure 21. Production of Neu5Ac via NanA-PhaC PHA bead and GiCLN particle biocatalysis after heat-treatment. Aliquots of NanA-PhaC beads and GiCLB particles containing 25 µg of fusion protein were heated for 10 min at the following temperatures: 4°C, 15°C, 25°C, 35°C, 45°C, 55°C, 65°C, 75°C, 85°C, and 95°C. Following heat-treatment the samples were mixed with a substrate solution, which consisted of 0.2 M *N*-acetyl-D-mannosamine and 1.0 M Sodium pyruvate, to a final reaction volume of 0.5 ml. The samples were then incubated under aerobic conditions at 50 ˚C, 200 rpm, for 48 h. Following incubation the samples were centrifuged at 16000 x g for 10 min, and the supernatants removed. The supernatants were then diluted and analysed by HPLC (2.19). All samples were assayed in triplicate for heat-treatment at each temperature. Error bars represent ± 1 standard deviation.

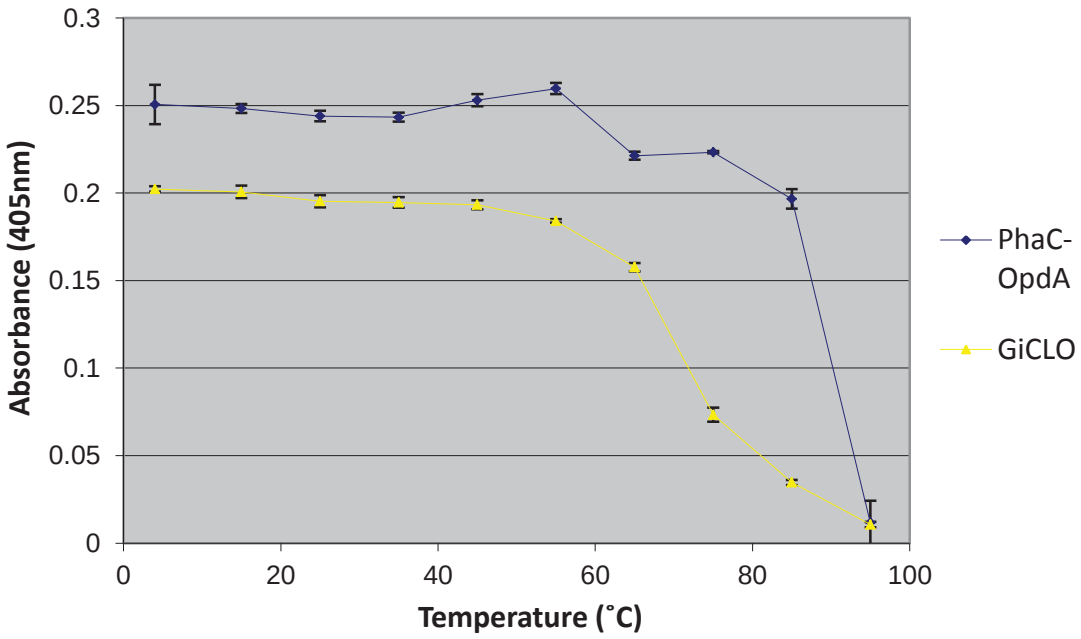

Figure 22. Production of *para*-nitrophenol via PhaC-OpdA PHA bead and GiCLO particle biocatalysis after heat-treatment. Aliquots of PhaC-OpdA beads and GiCLO particles containing 50 µg of fusion protein were heated for 10 min at the following temperatures: 4°C, 15°C, 25°C, 35°C, 45°C, 55°C, 65°C, 75°C, 85°C, and 95°C. Following heat-treatment the samples were mixed with 200 µM Methyl parathion substrate solution to a final reaction volume of 1.0 ml. The samples were then incubated under aerobic conditions at 25 ˚C, 200 rpm, for 12 h. Following incubation the samples were centrifuged at 16000 x g for 5 min, and the supernatants removed. The supernatants were then pipetted into separate 2-ml cuvettes, and the absorbance measured at 405 nm using an Ultrospec 2000 spectrophotometer (Pharmacia Biotech, UK). All samples were assayed in triplicate for heat-treatment at each temperature. Error bars represent ± 1 standard deviation.

As shown by Figures 20, 21, and 22, the amount of product produced via GFP particle biocatalysis remains constant over a range of temperatures. However, the range of temperatures that GFP particles can produce consistent levels of product appears to be different depending on the enzyme that is displayed. The enzyme activity of GiCLO particles displaying the OpdA enzyme is the least stable with increasing temperatures as the production of *para*-nitrophenol drops steadily above 55˚C. The enzyme activity of GiCLN particles displaying the NanA enzyme remains consistent across almost all temperatures tested with Neu5Ac production decreasing significantly after 85˚C. The enzymatic activity of GiCLB particles displaying Bla(-ss) enzyme appears to be the most stable of all the enzyme-bearing GFP particles under investigation. Product levels remain consistent across all temperatures tested.

Fluorescent images of GFP particles treated at different temperatures were also obtained as described above (2.17.1), and are presented in Figures 23, 24, and 25.

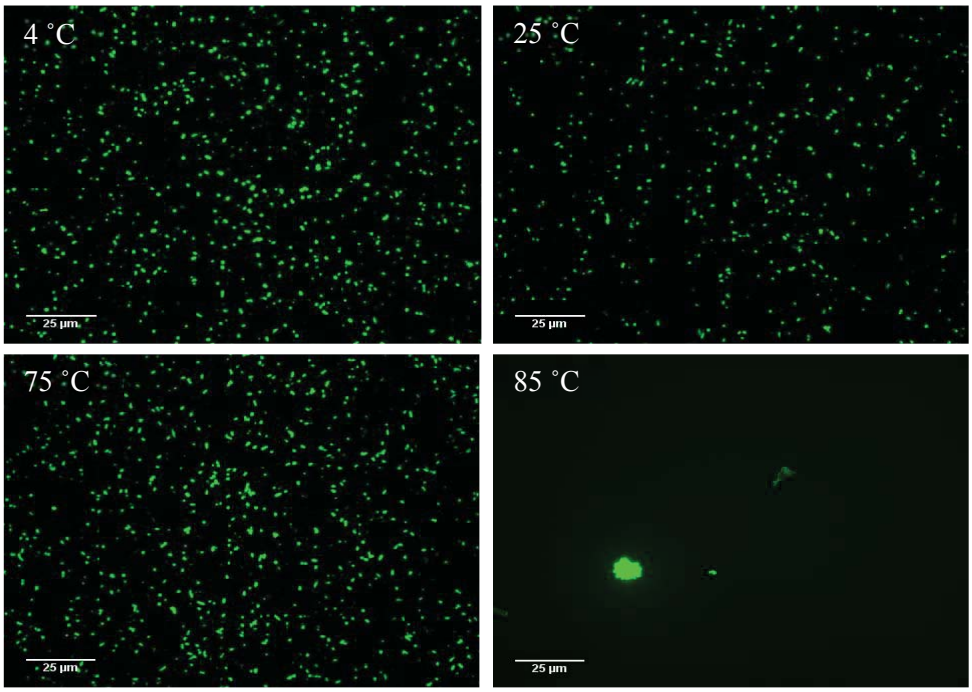

Figure 23. Fluorescent images of GiCLB particles after heat-treatment. GiCLB particles were heated for 10 min at the following temperatures: 4°C, 15°C, 25°C, 35°C, 45°C, 55°C, 65°C, 75°C, 85°C, and 95°C. Fluorescent images of the particles were obtained at 1000x magnification using a U-MWIBA2 Blue excitation filter cube fitted to an Olympus BX51 Fluorescent Light Microscope (Olympus Optical Co., Japan), an Optronics camera (Optronics, USA), and MagnaFire™ 2.1C Application software (Optronics, USA).

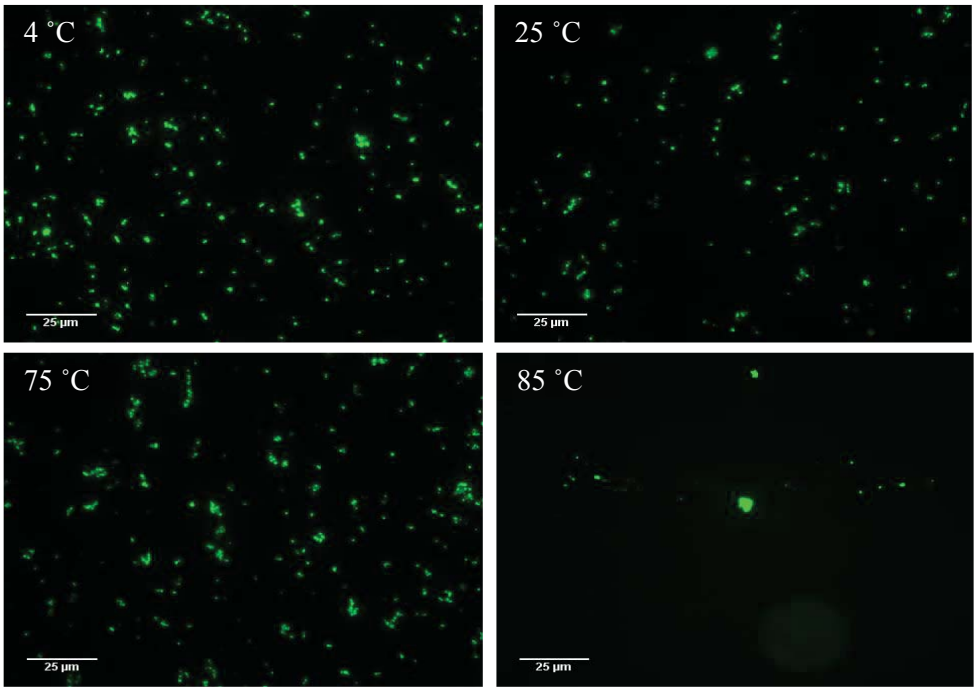

Figure 24. Fluorescent images of GiCLN particles after heat-treatment. GiCLN particles were heated for 10 min at the following temperatures: 4°C, 15°C, 25°C, 35°C, 45°C, 55°C, 65°C, 75°C, 85°C, and 95°C. Fluorescent images of the particles were obtained at 1000x magnification using a U-MWIBA2 Blue excitation filter cube fitted to an Olympus BX51 Fluorescent Light Microscope (Olympus Optical Co., Japan), an Optronics camera (Optronics, USA), and MagnaFire^{TM} 2.1C Application software (Optronics, USA).

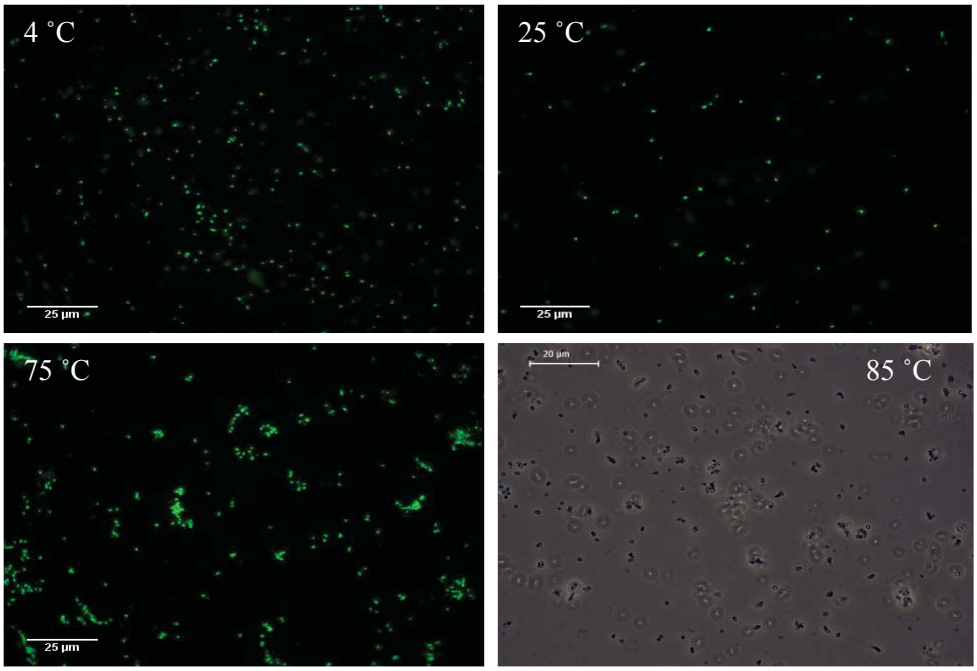

Figure 25. Fluorescent and Phase contrast images of GiCLO particles after heat-treatment. GiCLO particles were heated for 10 min at the following temperatures: 4°C, 15°C, 25°C, 35°C, 45°C, 55°C, 65°C, 75°C, 85°C, and 95°C. Fluorescent images of the particles were obtained at 1000x magnification using a U-MWIBA2 Blue excitation filter cube fitted to an Olympus BX51 Fluorescent Light Microscope (Olympus Optical Co., Japan), an Optronics camera (Optronics, USA), and MagnaFire^{TM} 2.1C Application software (Optronics, USA). The phase-contrast image of GiCLO particles after the 85 ˚C treatment was obtained at 1000x magnification using a Leica stereomicroscope.

All types of enzyme-bearing GFP particle retain their fluorescence after treatment with temperatures between 4˚C and 75˚C. However, at 85˚C fluorescence is lost, and although similar GFP particle shapes can be seen by phase-contrast microscopy it is not possible to determine whether they are in fact GFP particles. In contrast to fluorescence, the different types of enzyme-bearing GFP particle appear to be physically changed in different ways depending on temperature. First, the GiCLB particles retain their shape, size, and regular distribution between the temperatures that can be visualised by fluorescent microscopy. Second, the size of the GiCLN particles appears to be distributed across a larger range in comparison to the GiCLB particles, and as the temperature increases the GiCLN particles appear to aggregate. Third, the GiCLO particles retain similar distributions of size and shape between 4˚C and 75˚C. However, as the temperature increase they also appear to aggregate.

3.2.2 pH Stability

To assess pH stability, the GFP particles were pre-treated at pH ranging from 2 to 12 and their enzyme activity assessed as described above (2.21.3). The results are displayed in Figures 26, 27, and 28.

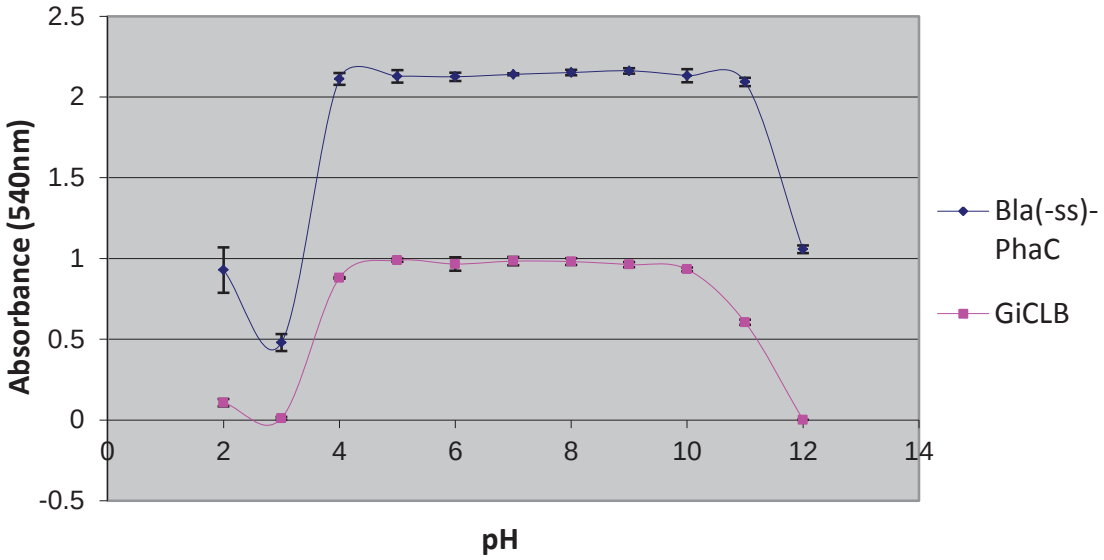

Figure 26. Production of maltose via Bla(-ss)-PhaC PHA bead and GiCLB particle biocatalysis after pH-treatment. Aliquots of Bla(-ss)-PhaC beads and GiCLB particles containing 50 µg of fusion protein were immersed for 10 min in buffers of the following pH: 2, 3, 4, 5, 6, 7, 8, 9, 10, 11, and 12. Following pH-treatment, the samples were washed with 20 mM Sodium phosphate buffer plus 6.7 mM Sodium chloride, pH 6.90, resuspended in their original volume, and then mixed with 1.0% (w/v) Soluble Starch solution (2.4.8) to a final reaction volume of 1.0 ml. The samples were then incubated under aerobic conditions at 25 ˚C, 200 rpm, for 12 h. Following incubation the samples were centrifuged at 16000 x g for 5 min, and 0.5 ml of supernatant was removed. The supernatants were then mixed with 0.5 ml of α-Amylase Colour Reagent Solution (2.4.7), and heated at 100 ˚C for 15min in a memmert OB 10 oil bath (memmert, Germany). After heating, the samples were cooled to room temperature (22 ˚C- 25 ˚C), and brought to a final volume of 6.0 ml with Milli-Q water. 1.0 ml of each sample was pipetted into separate 2-ml cuvettes, and the absorbance measured at 540 nm using an Ultrospec 2000 spectrophotometer (Pharmacia Biotech, UK). All samples, at each pH, were assayed in triplicate. Error bars represent ± 1 standard deviation.

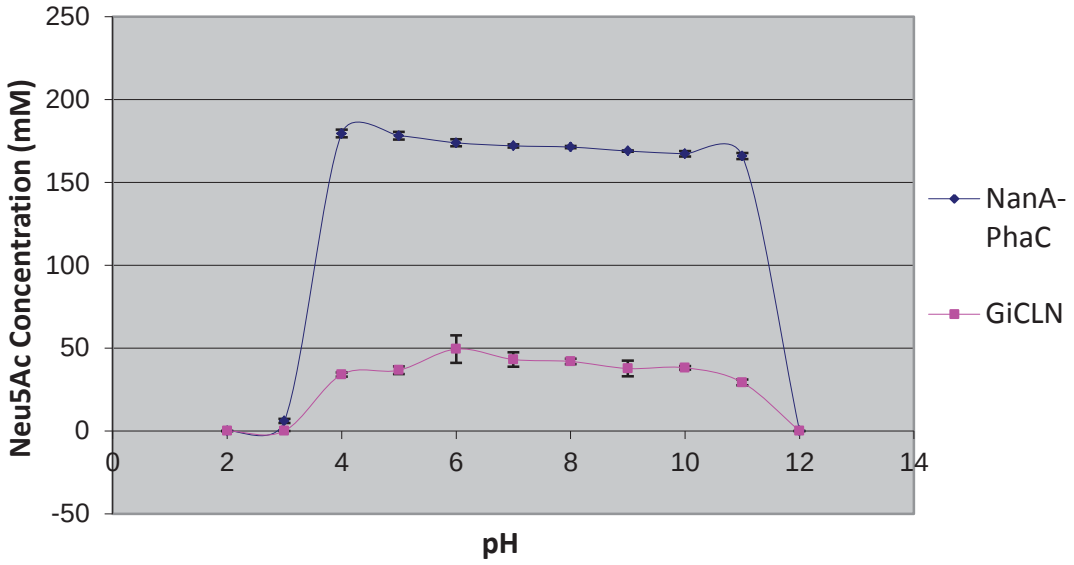

Figure 27. Production of Neu5Ac via NanA-PhaC PHA bead and GiCLN particle biocatalysis after pH-treatment. Aliquots of NanA-PhaC beads and GiCLB particles containing 25 µg of fusion protein were immersed for 10 min in buffers of the following pH: 2, 3, 4, 5, 6, 7, 8, 9, 10, 11, and 12. Following pH-treatment, the samples were washed with 50 mM Potassium phosphate buffer, pH 7.50, resuspended in their original volume, and then mixed with a substrate solution, which consisted of 0.2 M *N*-acetyl-D-mannosamine and 1.0 M Sodium pyruvate, to a final reaction volume of 0.5 ml. The samples were then incubated under aerobic conditions at 50 ˚C, 200 rpm, for 48 h. Following incubation the samples were centrifuged at 16000 x g for 10 min, and the supernatants removed. The supernatants were then diluted and analysed by HPLC (2.19). All samples, at each pH, were assayed in triplicate. Error bars represent ± 1 standard deviation.

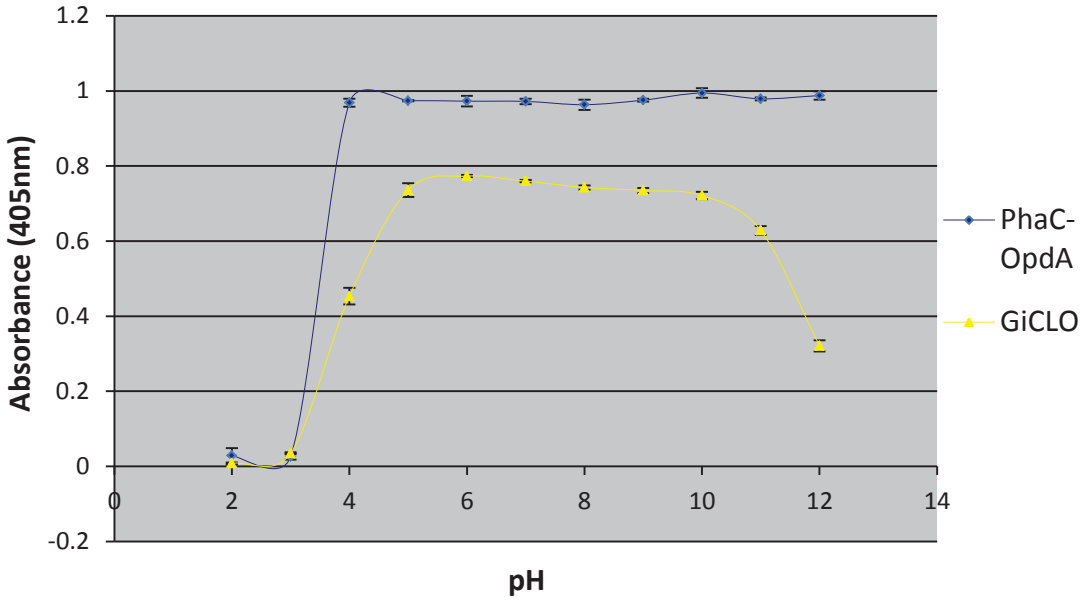

Figure 28. Production of *para*-nitrophenol via PhaC-OpdA PHA bead and GiCLO particle biocatalysis after pH-treatment. Aliquots of PhaC-OpdA beads and GiCLO particles containing 50 µg of fusion protein were immersed for 10 min in buffers of the following pH: 2, 3, 4, 5, 6, 7, 8, 9, 10, 11, and 12. Following pH-treatment, the samples were washed with 50 mM HEPES buffer, pH 8.00, resuspended in their original volume, and then mixed with 200 µM Methyl parathion substrate solution to a final reaction volume of 1.0 ml. The samples were then incubated under aerobic conditions at 25 ˚C, 200 rpm, for 12 h. Following incubation the samples were centrifuged at 16000 x g for 5 min, and the supernatants removed. The supernatants were then pipetted into separate 2-ml cuvettes, and the absorbance measured at 405 nm using an Ultrospec 2000 spectrophotometer (Pharmacia Biotech, UK). All samples, at each pH, were assayed in triplicate. Error bars represent ± 1 standard deviation.

The GFP particles tested share similar stability profiles after a range of pH-treatment. The enzyme activity of all types of particle is almost non-existent at the extremes of pH- pH 2,3, and 12; however, it rapidly increases at pH 4. This level of activity is relatively consistent between pH 5 and 10, and then begins to decrease. GiCLO particles exhibit the most stable activity at alkaline pH as *para*-nitrophenol can still be detected after treatment at pH 12. The production of maltose and Neu5Ac via GiCLB and GiCLN biocatalysis at this pH is undetectable. It is worth noting that the pattern of enzyme activity exhibited by the GFP particles is mostly shared by the PHA bead comparisons. Although the PHA beads show higher activity, this activity is significantly decreased, or non-existent, at the same extremes of pH, and maximum activity is observed through the same range.

Fluorescent images of GFP particles treated at different pH were also obtained as described above (2.12.1), and are presented in Figures 29, 30, and 31.

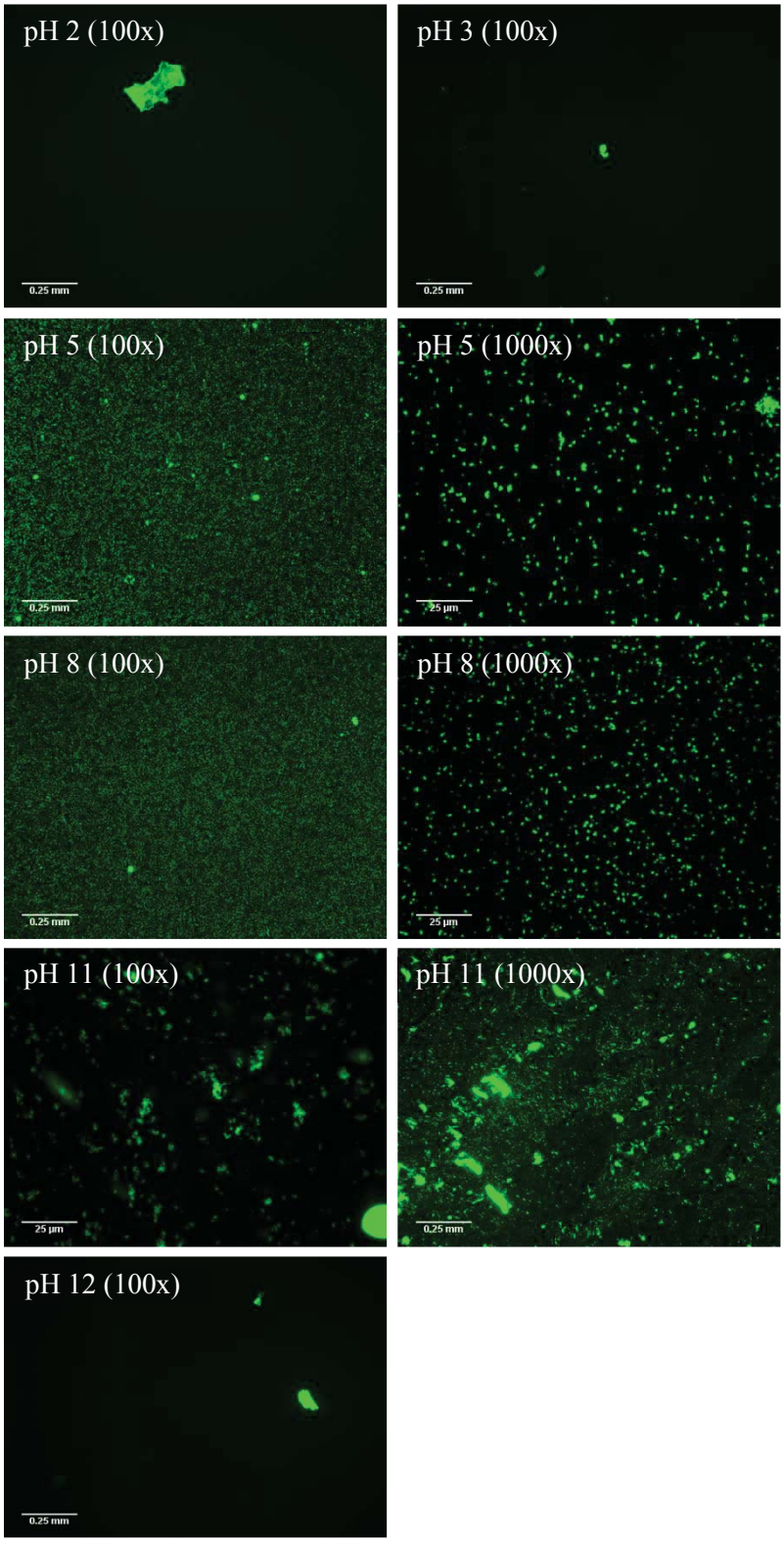

Figure 29. Fluorescent images of GiCLB particles after pH-treatment. GiCLB particles were immersed for 10 min in buffers of the following pH: 2, 3, 4, 5, 6, 7, 8, 9, 10, 11, and 12. Following pH-treatment, the samples were washed with 20 mM Sodium phosphate buffer plus 6.7 mM Sodium chloride, pH 6.90. Fluorescent images of the particles were obtained at 100x and 1000x magnification using a U-MWIBA2 Blue excitation filter cube fitted to an Olympus BX51 Fluorescent Light Microscope (Olympus Optical Co., Japan), an Optronics camera (Optronics, USA), and MagnaFire^{TM} 2.1C Application software (Optronics, USA).

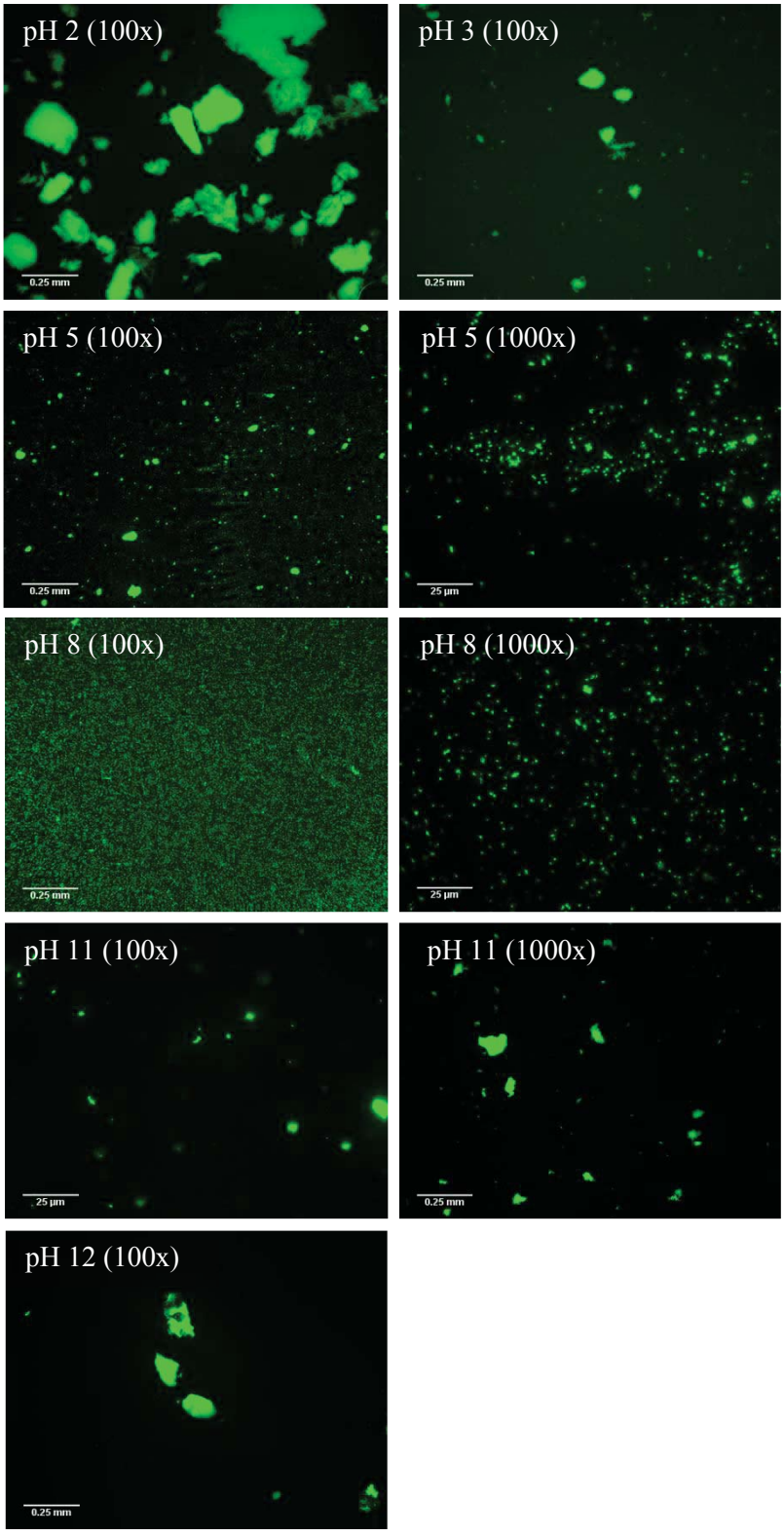

Figure 30. Fluorescent images of GiCLN particles after pH-treatment. GiCLN particles were immersed for 10 min in buffers of the following pH: 2, 3, 4, 5, 6, 7, 8, 9, 10, 11, and 12. Following pH-treatment, the samples were washed with 50 mM Potassium phosphate buffer, pH 7.50. Fluorescent images of the particles were obtained at 100x and 1000x magnification using a U-MWIBA2 Blue excitation filter cube fitted to an Olympus BX51 Fluorescent Light Microscope (Olympus Optical Co., Japan), an Optronics camera (Optronics, USA), and MagnaFire^{TM} 2.1C Application software (Optronics, USA).

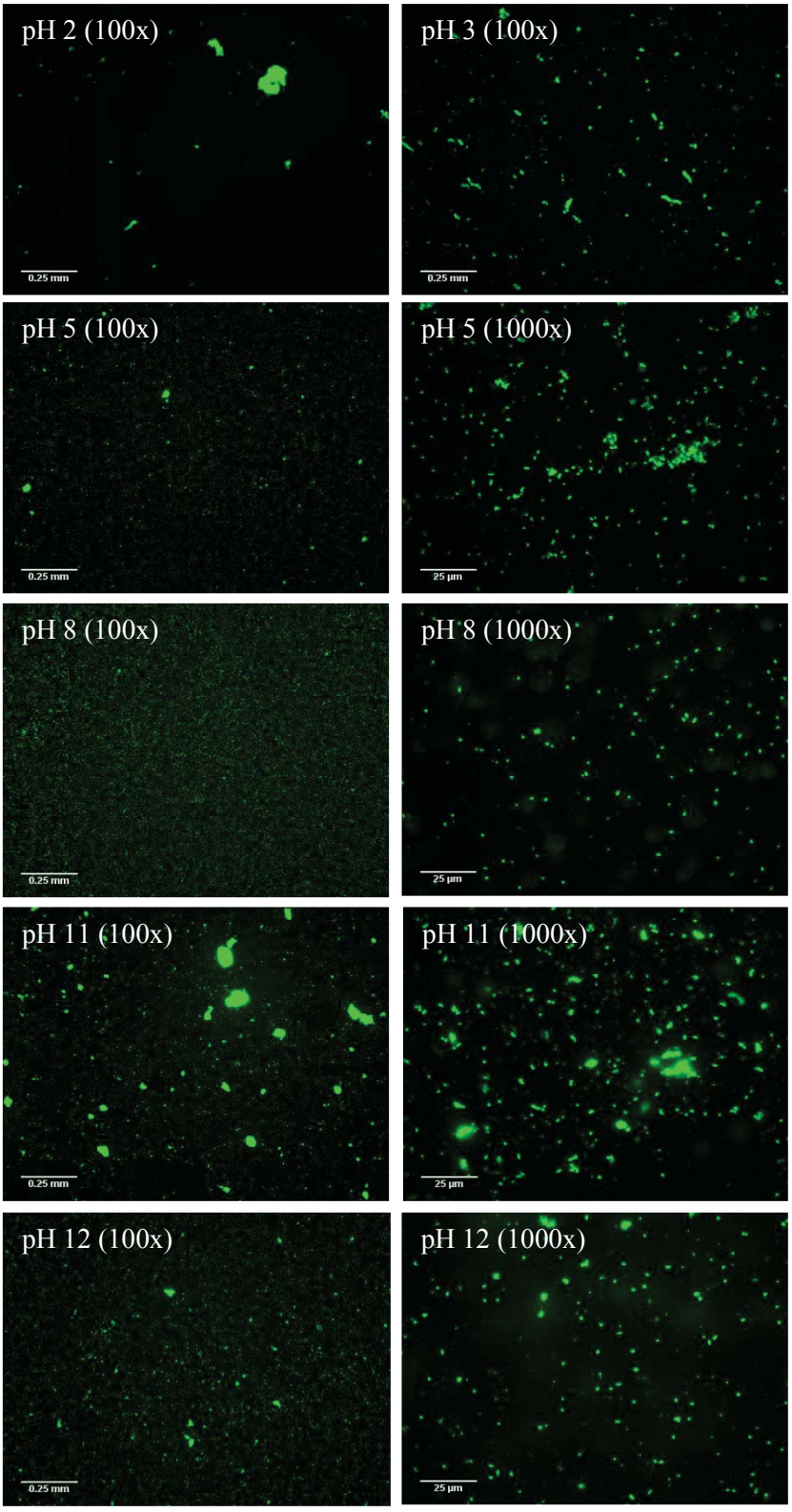

Figure 31. Fluorescent images of GiCLO particles after pH-treatment. GiCLO particles were immersed for 10 min in buffers of the following pH: 2, 3, 4, 5, 6, 7, 8, 9, 10, 11, and 12. Following pH-treatment, the samples were washed with 50 mM HEPES, pH 8.00. Fluorescent images of the particles were obtained at 100x and 1000x magnification using a U-MWIBA2 Blue excitation filter cube fitted to an Olympus BX51 Fluorescent Light Microscope (Olympus Optical Co., Japan), an Optronics camera (Optronics, USA), and MagnaFire™ 2.1C Application software (Optronics, USA).

In the same manner as how GFP particles share similarities in their activity profiles through a range of pH, they are also physically affected in similar ways. At pH 2, 3 and 12 single, fluorescent GFP particles cannot be observed, and in their place are fluorescent aggregates, presumably formed by the GFP particles. When the samples are centrifuged after treatment at these pH pellets do form; however, it is not certain whether the pellet is formed by intact GFP particles, partially dissolved particles, aggregates, or other types of debris. As the pH increases, however, single, fluorescent GFP particles can be observed, and the amount of aggregates diminishes. Around pH 11 the particles can be seen to aggregate; however, fluorescence is still retained. Despite these similarities there are also differences in the ways in which the GFP particles are affected by pH. GiCLB are affected as described above. However, at pH 2 and 3 significantly larger fluorescent aggregates can be seen in GiCLN samples, which are presumably formed by the GiCLN particles. As the pH increases the GiCLN particles behave as described above. At pH 2 and 3 small fluorescent aggregates can be observed in GiCLO samples. As the pH increases the aggregates decrease in size until only single, fluorescent GiCLO particles can be observed. Interestingly, at pH 11 and 12 fluorescent aggregates reappear; however, single, fluorescent GFP particles can still be observed.

3.2.3 Reusability

The GFP particles were tested for reusability. This was achieved by using the same incubation periods as for the temperature and pH stability assays, and repeating the activity assays with the same sample of particles for four cycles, as described above (2.21.4). The results of the reusability assays are displayed in Figures 32, 33, and 34.

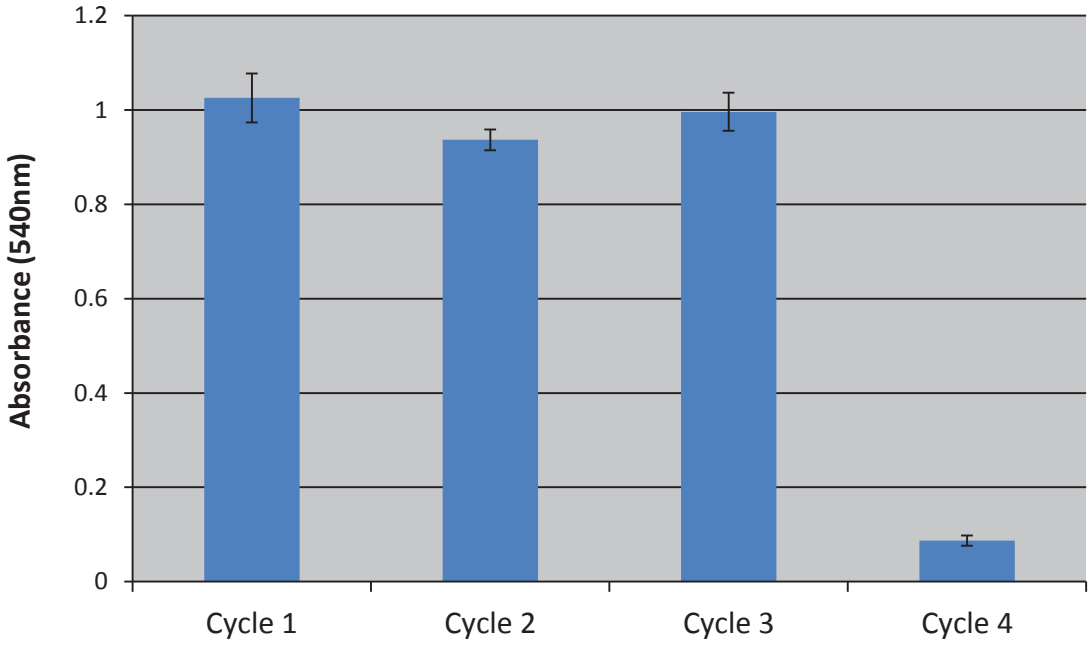

Figure 32. Production of maltose via GiCLB particle biocatalysis over four consecutive cycles. An aliquot of GiCLB particles that contained 50 µg of fusion protein was mixed with 1.0% (w/v) Soluble Starch substrate solution (2.4.8) to a final reaction volume of 1.0 ml. The sample was then incubated under aerobic conditions at 25 ˚C, 200 rpm, for 12 h. Following incubation the sample was centrifuged at 16000 x g for 5 min, and the supernatant removed. The pellet of GiCLB particles was resuspended in its original volume using 20 mM Sodium phosphate buffer plus 6.7 mM of Sodium chloride, pH 6.90, and then mixed with 1.0% (w/v) Soluble Starch substrate solution to a final reaction volume of 1.0 ml. The sample was then re-incubated as described above. 0.5 ml of the supernatant was mixed with 0.5 ml of α-Amylase Colour Reagent Solution (2.4.7), and heated at 100 ˚C for 15min in a memmert OB 10 oil bath (memmert, Germany). After heating the samples were cooled to room temperature (22 ˚C- 25 ˚C), and brought to a final volume of 6.0 ml with Milli-Q water. 1.0 ml of each sample was pipetted into separate 2-ml cuvettes, and the absorbance measured at 540 nm using an Ultrospec 2000 spectrophotometer (Pharmacia Biotech, UK). The above process was repeated for four cycles. The GiCLB particle sample was assayed in triplicate for each cycle. Error bars represent ± 1 standard deviation.

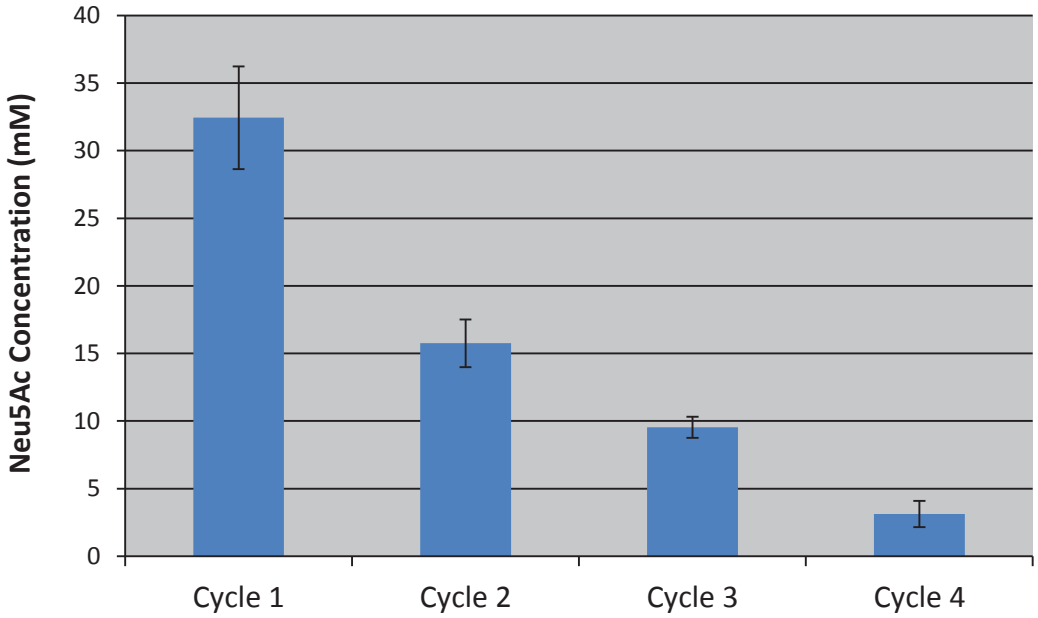

Figure 33. Production of Neu5Ac via GiCLN particle biocatalysis over four consecutive cycles. An **a**liquots of GiCLN particles that contained 25 µg of fusion protein was mixed with substrate solution, which consisted of 0.2 M *N*-acetyl-D-mannosamine (ManNAc) and 1.0 M Sodium pyruvate, to a final reaction volume of 0.5 ml. The samples were then incubated under aerobic conditions at 50 ˚C, 200 rpm, for 48 h. Following incubation the sample was centrifuged at 16000 x g for 10 min, and the supernatants removed. The pellet of GiCLN particles was resuspended in its original volume using 50 mM Potassium phosphate buffer, pH 7.50, and then mixed with 0.2 M ManNAc/ 1.0 M Sodium pyruvate substrate solution to a final reaction volume of 0.5 ml. The sample was then re-incubated as described above. The supernatant was diluted and analysed by HPLC (2.19). The above process was repeated for four cycles. The GiCLN particle sample was assayed in triplicate for each cycle. Error bars represent ± 1 standard deviation.

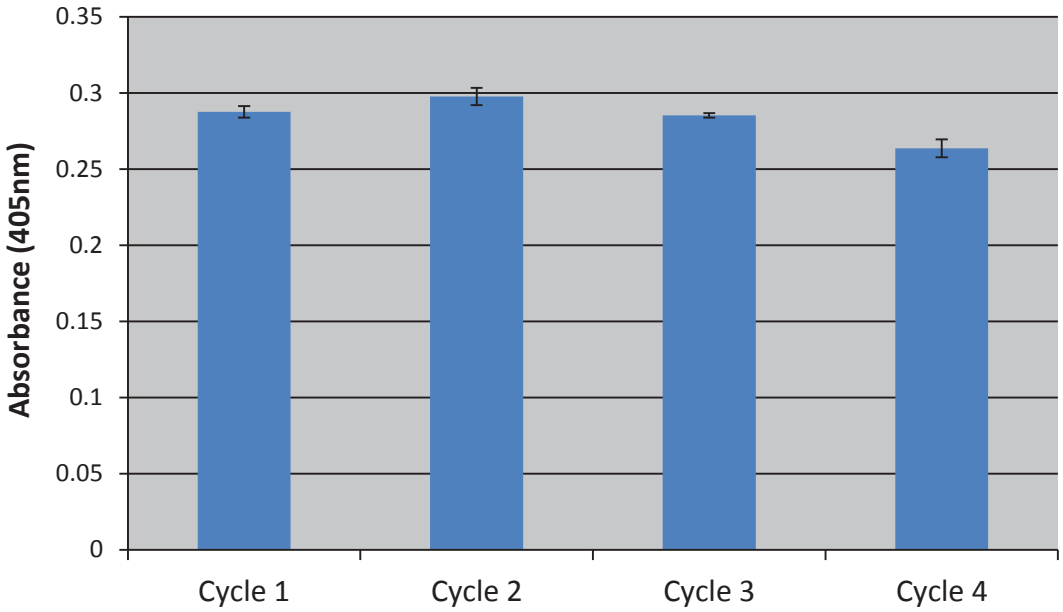

Figure 34. Production of *para*-nitrophenol via GiCLO particle biocatalysis over four consecutive cycles. An aliquot of GiCLO particles that contained 50 µg of fusion protein was mixed with 200 µM Methyl parathion substrate solution to a final reaction volume of 1.0 ml. The sample was then incubated under aerobic conditions at 25 ˚C, 200 rpm, for 12 h. Following incubation the sample was centrifuged at 16000 x g for 5 min, and the supernatant removed. . The pellet of GiCLO particles was resuspended in its original volume using 20% (v/v) Methanol in 50 mM HEPES buffer, pH 8.00, and then mixed with 200 µM Methyl parathion substrate solution to a final reaction volume of 1.0 ml. The sample was then re-incubated as described above. The supernatant was then pipetted into a 2-ml cuvette, and the absorbance measured at 405 nm using an Ultrospec 2000 spectrophotometer (Pharmacia Biotech, UK). The GiCLO particle sample was assayed in triplicate for each cycle. Error bars represent ± 1 standard deviation.

The GFP particles exhibited different activity profiles over the four consecutive cycles. The production of maltose via GiCLB particle biocatalysis is relatively constant over the first three cycles, but decreases significantly in the fourth cycle. In contrast, the production of Neu5Ac via GiCLN particle biocatalysis steadily decreases between each cycle. Finally, the production of *para*-nitrophenol via GiCLO particle biocatalysis remains consistent throughout all cycles with a slight decrease in production observable in the fourth cycle.

3.2.4 Long-term Storage Stability

Samples of each enzyme-bearing GFP particle were set aside and stored for long periods at 4 ˚C, room temperature (22 ˚C-25 ˚C) (R.T.), and -80 ˚C, as described above (2.16.5). This was done in order to reveal the optimal storage conditions in which to store extracted GFP particles, and the effect of this storage on enzyme activity. After the

storage period had ended, the particles were tested for activity. The results are displayed in Figures 35, 36, and 37.

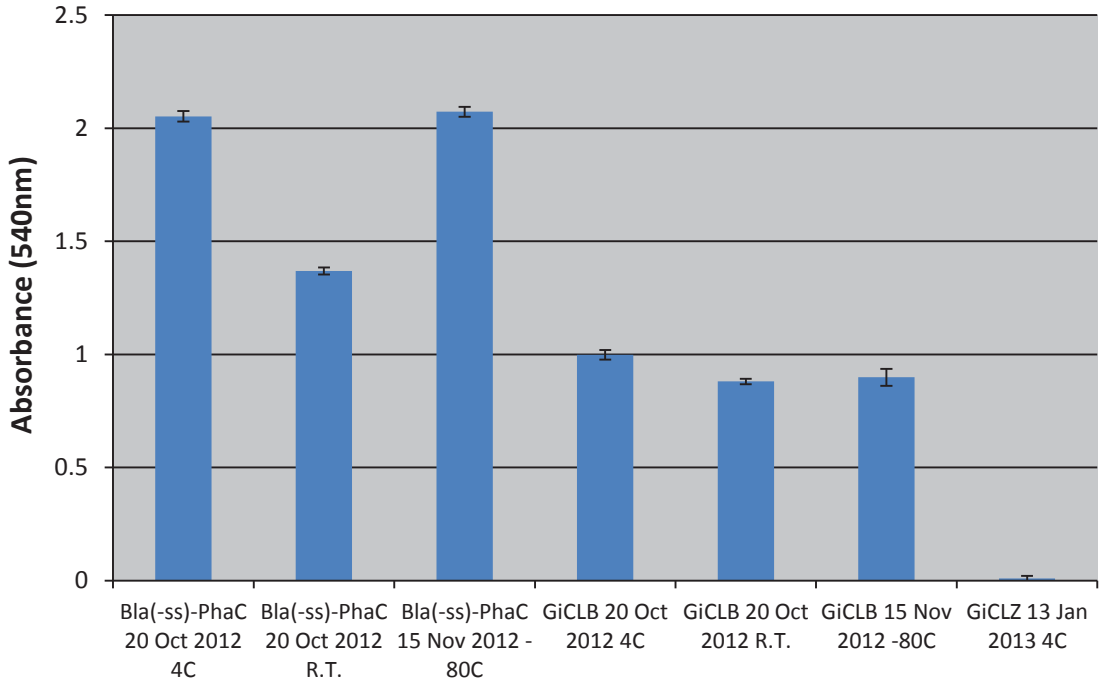

Figure 35. Production of maltose via Bla(-ss)-PhaC PHA bead and GiCLB particle biocatalysis after long-term storage at 4 ˚C, room temperature (22 ˚C- 25 ˚C) (R.T.), and -80 ˚C. Activity assays of Bla(-ss)-PhaC beads and GiCLB particles were conducted on the 23rd January 2013. This equates to a storage period of 95 days for samples stored from the 20th October 2012, and 69 days for samples stored from the 15th November 2012. Aliquots of each sample that contained 50 µg of fusion protein were mixed with 1.0% (w/v) Soluble Starch substrate solution (2.4.8) to a final reaction volume of 1.0 ml. The samples were then incubated under aerobic conditions at 25 ˚C, 200 rpm, for 12 h. Following incubation the samples were centrifuged at 16000 x g for 5 min, and 0.5 ml of supernatant was removed. The supernatants were then mixed with 0.5 ml of α-Amylase Colour Reagent Solution (2.4.7), and heated at 100 ˚C for 15min in a memmert OB 10 oil bath (memmert, Germany). After heating the samples were cooled to room temperature (22 ˚C- 25 ˚C), and brought to a final volume of 6.0 ml with Milli-Q water. 1.0 ml of each sample was pipetted into separate 2-ml cuvettes, and the absorbance measured at 540 nm using an Ultrospec 2000 spectrophotometer (Pharmacia Biotech, UK). All samples were assayed in triplicate. Error bars represent ± 1 standard deviation.

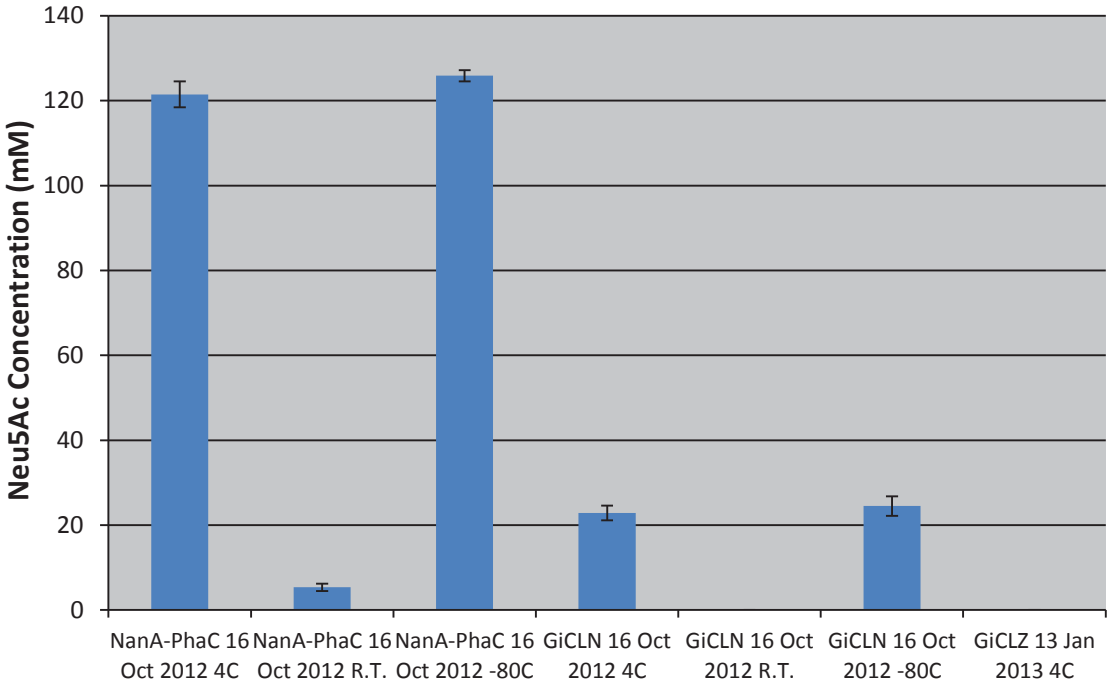

Figure 36. Production of Neu5Ac via NanA-PhaC PHA bead and GiCLN particle biocatalysis after long-term storage at 4 ˚C, room temperature (22 ˚C- 25 ˚C) (R.T.), and -80 ˚C. Activity assays of NanA-PhaC beads and GiCLN particles were conducted on the 21st January 2013. This equates to a storage period of 97 days for all samples. Aliquots of each sample that contained 25 µg of fusion protein were mixed with substrate solution, which consisted of 0.2 M *N*-acetyl-D-mannosamine (ManNAc) and 1.0 M Sodium pyruvate, to a final volume of 0.5 ml. The samples were then incubated under aerobic conditions at 50 ˚C, 200 rpm, for 48 h. Following incubation the samples were centrifuged at 16000 x g for 10 min, and the supernatants removed. The supernatants were then diluted and analysed by HPLC (2.19). All samples were assayed in triplicate. Error bars represent ± 1 standard deviation.

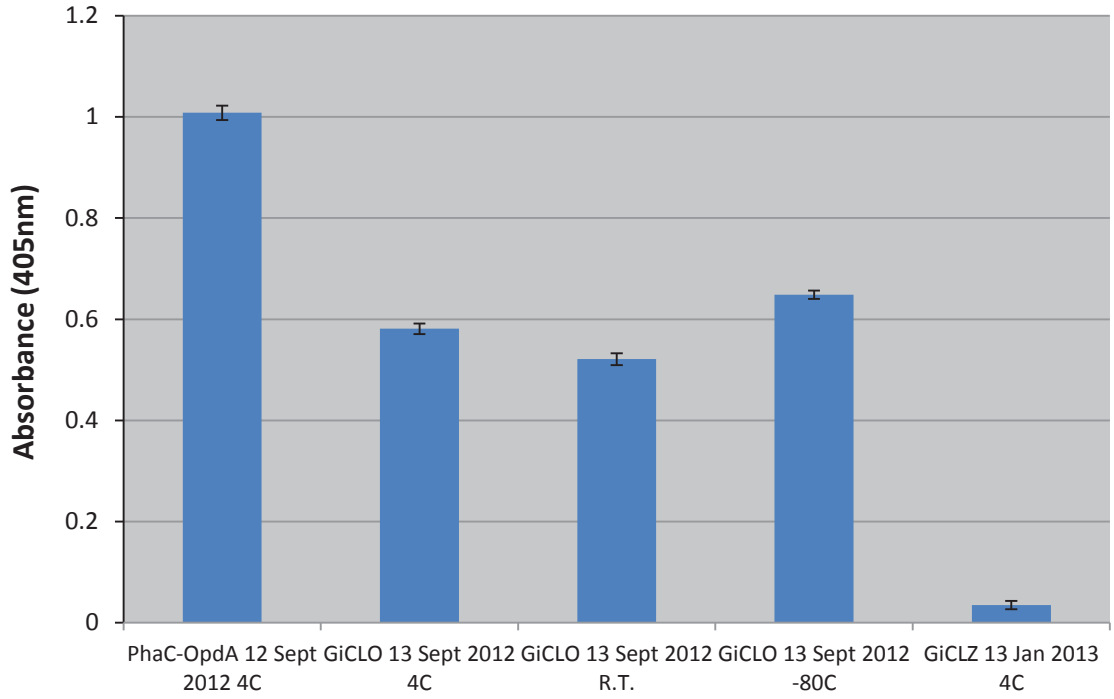

Figure 37. Production of *para*-nitrophenol via PhaC-OpdA PHA bead and GiCLO particle biocatalysis after long-term storage at 4 ˚C, room temperature (22 ˚C- 25 ˚C) (R.T.), and -80 ˚C. Activity assays of PhaC-OpdA beads and GiCLB particles were conducted on the 23rd January 2013. This equates to a storage period of 133 days for the PhaC-OpdA bead sample stored from the 12th September 2012, and 132 days for the GiCLO samples stored from the 13th September 2012. Aliquots of each sample that contained 50 µg of fusion protein were mixed with 200 µM Methyl parathion substrate solution to a final volume of 1.0 ml. The samples were then incubated under aerobic conditions at 25 ˚C, 200 rpm, for 12 h. Following incubation the samples were centrifuged at 16000 x g for 5 min, and the supernatants removed. The supernatants were then pipetted into separate 2-ml cuvettes, and the absorbance measured at 405 nm using an Ultrospec 2000 spectrophotometer (Pharmacia Biotech, UK). All samples were assayed in triplicate. Error bars represent ± 1 standard deviation.

The different types of enzyme-bearing GFP particle are affected in different ways by the long-term storage. The activity assays for Bla(-ss) and OpdA bearing PHA beads/ GFP particles were performed on the 23rd January 2013, while the activity assay for NanA bearing PHA beads/ GFP particles was performed on the 21st January 2013. First, the GiCLB 4˚C and room temperature samples were stored for a period of 95 days, while the -80˚C sample was stored for 69 days. Despite a difference of 26 days, the production of maltose via each sample is relatively constant. The average maltose absorbance values measured for the 4 ˚C, R.T., and -80 ˚C GiCLB particle samples after storage were 0.998, 0.880, and 0.899 (3s.f.), respectively. The Bla(-ss)-PhaC beads continue to exhibit higher activity in comparison to the GiCLB particles; however, the enzyme activity of Bla(-ss)-PhaC beads appears to be more unstable when stored at room temperature. The average maltose absorbance values measured for the 4 ˚C, R.T., and

-80 ˚C Bla(-ss)-PhaC bead samples after storage were 2.05, 1.37, and 2.07 (3s.f.), respectively. Second, all GiCLN samples were stored for a period of 97 days. However, there are significant differences in Neu5Ac production. The 4˚C and -80˚C samples were able to catalyse the production of similar amounts of Neu5Ac; however, the production of Neu5Ac via GiCLN particles stored at room temperature was not measurable. The average quantities of Neu5Ac catalysed by the 4 ˚C and -80 ˚C GiCLN particle samples after storage were 22.8 mM and 24.5 mM (3s.f.), respectively. This pattern is repeated in the NanA-PhaC bead samples where, again, the 4˚C and -80˚C samples catalyse the production of similar amounts of Neu5Ac, while production via beads stored at room temperature is significantly diminished. The average quantities of Neu5Ac catalysed by the 4 ˚C, R.T., and -80 ˚C NanA-PhaC bead samples after storage were 121 mM, 5.34 mM, and 126 mM (3s.f.), respectively. Third, PhaC-OpdA beads were stored for a period of 133 days, while the GiCLO particle samples were stored for a period of 132 days. As shown in Figure 37, the GiCLO samples were able to catalyse the production of similar amounts of *para*-nitrophenol. The average *para*-nitrophenol absorbance values of the 4 ˚C, R.T., and -80 ˚C GiCLO particle samples after storage were 0.581, 0.521, and 0.648 (3s.f.), respectively. Unfortunately, no PhaC-OpdA bead room temperature or -80 ˚C samples were set aside. However, the sample stored at 4 ˚C continued to produce higher amounts of *para*-nitrophenol in comparison to the GiCLO particles. The average *para*-nitrophenol absorbance value of this sample was 1.01 (3s.f.).

Fluorescent images of GFP particles after long-term storage were also obtained as described above (2.17.1), and are presented in Figures 38, 39, and 40.

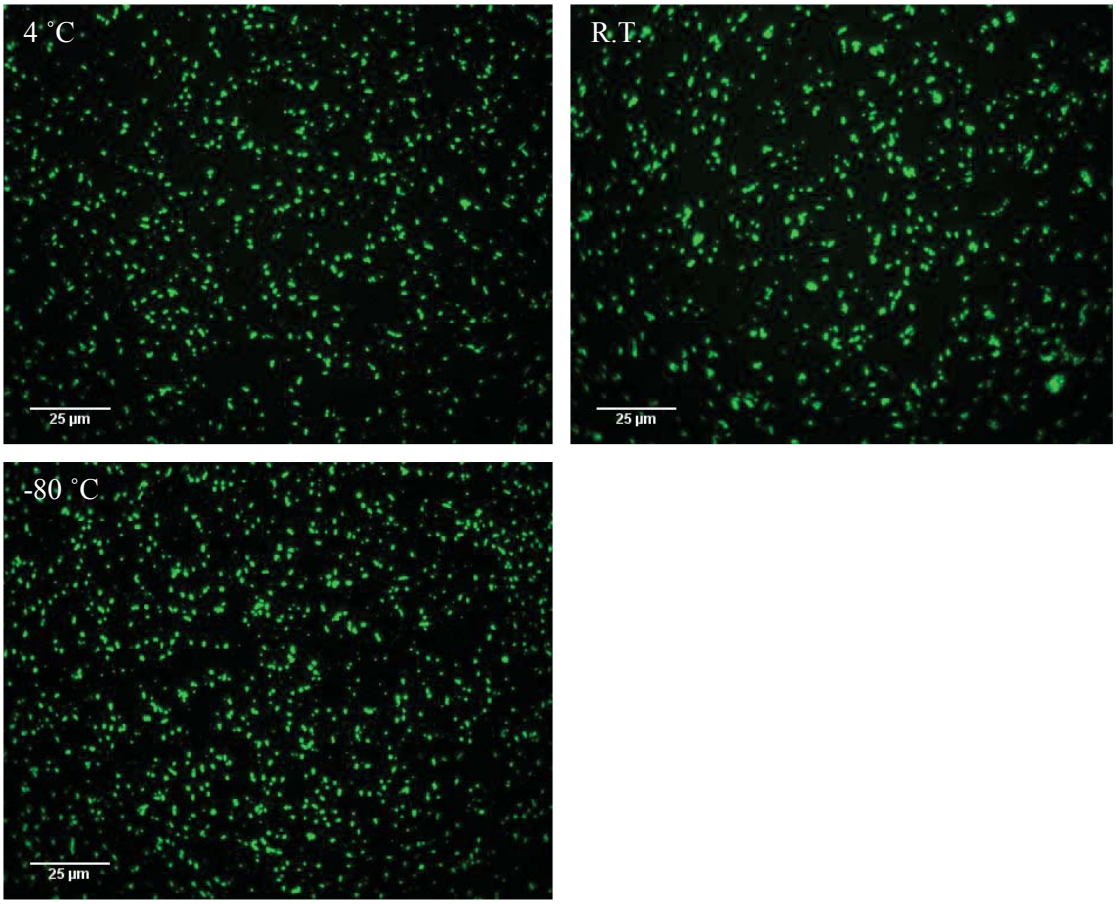

Figure 38. Fluorescent images of GiCLB particles after long-term storage at 4 ˚C, room temperature (22 ˚C-25 ˚C) (R.T.), and -80 ˚C. Aliquots of GiCLB particles were stored for 95 days at 4 ˚C and at room temperature (22 ˚C- 25 ˚C) (R.T.) in 20% (v/v) Ethanol in 50 mM Potassium phosphate buffer. An aliquot was also stored for 69 days at -80 ˚C in 25% (v/v) Glycerol in 50 mM Potassium phosphate buffer. Fluorescent images of the particles were obtained at 1000x magnification using a U-MWIBA2 Blue excitation filter cube fitted to an Olympus BX51 Fluorescent Light Microscope (Olympus Optical Co., Japan), an Optronics camera (Optronics, USA), and MagnaFire^{TM} 2.1C Application software (Optronics, USA).

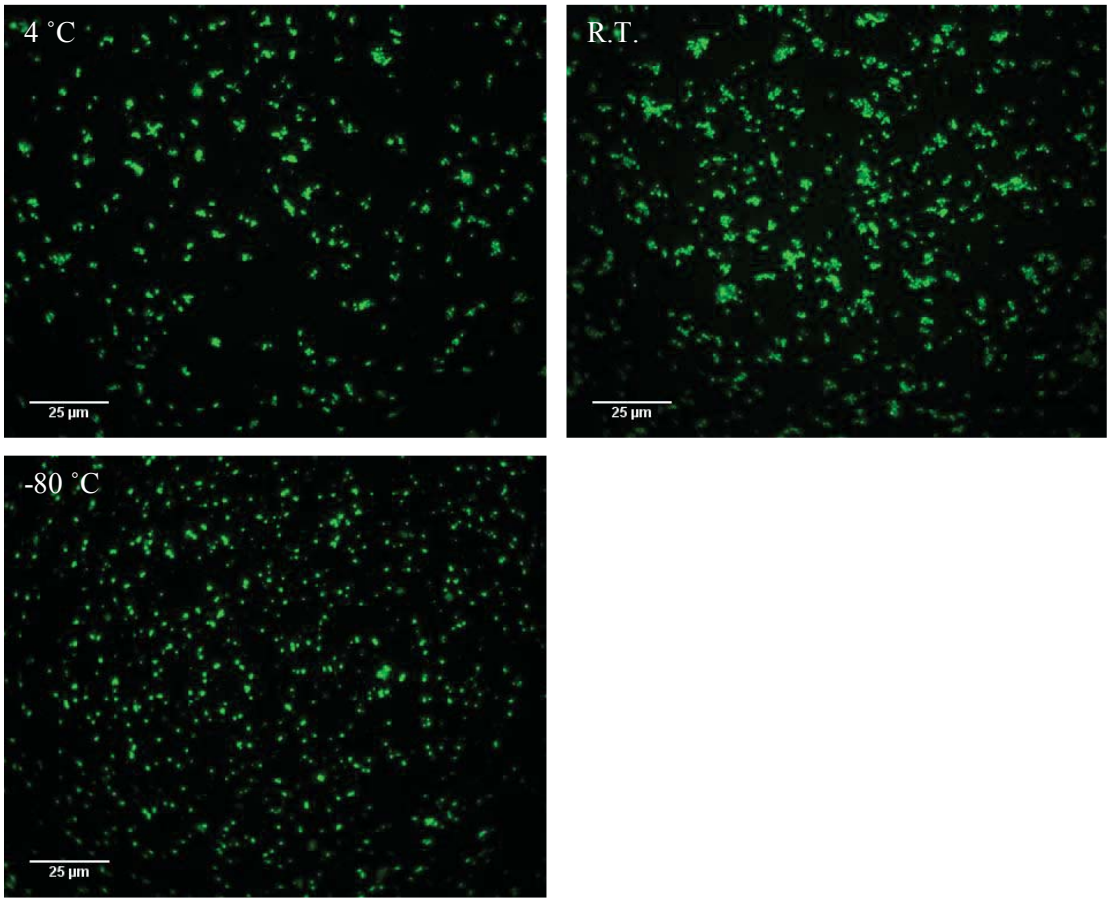

Figure 39. Fluorescent images of GiCLN particles after long-term storage at 4 ˚C, room temperature (22 ˚C-25 ˚C), and -80 ˚C. Aliquots of GiCLN particles were stored for 97 days at 4 ˚C and at room temperature (22 ˚C- 25 ˚C)(R.T.) in 20% (v/v) Ethanol in 50 mM Potassium phosphate buffer, and at -80 ˚C in 25% (v/v) Glycerol in 50 mM Potassium phosphate buffer. Fluorescent images of the particles were obtained at 1000x magnification using a U-MWIBA2 Blue excitation filter cube fitted to an Olympus BX51 Fluorescent Light Microscope (Olympus Optical Co., Japan), an Optronics camera (Optronics, USA), and MagnaFire™ 2.1C Application software (Optronics, USA).

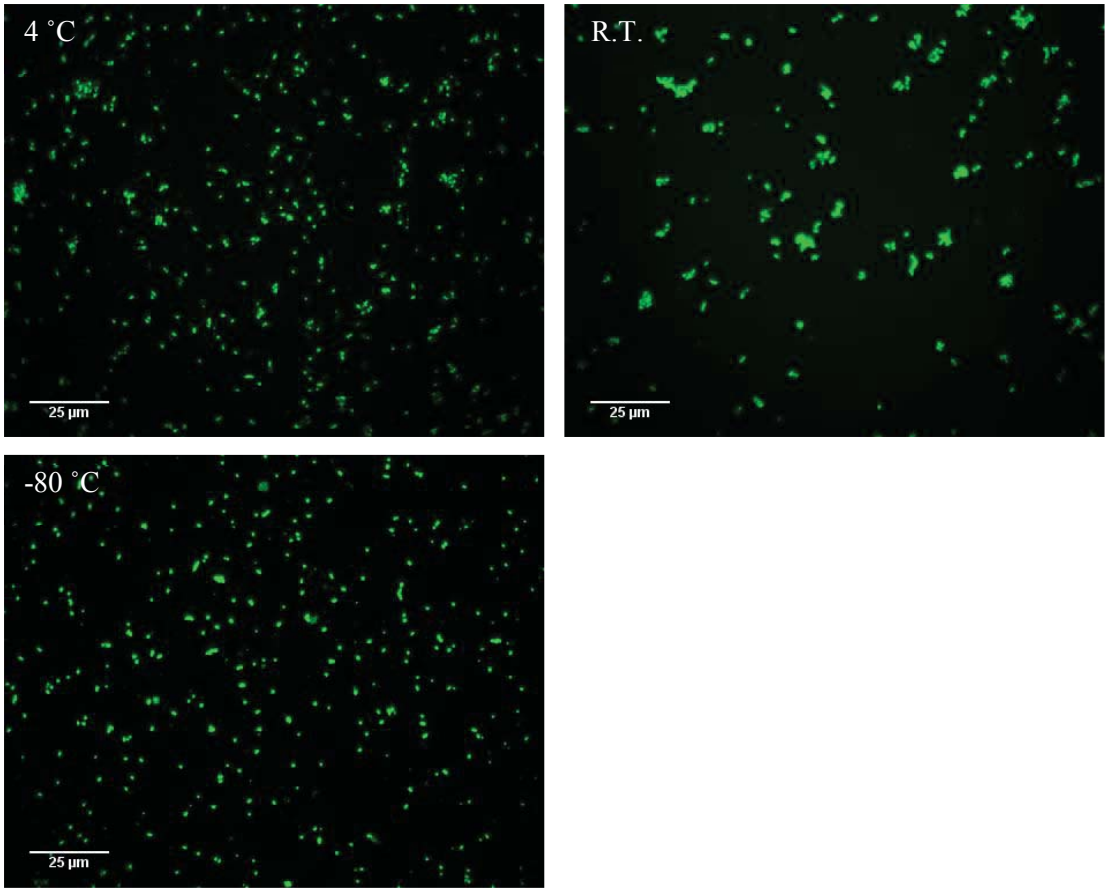

Figure 40. Fluorescent images of GiCLO particles after long-term storage at 4 ˚C, room temperature (22 ˚C- 25 ˚C) (R.T.), and -80 ˚C. Aliquots of GiCLO particles were stored for 132 days at 4 ˚C and at room temperature (22 ˚C- 25 ˚C) (R.T.) in 20% (v/v) Ethanol in 50 mM Potassium phosphate buffer, and at -80 ˚C in 25% (v/v) Glycerol in 50 mM Potassium phosphate buffer. Fluorescent images of the particles were obtained at 1000x magnification using a U-MWIBA2 Blue excitation filter cube fitted to an Olympus BX51 Fluorescent Light Microscope (Olympus Optical Co., Japan), an Optronics camera (Optronics, USA), and MagnaFire^{TM} 2.1C Application software (Optronics, USA).

The enzyme-bearing GFP particles are affected differently by long-term storage and the storage conditions. First, between storage conditions there appears to be little difference in the physical state of GiCLB particles. All samples contained particles that were randomly distributed throughout the field with perhaps a slight increase in aggregation observable in the room temperature sample. Second, GiCLN particles appear to be prone to aggregation when stored at 4˚C and room temperature, with more aggregation observable in the room temperature sample. GiCLN particles stored at -80˚C appear to be the most randomly distributed, and, perhaps, larger in size. Third, slight aggregation is observable in the GiCLO sample stored at 4˚C with most aggregation seen in the

room temperature sample. Again, the GiCLO -80˚C sample appears to have the most randomly distributed single particles which, perhaps, are of a larger size.

Throughout this study the enzyme activity and physical characteristics exhibited by the enzyme-bearing GFP particles were assessed on several fronts. First, in terms of their ability to form and display enzyme, it has been shown that using the methodology outlined above it is possible to produce particles consisting of GFP fusion proteins which can also display active enzyme. Second, in terms of the level of enzyme activity exhibited and stability throughout a range of treatments, it has been shown that each type of enzyme-bearing GFP particle behaves differently. These GFP particles, and their individual characteristics, could be useful for a variety of industrial processes, and there is the possibility of engineering them further in order to improve performance for a particular purpose.

CHAPTER FOUR: DISCUSSION

Inclusion bodies are more than aggregates of misfolded and inactive protein. It has been demonstrated that inclusion bodies consist of homologous proteins that display a range of structural conformations, including correctly folded and active proteins (Garcia-Fruitos et al., 2005; Garcia-Fruitos et al., 2011; Peternel & Komel, 2011). This realisation has changed how inclusion bodies are perceived, and has led to numerous studies that explore their potential in industrial processes (Garcia-Fruitos et al., 2012). This study has focused on a unique type of fluorescent inclusion body formed from GFP fusion proteins (GFP particles). GFP particles were first investigated by Jahns *et al.* (2011). In this study the formation of GFP particles was shown to be reliant on a short N-terminal extension of GFP and a C-terminal extension of GFP consisting of a polyester synthase (PhaC), or a *N*-acetyl-D-neuraminic acid aldolase (NanA). Furthermore, GFP particles were able to display functional binding sites that compete favourably with similar commercial products. Using this study as a foundation, the focus of this thesis has been to explore the potential of GFP particles to immobilise and display active enzyme. The demonstration of active enzyme-bearing GFP particles would deepen knowledge concerning GFP particle formation, as well as highlight their potential use in industrial biocatalysis processes.

4.1 GFP fusion proteins containing enzymes are capable of forming GFP particles

The enzymes chosen for this study were: an α-amylase lacking its signal sequence (Bla(-ss)); an *N*-acetyl-D-neuraminic acid aldolase (NanA); and an organophosphohydrolase (OpdA). These enzymes were chosen to demonstrate the versatility of GFP particles in displaying enzymes that catalyse different types of reactions, and which consist of different quaternary structure- Bla(-ss) is a monomer; NanA is a tetramer; and OpdA is a dimer. The enzymes were fused to the C-terminus of extGFP-PhaC(C319A) fusion proteins which were then overexpressed from pET14b vectors in *E. coli* BL21(DE3) host cells under the control of the strong T7 promoter. The inactive PhaC (PhaC(C319A)) was chosen to be the central domain of the fusion protein as it has been shown to facilitate the formation of only proteinaceous GFP particles, even in the presence of the PhaC substrate (*R*)-3-hydroxyacyl-CoA (Jahns et al., 2013). In all three instances (Fig. 10 & 16), fluorescent GFP particles were able to

form. This is interesting due to the conformational requirements for GFP fluorescence. GFP fluorescence is generated by a hexapeptide chromophore consisting of the amino acids Phe64-Ser65-Tyr66-Gly67-Val68-Gln69 with autocatalytic cyclisation occurring between Ser65-Tyr66-Gly67 (Zimmer, 2002). The structure of the entire GFP molecule is important in creating the correct environment for this cyclisation to occur (Zimmer, 2002). It has been shown through deletion experiments that most of the GFP protein is required in order to form the chromophore and achieve fluorescence (Dopf & Horiagon, 1996). Therefore, it is reasonable to assume that fusing GFP to other proteins with complex structure, such as enzymes, would disrupt the precise folding of GFP required for fluorescence. The GFP fusion proteins used in this study consisted of three sections: the extended enhanced GFP protein at the N-terminus; the dimeric PhaC enzyme or tetrameric NanA enzyme as the central domain; and either Bla(-ss), NanA, or OpdA at the C-terminus. With three sections folding simultaneously, and within close proximity, one would assume that each section would disrupt the folding of the others through steric hindrance. Furthermore, Jahns *et al* observed in their study that different C-terminal functionalities could encourage or discourage the formation of GFP particles. However, as shown in this study, the GFP molecules were able to fold correctly to emit fluorescence, and the enzyme-bearing GFP fusion proteins were able to aggregate to form GFP particles as observed by fluorescence microscopy.

Further work is required in order to completely explain the formation process and structure of enzyme-bearing GFP particles. First, Transmission Electron Microscopy (TEM) and Scanning Electron Microscopy are necessary to determine the exact dimensions and texture of the particles. The texture of GFP particles is particularly important as porous particles can be expected to permit efficient mass transfer of substrate to active enzyme within the particles. (Garcia-Fruitos et al., 2012). Furthermore, the internal structure of GFP particles needs to be examined using techniques such as infra-red spectroscopy, and circular dichroism. Such investigations would determine the organisation of proteins within GFP particles, and show whether they share similar structural properties, such as amyloid-like cross-molecular β-sheet formations, as other types of inclusion body (M. Carrio et al., 2005; Garcia-Fruitos et al., 2012). Second, the formation of GFP particles inside *E. coli* BL21 (DE3) cells needs to be monitored over time to determine the mechanism by which GFP particles form. Fluorescent microscopy images show that enzyme-bearing GFP particles exhibit a

similar shape and distribution in comparison to other types of inclusion body. The particles appear to be casts of the inside of their host cell, and only one or two particles can be found in each cell, attributes observed for other types of inclusion bodies (Peternel & Komel, 2011). However, a more detailed examination of GFP particle formation over time would be beneficial not only in terms of explaining GFP particle formation, but also in terms of a general model for inclusion body formation. Third, GFP particle formation conditions need to be examined in more depth. The conditions used in this study were shown by Jahns *et al.* to be able to facilitate the formation of GFP particles. However, previous studies have shown that inclusion body formation, and the quality of their constituent proteins, is influenced by a variety of factors including: promoter strength; the genetic background of host cells; culture conditions; and particle extraction methods (Garcia-Fruitos, 2010; Garcia-Fruitos et al., 2009; Peternel & Komel, 2011). Each feature of GFP particle production can be optimised in order to produce particles that exhibit different or improved properties.

4.2 GFP particles are capable of displaying active enzyme

GFP fusion proteins containing enzyme can not only self-aggregate into fluorescent GFP particles, but they can also immobilise and display active enzyme. All three types of enzyme-bearing GFP particles were able to exhibit the activity of their constituent enzymes. This adds more complexity to the manner in which GFP particles form, as not only can the delicate chromophore of GFP successfully form to emit fluorescence, but enzymes of differing quaternary structure can also fold correctly to exhibit activity. The strength of activity, however, appears to be dependent on the position of the enzyme within the GFP fusion protein, and on the type of enzyme displayed.

As mentioned in Chapter Three, initial tests were conducted with GFP particles displaying NanA. Three different types of GFP fusion protein were assessed for their ability to form GFP particles, and whether the resultant particles could exhibit NanA activity, as measured by Neu5Ac production. Within these fusion proteins NanA was situated as the central domain (GNLZ), as the C-terminus (GiCLN), and as a central domain/ C-terminus double fusion (GNLN). As shown in Figure 12, after 16 hours and 48 hours of incubation GFP particles consisting of GiCLN fusion proteins produced the highest quantity of Neu5Ac, and, therefore, exhibited the strongest enzyme activity. The

next strongest activity was exhibited by GNLZ particles, while the weakest activity was exhibited by GNLN particles. This difference in activity could be due to several reasons. First, placing NanA at the C-terminus could make it more available to substrate. At this position is has more opportunity to be displayed at the surface of GFP particles and in the correct orientation. Other studies have shown that the enzyme lipase is more active when it is surface displayed, and its active site is directed towards substrate (Brady et al., 2008). Furthermore, at the C-terminus the enzyme could have more space to fold correctly as it is only attached at one end to another potentially hindering protein. Second, placing NanA as the central domain could restrict its access to substrate, as well as limit its ability to fold correctly. It is interesting that NanA activity could be observed from GNLZ particles as it is 'sandwiched' between two other proteins which one would assume would disrupt the folding of the NanA subunits. Perhaps disruption did occur, but was not sufficient to abolish activity. NanA access to substrate for GNLZ particles could also be restricted and lead to decreased activity due to the increased probability of it being buried within the GFP particles, or surface displayed in an unfavourable orientation. The observation that NanA can fold to an active state when positioned as the central domain has implications for GiCLN particles. In GiCLN particles, NanA is fused to the C-terminus of an inactive PhaC (PhaC(C319A)) where the mutation occurs at a cysteine residue at the active site that is essential for PhaC activity (Jahns et al., 2013). This does not mean that the structure of PhaC is affected in a dramatic way, and so it is possible that it can still fold into its dimeric form. Fusing NanA to another enzyme that exhibits such quaternary structure could hinder its own conformation and lead to decreased activity. In addition, GNLZ has already been shown to exhibit excellent IgG binding activity via the ZZ domain (Jahns et al., 2013). The fact that it can also exhibit enzyme activity could lead to novel applications where targeting and catalysis are required. For example, using binding domains to target GFP particles to tumour cells where the enzyme activates a pro-drug to destroy the tumour. Third, it is probable that fusing two complex enzymes adjacent to one another, as in GNLN particles, would cause enough steric hindrance to disrupt protein folding. The decreased activity exhibited by GNLN particles in comparison to GNLZ and GiCLN particles is indicative of this effect. However, it is interesting that the GFP within GNLN particles can still fluoresce despite its fusion to two complex enzymes. It appears that locating enzymes at the C-terminus of GFP fusion proteins is optimal for correct protein folding. The results of this initial study laid the foundation

for the production of further enzyme-bearing GFP particles. Due to the strong activity exhibited by GiCLN particles it was decided to position other enzymes at the C-terminus of extGFP-PhaC(C319A) fusion proteins. Presumably, this would increase the probability of successfully displaying other active enzymes that exhibit the highest possible activity. As stated previously, N-terminal fusions of enzymes were not investigated in order to utilise the GFP particle promoting effect of the N-terminal extension of GFP. It is possible that an N-terminal fusion of enzyme to GFP could produce GFP particles that exhibit enzyme activity. However, this possibility and the level of enzyme activity needs to be investigated.

As mentioned above, all enzyme-bearing GFP particles assessed in this study exhibited the activity of their constituent enzymes. This can be observed by increases in product that are measured by changes in absorbance as detected by spectrophotometer, or UV detection as detected by HPLC. However, the strength of activity appears to be dependent on the type of enzyme. GiCLB and GiCLO particles catalysed the highest rates of product synthesis, thereby exhibiting the strongest enzyme activity of enzyme-bearing GFP particles (Fig. 17 & 19). Both types were able to catalyse their reactions to their end-points within 72 hours, while GiCLN particles did not complete their reaction within this timeframe (Fig. 18). The reason for this difference in the strength of enzyme activity could be due to differences in quaternary structure. Bla(-ss) and OpdA are monomeric and dimeric enzymes, respectively. NanA is a tetramer, so it is possible that Bla(-ss) and OpdA have more capacity to fold correctly due to decreased structural complexity, and so exhibit higher enzyme activity. However, it must be noted that the difference in activity is most probably due to the type of reaction that each enzyme catalyses and the affinity that each enzyme has for its substrate. Both Bla(-ss) and OpdA are hydrolysing enzymes which cleave the α-1,4 glycosidic and phosphotriester bonds in their substrates, respectively. In contrast, the reaction investigated for NanA in this study involves the condensation of two substrates, *N*-acetyl-D-mannosamine (ManNAc) and Sodium pyruvate, to produce *N*-acetyl-D-neuraminic acid (Neu5Ac). Although NanA can catalyse the reaction in both directions, the reaction investigated in this study is the least favourable, but important for the production of Neu5Ac for the manufacture of pharmaceuticals. The K_M value for free BLA enzyme for starch is 9.6 μM, while the K_M value for free OpdA enzyme for Methyl parathion is 160 μM (Blatchford et al., 2012; Shewale & Pandit, 2007). In contrast, the K_M value for NanA for ManNAc is 0.7

M (Kragl, Gygax, Ghisalba, & Wandrey, 1991). Therefore, the affinity of Bla(-ss) and OpdA for their respective substrates is much higher than NanA for ManNAc, and so the rate of catalysis will also be much higher. Comparing the rate of Neu5Ac hydrolysis to the Bla(-ss) and OpdA catalysed reactions would be more appropriate, although the K_M value of NanA for Neu5Ac is 3.3 mM (Aisaka, Igarashi, Yamaguchi, & Uwajima, 1991). This is still much higher than the K_M values for Bla(-ss) and OpdA, and a slower reaction is also expected. In any case, further research into the structure of enzyme-bearing GFP particles is required to determine how enzyme is displayed, and how the particles could be engineered to optimise enzyme activity.

A feature shared by all enzyme-bearing GFP particles used in this study is their weaker activity in comparison to PHA bead controls. The PHA bead controls served as established and peer-reviewed functional inclusion bodies to which GFP particles could be compared. The time periods required for the PHA beads and GFP particles to catalyse reactions to their the end-points are displayed in Table 10.

Table 10. The duration of incubation required for enzyme-bearing PHA beads and GFP particles to catalyse reactions to their end-points.

Type of Particle	**Length of Incubation (h)**
Bla(-ss)-PhaC PHA beads	12
GiCLB particles	48
NanA-PhaC PHA beads	~35
GiCLN particles	>72
PhaC-OpdA PHA beads	4
GiCLO particles	72

These differences in strength of activity could be attributable to differences in the way in which PHA beads and GFP particles form, and the resultant display of enzyme. Fusion of different functionalities to the polyester synthase (PhaC) that is responsible for synthesising PHA beads has been achieved in numerous studies (Grage & Rehm, 2008; Jahns et al., 2008; Parlane et al., 2011; Peters & Rehm, 2005, 2006). The advantage of this system is that once bead synthesis has been completed PhaC remains covalently attached to the surface of the polyester bead (Grage et al., 2009). Therefore,

any protein that is fused to PhaC is also displayed on the bead surface. In this study, the amount of fusion protein used in each reaction was standardised in order to be able to directly compare effects caused by PHA beads and GFP particles. All of the fusion protein used in the PHA bead reactions was displayed on the surface of the beads due to the positioning of PhaC. However, the positioning of enzyme on GFP particles is less certain. The GFP particles used in this study consisted entirely of GFP fusion protein. Therefore, most of the fusion protein used in each GFP particle reaction was below the surface of the particle, and, therefore, separated from substrate. This would account for the decreased activity in comparison to PHA beads in itself; however, there is also no reason to assume that GFP fusion protein at the surface of the particles would be arranged in as organised a manner as for PHA beads. The enzyme portion of the surface fusion proteins could still be buried below the surface of the particles, or have its movement restricted by other proteins, therefore, resulting in decreased activity. Moreover, if the formation of GFP particles abides by the current model of inclusion body formation not all of the fusion protein of the GFP particles will be correctly folded (Garcia-Fruitos et al., 2012; Peternel & Komel, 2011). Therefore, only a fraction of the fusion protein in GFP particles will consist of active enzyme of which only fraction will have access to substrate. Comparing PHA bead and GFP particle activity based on the amount of fusion protein shows GFP particles to be less active than PHA beads, but does not provide a complete comparison of enzyme activity. Another comparison would be to standardise the reactions based on bead/ particle weight. The results gathered by Jahns *et al.* demonstrated that when using this method of standardisation GFP particles function as effectively, or even more effectively, in the purification of IgG from human serum (Jahns et al., 2013). However, despite showing significant differences in enzyme activity, the standardisation by fusion protein quantity shows that GFP particles do display active enzyme, and illuminates potential models for the formation of GFP particles that can be investigated in future research.

4.3 Consistency of GFP particle activity with changes in temperature depends on the enzyme displayed

The enzyme-bearing GFP particles used in this study exhibited consistent levels of product synthesis, and therefore enzyme activity, after being pre-treated with a range of temperatures. However, it appears that the size of the range within which a particle

maintains consistent activity is dependent on the enzyme displayed. GiCLB and GiCLN particles were able to maintain reasonably constant levels of activity with slight decreases occurring after 45 ˚C and 25 ˚C, respectively (Fig. 20 & 21). Both particles display a sharper decrease when treated at 95 ˚C although activity is still measureable. In contrast, GiCLO particles appear to be the most sensitive to heat-treatment. Activity is constant between 4 ˚C and 45 ˚C; however, after this point it steadily decreases until after the 95 ˚C treatment where activity is almost non-existent (Fig. 22). The reason for these differences in activity is presumably due to the natural properties of the enzymes. Previous research on the α-amylase (Bla) derived from *Bacillus licheniformis* has shown that it can retain 45% of maximal activity when used at 110 ˚C (Vihinen & Mantsala, 1989). Furthermore, Bla(-ss) is a derivative of a stabilised variant of Bla which exhibits increased thermostability beyond that exhibited by the wild-type enzyme (Machius, Declerck, Huber, & Wiegand, 2003). Therefore, it is expected that the level of activity exhibited by GiCLB particles would remain relatively unchanged after the range of heat-treatments that were used. NanA has also been used at high temperatures. A previous study demonstrated that the optimal temperature for Neu5Ac hydrolysis facilitated by soluble NanA is 80 ˚C (Aisaka et al., 1991). Another study that immobilised NanA on the surface of *Bacillus subtilis* spores observed an optimal temperature of 50 ˚C for the condensation of ManNAc and pyruvate to form Neu5Ac (X. Xu et al., 2011). These results show that NanA can function at elevated temperatures, and so the consistency of GiCLN activity throughout the heat-treatments in this study is in agreement with the established literature. OpdA activity deteriorates as temperature increases. Blatchford *et al*. measured the activity of soluble OpdA and PhaC-OpdA beads, relative to maximal activity, after heat-treatment using the same protocol as used in this study (Blatchford et al., 2012). The researchers observed that after heat-treatment at 30 ˚C- 65 ˚C soluble OpdA exhibited relatively stable activity, while the activity of PhaC-OpdA PHA beads decreased by approximately 30%. However, after this point, the activity of both soluble and PHA bound OpdA decreased rapidly. Although this study measured changes in activity with temperature with respect to maximal activity, the pattern of activity loss is similar to that observed for GiCLO particles. The rate of *para*-nitrophenol production by GiCLO particles is consistent after treatment with temperatures between 4 ˚C and 45 ˚C, indicating that maximal activity under the experimental conditions is occurring. However, heat-treatment at higher temperatures causes a rapid decrease in *para*-nitrophenol production, and therefore

OpdA activity, which is comparable to the decreases in activity of soluble OpdA and PhaC-OpdA beads under similar conditions. Although the activity of PhaC-OpdA beads and GiCLO particles in this study initially appear to be more stable than what was observed by Blatchford *et al.*, there is a rapid loss in activity from both types of particle after 55 ˚C. It is interesting that the patterns of enzyme activity displayed in Figures 20, 21, and 22 by the PHA bead controls are similar to those exhibited by the GFP particles. This is further evidence that the thermostability of the activity of enzyme-bearing GFP particles is dependent on the enzyme that is displayed.

Fluorescent images of the GFP particles that were obtained after heat-treatment also reveal differences (Fig. 23, 24, & 25). As described above (3.2.1), all types of enzyme-bearing GFP particle retain their fluorescence after treatment with temperatures between 4 ˚C and 75 ˚C. However, at 85 ˚C fluorescence is lost, and although similar GFP particle shapes can be seen by phase-contrast microscopy it is not possible to determine whether they are in fact GFP particles. In contrast to fluorescence, the different types of enzyme-bearing GFP particle appear to be physically changed in different ways depending on temperature. First, the GiCLB particles retain their shape, size, and regular distribution between the temperatures that can be visualised by fluorescent microscopy. This corresponds well to the consistency of activity exhibited by GiCLB particles after heat-treatment. Second, the size and shape of GiCLN particles is retained after all heat-treatments; however, as the treatment temperature increases the particles appear to aggregate. This seems to have little effect on enzyme activity, although it may be the cause of the decrease in activity between 25 ˚C and 75 ˚C. Third, the GiCLO particles retain similar distributions of size and shape between 4˚C and 75˚C. However, as the temperature increases they also appear to aggregate. This aggregation, although only slight, may be an additional cause of the decrease in activity observed after 45 ˚C.

4.4 GFP particles exhibit similar patterns of activity throughout a range of pH

The enzyme-bearing GFP particles were pre-treated with buffers of pH 2 to 12. Following treatment, the particles were assessed for activity. All GFP particles demonstrated similar patterns of activity, as evidenced by the quantities of product detected (Fig. 26, 27 & 28). At pH 2,3 and 12 activity was generally non-existent or very low. However, between pH 4 and 10 the enzymatic activity of all types of particle

was remarkably stable with a significant decrease observed at pH 11. Interestingly, GiCLO particles demonstrated the most stable activity under the conditions tested. At pH 2 and 3 activity was again very low. However, as the pH of the treatments increased the enzyme activity of GiCLO particles also increased to reach maximum activity after the pH 6 treatment. GiCLO activity remained relatively constant until the pH 11 treatment where it decreased significantly. However, in contrast to GiCLB and GiCLN particles which did not exhibit any activity after the pH 12 treatment, GiCLO particles were still reasonably active, exhibiting ~30% of observed maximal activity. This is surprising given that GiCLO particles exhibited the least consistent activity after pre-treatment at different temperatures.

Previous research on the pH stability of soluble α-amylase from *Bacillus licheniformis* described contrasting results to those seen in this study. Enzyme activity was measured after treatment at pH 4 to 9 for 1 h at 25 ˚C (Ivanova, Dobreva, & Emanuilova, 1993). Enzyme activity was approximately 70% of maximum at pH 4 and increased to 100% at pH 6.0. This activity was stable until pH 8.5 after which it dropped to approximately 90% at pH 9. Ivanova *et al.* showed that the α-amylase from *Bacillus licheniformis* exhibits maximal activity within a much narrower range than that observed in this study. The rate of maltose production via GiCLB particle biocatalysis, as detected by absorbance, remains relatively unchanged between pH 4.0 and 10.0, indicating that maximal activity has been achieved and retained within this range (Fig. 26). However, maximal activity as observed by Ivanova *et al.* only occurs between pH 6.0 and 8.5. These contrasting results may be due to differences in how the pH stability assays were performed. As described above, Ivanova *et al.* incubated their samples at different pH for 1 h, while in this study they were incubated for 10 min. It is possible that if the GFP particles were pH-treated for 1 h they would exhibit a different activity profile. However, it is also possible that the GFP particles confer stability to their constituent enzymes, as is often the case in enzyme immobilisation, although further research using extended pH-treatments needs to be conducted for confirmation. In addition, there are also differences in the pH stability observed in the original investigation of Bla(-ss)-PhaC PHA beads, and that observed for the same beads in this study. Whereas in this study the Bla(-ss)-PhaC beads appeared to exhibit maximal activity between pH 4 to 11 the previous study observed that maximum activity occurs at pH 8 and steadily decreases as conditions become more acidic or basic (Rasiah & Rehm, 2009). These

contrasting results are also most likely due to differences in the conduct of the pH stability assays. The conditions used involved incubation at 75 ˚C for at least 30 min. This reinforces the need for a more extensive investigation of the stability of GFP particle activity with changes in pH. However, it is interesting to note the similarities between the patterns of enzyme activity between Bla(-ss)-PhaC beads and GiCLB particles, as observed in this study. It is possible that under the same conditions used by Rasiah & Rehm the GiCLB particles might favour a similar optimal pH as Bla(-ss)-PhaC beads.

Previous research on the pH stability of soluble NanA has also produced conflicting results. Aisaka *et al.* showed that NanA exhibits stable activity between pH 6.0 and 7.0; however, at pH 5.0 and 8.0 activity decreased by approximately 60% and 30%, respectively (Aisaka et al., 1991). Although this assay was conducted in a similar fashion to that used in this study the differences may have led to contrasting results. The NanA samples were incubated in 50 mM Potassium phosphate buffer of varying pH for 15 min at 75 ˚C, whereas the samples in this study were incubated in different buffers of varying pH for 10 min at room temperature (22 ˚C- 25 ˚C). The increased incubation time and choice of buffer are not expected to have a significant effect over those used in this study; however, it is possible that the elevated incubation temperature used by Aisaka *et al.* might destabilise the enzyme and make it more vulnerable to changes in pH. It is also possible that immobilisation of NanA to GFP particles genuinely stabilises the enzyme. Again, it is interesting to note the similar patterns of activity exhibited by NanA-PhaC PHA beads and GiCLN particles. The effect of pH treatment has not been previously investigated for NanA-PhaC beads, and so comparisons with previous literature cannot be made. However, as is the case for GiCLB particles, further research is required using different incubation periods and temperatures to provide more information on the stability of GiCLN activity with changes in pH.

Research on the pH stability of OpdA from *Agrobacterium radiobacter* has not been previously conducted; however, similar organophosphohydrolases have been characterised. Previous studies of organophosphohydrolases from *Streptomyces lividans*, *Nocardiodes simplex*, and *Penicillium lilacinum* have been performed (Liu et al., 2004; Mulbry, 2000; Rowland, Speedie, & Pogell, 1991). First, the organophosphohydrolase from *Streptomyces lividans* was shown to have high activity

between pH 7.5 to 10.5 with an optimal activity observed at pH 9.5. Activity was rapidly lost below pH 6.5. Second, enzyme from *Nocardiodes simplex* exhibited a narrow optimum of pH 8.5. Third, enzyme from *Penicillium lilacinum* exhibited maximum activity at pH 7.5, and was shown to exhibit stable activity between pH 6.5 to 9.5. Beyond these points activity decreased rapidly. Again, the pH stability assays used in these studies were conducted in different ways compared to this study. Furthermore, all of the organophosphohydrolases described are different in terms of size and quaternary structure in comparison to OpdA. All enzymes are assumed to be monomeric and are 34 kDa, 45 kDa, and 59kDa, respectively. However, a common theme shared by these enzymes is high activity at slightly alkaline to moderately alkaline pH. GiCLO particles exhibited maximum absorbance, indicating maximum activity, between pH 5 to 10. Beyond these points absorbance decreases rapidly. This is a much broader range than that exhibited by organophosphohydrolases from the species above. This is possibly due to the natural stability exhibited by OpdA derived from *Agrobacterium radiobacter*; stability imposed by immobilisation to GFP particles; or a combination of both facets. Studies on pH stability need to be performed on soluble OpdA from *Agrobacterium radiobacter* in order to quantify stabilisation effects exerted by GFP particles. In addition, it is again interesting to note the similarity in absorbance patterns exhibited by PhaC-OpdA PHA beads and GiCLO particles. However, PhaC-OpdA beads appear to exhibit more stable enzyme activity than GiCLO particles under the conditions tested.

The enzyme-bearing GFP particles not only share similarities in their patterns of activity through a range of pH, but are physically affected in similar ways, as described above (3.2.2). At pH 2, 3 and 12 single, fluorescent GFP particles cannot be observed, and in their place are fluorescent aggregates, presumably formed by the GFP particles (Fig. 29, 30, & 31). When the samples are centrifuged after treatment at these pH pellets do form; however, it is not certain whether the pellet is formed by intact GFP particles, partially dissolved particles, aggregates, or other types of debris. As the pH increases, however, single, fluorescent GFP particles can be observed, and the amount of aggregates diminishes. Around pH 11 the particles can be seen to aggregate; however, fluorescence is still retained. Despite their similarities the different GFP particles are also affected in different ways. First, GiCLB particles are affected as described above with no single fluorescent particles observable after treatment at pH 2, 3, and 12 (Fig.

29). Second, at pH 2 and 3 significantly larger fluorescent aggregates can be seen in GiCLN samples, which are presumably formed by the GFP particles (Fig. 30). However, as the pH increases the particles behave as described above. Third, at pH 2 and 3 small fluorescent aggregates can be observed in GiCLO samples (Fig. 31). As the pH increases the aggregates decrease in size until only single, fluorescent GFP particles can be observed. Interestingly, at pH 11 and 12 fluorescent aggregates reappear; however, single, fluorescent GFP particles can still be observed. The physical behaviour of the GFP particles at different pH may explain the patterns of enzyme activity observed for each particle. At pH 2 and 3 little to no activity can be observed from any particle, and this might be due to structural changes in the particles and their enzymes that cause them to aggregate as seen by fluorescence microscopy. As the pH increases the enzyme activity of the particles also increases. Simultaneously, the large aggregates disappear and single, fluorescent GFP particles can be observed. It appears that single, fluorescent GFP particles are required for the demonstration of significant enzyme activity, and are indicative of the presence active enzyme. As the pH increases to 11 and 12 the enzyme activity of GiCLB and GiCLN particles rapidly decreases, which may be due to the aggregation of GFP particles presumably caused by structural changes as mentioned above. Interestingly, GiCLO particles are able to display significant activity at pH 11 and 12 which may be due to the persistence of single, fluorescent particles as seen by fluorescence microscopy. In terms of enzyme activity stability with changes in pH, it appears that GiCLO particles are the most stable, while GiCLB and GiCLN particles are the least stable. This continues the trend that the activity profile exhibited by enzyme-bearing GFP particles is dependent on the enzyme displayed, and is presumably also dependent on the natural properties of enzymes.

4.5 GFP particles exhibit different patterns of activity when recycled

The GFP particles exhibit different patterns of activity when reused over consecutive cycles. The activity of GiCLB particles appears to be relatively constant over the first three cycles, but decreases significantly in the fourth cycle (Fig. 32). This could be due to degradation of Bla(-ss) enzyme between the third and fourth cycles. After Cycle 4 samples were centrifuged a white pellet was observed around the yellow/ green pellet of the GiCLB particles. This white pellet was observed in the first 6 hours of the GiCLB time course, and it is suggested that the GiCLB particles somehow cause precipitation

to occur in the soluble starch substrate. At 12 hours incubation the white pellet was not visible, which suggested that GiCLB particles can degrade the precipitate if incubated for an appropriate period. As Cycle 4 was incubated for 12 hours, it was expected that the white pellet would not form. However, as the white pellet did form it is suggested that the Bla(-ss) enzyme activity displayed by the GiCLB particles had decreased so that it could not degrade the precipitate within the 12 hours. This could be due to structural changes that occurred with repeated use, and which reached a critical point after Cycle 3. Bla(-ss)-PhaC PHA beads have also been assessed for reusability (Rasiah & Rehm, 2009). In this study a 28% decrease in activity was observed in Cycle 2; however, activity was then maintained at this level in Cycle 3. The reusability assays were conducted in a similar manner in both studies, and so it is assumed that the differences in activity between the first and second cycles are due to experimental variation.

The activity of the GiCLN particles appears to steadily decrease between each cycle (Fig. 33). This could be due to degradation of the NanA displayed on GiCLN particles with each cycle which would mean that the display of NanA is very delicate. In addition, a more likely explanation could be that the regular decrease in activity is due to loss of sample with each consecutive cycle. It was observed that when the supernatants of each cycle were removed and centrifuged again a faint pellet would form at the bottom of the tubes. This pellet could be residual GiCLN particles that were not pelleted in the first centrifugation at the end of each cycle, and were, therefore, removed from subsequent cycles. Care was taken to avoid disturbing the particle pellets while removing the supernatants; however, it is possible that prolonged incubation at 50 ˚C could cause GiCLN particles to break up into smaller particles that are not pelleted using the regular centrifugation protocol. NanA-PhaC beads were also assessed for reusability in a previous study (Hooks et al., 2013). This study was conducted in a similar manner to this study; however, the concentration of ManNAc and pyruvate was lower- 100 mM and 250 mM, respectively, as opposed to 0.2 M and 1.0 M. It was observed that the Neu5Ac yield as a percentage of ManNAc consumed by NanA-PhaC beads increased from Cycle 1 (73%) to maximum yield at Cycle 2 (97%) with subsequent cycles decreasing in Neu5Ac yield. In contrast, the Neu5Ac yield catalysed by GiCLN particles decreased steadily from 16.2% (3s.f.), as observed in Cycle 1, to 1.56% (3s.f.) as observed in Cycle 4. Despite the differences in Neu5Ac yield NanA-PhaC beads, as shown by Hooks *et al.,* appear to exhibit more stability in terms of

NanA activity when reused. This could be due to increased stability of the enzyme on NanA-PhaC beads, and no loss of beads between each cycle. Further research on the physical properties of GiCLN particles after prolonged incubation needs to be conducted in order to ascertain whether the particles do in fact shrink and are lost from the reaction, or that NanA enzyme displayed on GiCLN particles degrades with each cycle.

The activity of GiCLO particles appears to remain consistent throughout all cycles with a slight decrease in activity observable in Cycle 4 (Fig. 34). PhaC-OpdA beads have not as yet been assessed for reusability, and were not tested in this study. Therefore, a comparison between the two immobilisation platforms is not possible. However, in terms of the GFP particles assessed, GiCLO particles exhibit the most consistent enzyme activity when reused, while GiCLN particles exhibit the least.

4.6 Long-term storage of GFP particles is affected by temperature

The different types of enzyme-bearing GFP particle are affected in different ways by long-term storage, as assessed in this study. Samples of PHA beads and GFP particles displaying the relevant enzymes were stored in either 20% Ethanol in 50 mM Potassium phosphate buffer or 25% Glycerol in 50 mM Potassium phosphate buffer at 4 ˚C, room temperature (22 ˚C-25 ˚C), and -80 ˚C. Activity assays for Bla(-ss) and OpdA bearing PHA beads/ GFP particles were performed on the 23rd January 2013, while the activity assay for NanA bearing PHA beads/ GFP particles was performed on the 21st January 2013. The GiCLB 4 ˚C and room temperature samples were stored for a period of 95 days, while the -80 ˚C sample was stored for 69 days. Despite this difference of 26 days, the enzyme activity exhibited by all samples is relatively constant (Fig. 35). The average absorbance value measured using the same activity assay conditions for GiCLB particles soon after particle extraction was 0.961 (3s.f.), while the average absorbance values measured for the 4 ˚C, R.T., and -80 ˚C samples after storage were 0.998, 0.880, and 0.899 (3s.f.), respectively. Therefore, there appears to be a slight increase in activity for samples stored at 4 ˚C, and an 8.43% and 6.45% (3s.f.) decrease in activity for samples stored at R.T. and -80 ˚C, respectively. The Bla(-ss)-PhaC beads continued to exhibit higher activity in comparison to the GiCLB particles; however, the activity of the beads appears to be more unstable when stored at room temperature. The average

absorbance value measured using the same activity assay conditions for Bla(-ss)-PhaC beads soon after bead extraction was 2.08 (3s.f.), while the average absorbance values measured for the 4 ˚C, R.T., and -80 ˚C samples after storage were 2.05, 1.37, and 2.07 (3s.f.), respectively. This is a decrease in activity of 1.39%, 34.2%, and 0.410% (3s.f.), respectively, in comparison to activity measured post-extraction. Therefore, GiCLB particles demonstrate comparable retention of activity in comparison to Bla(-ss)-PhaC beads under the storage conditions used in this study.

All GiCLN samples were stored for a period of 97 days; however, there are significant differences in enzyme activity. The 4 ˚C and -80 ˚C samples exhibited similar levels of activity; however, the activity of GiCLN particles stored at room temperature was undetectable (Fig. 36). This trend is also observable in the NanA-PhaC bead samples where, again, the 4 ˚C and -80 ˚C samples exhibit similar levels of activity, while the activity of beads stored at room temperature is significantly less. The quantity of Neu5Ac produced by GiCLN particles under the same activity assay conditions soon after cell extraction was 50.6 mM (3s.f.), while the quantities produced after 4 ˚C, R.T., and -80 ˚C storage were 22.8 mM, undetectable, and 24.5 mM (3s.f.), respectively. Therefore, storage under the specified conditions led to a decrease in GiCLN enzyme activity of 54.9%, ~100%, and 51.6% (3s.f.), respectively. The quantity of Neu5Ac produced by NanA-PhaC beads under the same test conditions soon after extraction was 163.0 mM (3s.f.), while the quantities produced after 4 ˚C, R.T., and -80 ˚C storage were 121.0 mM, 5.34 mM, and 126.0 mM (3s.f.), respectively. This equates to a decrease in activity of 25.6%, 96.7%, and 22.9%, respectively, in comparison to activity measured post-extraction. Therefore, GiCLN particles demonstrate significantly less retention of activity in comparison to NanA-PhaC beads under the storage conditions used in this study. It appears that GiCLN particles exert less stabilising effects over the NanA enzyme in comparison to NanA-PhaC beads under the storage conditions used.

All GiCLO samples were stored for a period of 132 days, and exhibit similar levels of activity (Fig. 37). However, samples stored at -80 ˚C appear to exhibit slightly greater activity. Unfortunately, no PhaC-OpdA bead room temperature or -80 ˚C samples were set aside; however, the sample stored at 4 ˚C continued to exhibit higher activity in comparison to the GiCLO particles. The long-term stability of PhaC-OpdA beads stored in tap water at 25 ˚C has been previously assessed (Blatchford et al., 2012). In this study

it was shown that the enzyme activity of PhaC-OpdA beads only slightly decreased over 11 days of storage. However, after 5 months of storage activity was ~15% of the original activity. It must be noted that there are large differences in absorbance exhibited by GiCLO particles between assays. For example, during the Time Course assay the average absorbance exhibited by the action of GiCLO particles after 12 hours was 0.321 (3s.f.) (Fig. 19). However, during the temperature stability, pH stability, and reusability assays the absorbance values for the same period of incubation, temperature, pH, and number of cycles were 0.195 (3s.f.), 0.743, and 0.287 (3s.f.), respectively (Fig. 22, 28, & 34). These values were expected to be the same as that of the Time Course. Although the particles used to conduct the pH stability assay were of a different batch to that used to conduct the Time Course, temperature stability, and reusability assays, all variables used to produce the particles were the same. Therefore, it is not expected that the activity of particles between batches would be significantly different. However, the manner in which the Methyl parathion substrate was prepared for each assay may have introduced the variability. The Methyl parathion crystals were difficult to dissolve in 50 mM HEPES buffer, even with the addition of 20% (v/v) Methanol as described previously (Blatchford et al., 2012). Therefore, to facilitate dissolution the 20% Methanol (v/v) in 50 mM HEPES buffer, pH 8.0, was pre-heated in an incubator to bring the solution to the melting temperature of Methyl parathion crystals- 35-38 ˚C. The temperature of the solution was not measured before adding the crystals, and since the substrate was prepared fresh for each assay it is possible that some solutions were hotter than others which dissolved the Methyl parathion with different efficiencies. This would account for the variability in absorbance observed in each assay as different amounts of soluble substrate were available. Although the differences in absorbance between assays are not ideal, it is the differences within the assays that are most important. Within each assay the concentration of Methyl parathion is constant, and so differences in absorbance can be attributed to the particular treatment. Unfortunately, the difference in absorbance observed in the Long-term Storage assay in comparison to that observed post-extraction cannot, therefore, be made. However, it is still possible to compare the differences in absorbance due to the different storage conditions within the assay.

The fluorescent images of the GFP particles obtained after long-term storage showed that the enzyme-bearing GFP particles are affected differently by long-term storage and

the storage conditions, as described above (3.2.4). First, between storage conditions there appears to be little difference in the physical state of GiCLB particles. All samples contained particles that were randomly distributed with perhaps a slight increase in aggregation observable in the room temperature sample (Fig. 38). This consistency in physical characteristics could lead to the consistency and retention of enzyme activity that was observed. Second, GiCLN particles appear to be prone to aggregation when stored at 4 ˚C and room temperature, with more aggregation observable in the room temperature sample (Fig. 39). GiCLN particles stored at -80 ˚C appear to be the most randomly distributed, and, perhaps, larger in size. In contrast to GiCLB particles, there does not appear to be an obvious link between physical appearance and activity. Aggregation can be observed in both the 4 ˚C and R.T. samples, and there is not significantly more aggregation in the R.T. sample in comparison to the other two samples. Therefore, the lack of activity exhibited by GiCLN particles stored at room temperature does not appear to be linked to aggregation. Perhaps at this temperature, and in the storage buffer used, the NanA enzyme is inherently unstable, which is also suggested by the decreased activity exhibited by NanA-PhaC beads stored under the same conditions. In any case, the activity of NanA appears to be significantly affected by the storage conditions used and the duration of storage as both GiCLN particles and NanA-PhaC beads exhibited decreased activity in comparison to beads/ particles post-extraction. It is possible that the NanA enzyme is inherently unstable during long-term storage. Third, slight aggregation is observable in the GiCLO sample stored at 4 ˚C with more aggregation seen in the room temperature sample (Fig. 40). The GiCLO -80 ˚C sample appears to have the most randomly distributed single fluorescent particles which, perhaps, are of a larger size. Again, aggregation does not appear to affect the enzyme activity of GiCLO particles. Enzyme activity appears to be consistent regardless of aggregation suggesting that OpdA displayed on GFP particles is inherently stable under the storage conditions used.

It appears that the activity exhibited by enzyme-bearing GFP particles depends on two factors: the type of enzyme displayed; and the temperature at which the particles are stored. The use of 20% (v/v) Ethanol in 50 mM Potassium phosphate buffer or 25% (v/v) Glycerol in 50 mM Potassium phosphate buffer appears to have a negligible effect as samples stored at 4 ˚C and -80 ˚C exhibited similar activity for all types of GFP particle tested. Previous research has demonstrated that GFP inclusion bodies are stable

when stored for long periods at 4 ˚C, 25 ˚C, 37 ˚C, and -80 ˚C (Garcia-Fruitos et al., 2009). However, this is in terms of fluorescence emitted and the architecture of the inclusion bodies. Although changes in fluorescence were not measured, all samples for all types of GFP particle used in this assay retained fluorescence, and exhibited only minor changes in physical characteristics as observed by fluorescence microscopy. Furthermore, the storage buffer used in this previous study was different to that used in this study, and might exert different effects on long-term stability. In addition, in order to demonstrate the compatibility of enzyme-bearing GFP particles for commercial use, stability during lyophilisation and freeze-thawing needs to be assessed in future research.

4.7 Limitations of Study

This study provides an overview on the activity and stability of enzyme-bearing GFP particles under a variety of conditions. Through each assay it was demonstrated that enzyme-bearing GFP particles are capable of forming and displaying active enzyme, and that enzyme activity is influenced by changes in: temperature, pH, the number of cycles of use, duration of storage, and the type of enzyme that is displayed. However, there are limitations to this study that influence the conclusions that can be made.

It has already been described how mistakes were made in the preparation of the substrate solutions for the amylase and organophosphohydrolase assays. In terms of the 1.0% (w/v) Soluble Starch Solution, it is acknowledged that volume adjustments should have been achieved with distilled water. By using more 20mM Sodium phosphate buffer plus 6.7mM Sodium chloride, pH 6.9, the concentration of Sodium phosphate and Sodium chloride in the solution was changed from that outlined in protocols by Sigma-Aldrich and Rasiah *et al.* on which the amylase assays in this study are based. Therefore, it is difficult to make comparisons of the data collected in this study with other studies that use the same protocols. In terms of the Methyl parathion substrate, it is not possible to make comparisons between assays as the absorbance signal observed in each assay varies considerably. This means that it is not possible to quantitate changes in activity over time, as is the case for observing changes due to long-term storage, or to compare absorbance signals to previous studies. However, as the Methyl

parathion substrate was prepared fresh for each assay its concentration within each assay is constant and so the effects of treatments within each assay can still be deduced.

Most studies report the activity of enzymes using specific activity, and examine the kinetics of enzyme activity using a variety of substrate concentrations and experimental conditions. However, in this study the amount of product produced by enzymes in terms of concentration or absorbance signal was displayed. This was done for several reasons. First, the calculation of specific activity and enzyme kinetics using the GFP particles examined in this study was either too difficult or not possible within the time constraints of this study. The NanA activity of GiCLN particles is quite weak, and it was not possible to calculate specific activity using standard protocols. Furthermore, as the measurement of Neu5Ac requires HPLC that requires 25min to process each sample it was not feasible to analyse the number of samples that would be required to examine enzyme kinetics. Moreover, the substrate ManNAc is quite expensive and the quantities that would be required to calculate enzyme kinetics using different substrate concentrations, temperatures, pH, and time points is again not feasible. Producing ManNAc from the epimerisation of *N*-acetyl-D-glucosamine is possible, but would add another level of complexity to the experiments that was not feasible within the duration of this study. In addition, the nature of the display of enzyme on the surface of GFP particles meant that conducting enzyme kinetics on GiCLB and GiCLO particles, which exhibited the strongest activity, would have been difficult. To extract the supernatants required to measure absorbance required centrifugation to remove the GFP particles. To perform this operation on the number of samples required to measure enzyme kinetics at different substrate concentration, temperature, pH, and time points would require excessive pipetting and centrifugation which were not possible within the time restraints of this study. Therefore, in the interests of standardising the types of assays used to examine each type of enzyme-bearing GFP particle, specific activity and enzyme kinetics assays were forgone, and the measurement of enzyme product was recorded. In this manner the activity of enzyme-bearing GFP particles could still be observed, and measured under different conditions. One might argue that it might have been more appropriate to investigate only one type of enzyme-bearing GFP particle and perform specific activity and enzyme kinetics, in line with other enzyme studies. However, in order to demonstrate the versatility of GFP particles in immobilising and displaying different types of enzyme it was deemed important to investigate enzymes with different

structure and mechanism of activity. Therefore, a broader, more superficial investigation was required.

The GFP particles investigated in this study were not tested against soluble enzyme. Instead, they were tested against PHA bead comparisons which themselves had, in most cases, been previously tested against soluble enzyme. Soluble NanA and OpdA were difficult to procure, and so it was decided that any comparisons to soluble enzyme would be made based on the literature, and the comparisons to PHA beads. It is acknowledged that testing soluble enzyme within the assays of this study would have been best; however, under the circumstances a literature comparison was deemed sufficient.

In previous studies, the amount of PHA beads or GFP particles used per assay was standardised on a bead/ particle weight basis, or by enzyme units. However, in this study samples were standardised on the amount of fusion protein used per assay. Again, this makes it difficult to make direct comparisons from this study to those previous, and assessing enzyme-bearing GFP particles using standardised particle weight might have changed the results of comparisons to PHA beads. However, standardisation based on fusion protein mass has revealed important insights into the structure of GFP particles. Furthermore, as the specific activity of the GFP particles used in this study was not calculated, standardisation based on enzyme units per assay was not possible.

CHAPTER FIVE: CONCLUSION

The enzyme industry is worth billions of dollars, and is set to grow as novel ways to use enzymes are discovered and demand increases. Enzymes provide a method of chemical catalysis that is more efficient, productive, and able to function under milder conditions in comparison to inorganic catalysts. However, the production and use of enzymes is also expensive, and cost is seen as a major hurdle for the widespread use of enzyme in industry. Immobilisation of enzymes to solid supports allows enzymes to be reused, thus balancing the expense of their production. However, current methods of immobilisation are laborious, and can lead to toxic waste products. Recent research, for example PHA beads, has led to the one-step production of solid support and enzyme leading to self-immobilisation of enzymes within recombinant cells. Such research has provided methods for enzyme immobilisation that are more efficient and less toxic. In this study, a similar one-step process of enzyme immobilisation to novel GFP fusion protein particles (GFP particles) was investigated. Enzyme-bearing GFP particles have been demonstrated to exhibit enzyme activity, and are capable of displaying enzymes of different quaternary structure and mechanism of catalysis. Furthermore, they have been demonstrated to possess considerable thermal, pH, and long-term storage stability in terms of enzyme activity and physical characteristics, as well as potential reusability which highlights their use in a variety of industrial applications. Due to the novel nature of GFP particles further research is required to characterise them completely, and to engineer them for optimal performance towards specific applications.

Ideas for future research have already been mentioned above. These include: investigating the structure of GFP particles; conducting temperature and pH stability studies under different conditions; and standardising samples by bead/ particle weight or enzyme units to obtain results that are more directly comparable to previous studies. These ideas were made to overcome the limitations of this study; however, there are other areas that should be explored in order to completely characterise GFP particles. First, an investigation into the bonds that hold GFP particles together would be useful. This would provide a gauge on the strength of GFP particles, and would highlight applications to which they would be more suited, or should not be used. Furthermore, such an investigation would provide insights into the structure of inclusion bodies in general. Second, and in relation to structural studies, GFP particles need to be

investigated in order to see whether GFP fusion protein leaches from the particles during the course of an assay. In commercial applications such leaching could be detrimental to the use of GFP particles, unless they were used as a slow-release source of fusion protein. In any case, investigation is required to quantitate leaching, and devise steps to counteract it, or exploit it. Previous studies have shown that inclusion bodies release very low amounts of protein during the first minutes of incubation, and then are quite stable under long-term storage and further incubation without any observable changes in size, shape, or activity (Garcia-Fruitos et al., 2007; Garcia-Fruitos et al., 2009). It would be interesting to see if GFP particles follow the same trend. Finally, investigation into the mechanical stability of GFP particles would be useful. GFP particles were isolated using a protocol developed by Rehm *et al.* for the isolation of PHA beads. As mentioned previously, the quality of inclusion bodies and their constituent proteins is affected by the methods of extraction, and so determining a procedure that is customised to GFP particles would optimise their production and use. Furthermore, such a protocol may be useful in the extraction of other types of inclusion body.

Despite questions concerning characterisation and performance, enzyme-bearing GFP particles have been demonstrated to be an efficient platform technology for the immobilisation and display of active enzyme under a variety of conditions. The added benefit of fluorescence remains to be effectively exploited; however, the future appears bright for their use in industry.

CHAPTER SIX: REFERENCES

Aisaka, K., Igarashi, A., Yamaguchi, K., & Uwajima, T. (1991). Purification, crystallisation and characterisation of *N*-acetylneuraminate lyase from *Escherichia coli*. *Biochemical Journal, 276*(2), 541-546.

Amara, A., & Rehm, B. H. A. (2003). Replacement of the catalytic nucleophille cysteine-296 by serine in class II polyhydroxyalkanoate synthase from *Pseudomonas aeruginosa*- mediated synthesis of a new polyester: identification of catalytic residues. *Biochemical Journal, 374*, 413-421.

Baird, G. S., Zacharias, D. A., & Tsien, R. Y. (1999). Circular permutation and receptor insertion within green fluorescent proteins. *Proceedings of the National Academy of Sciences USA, 96*(20), 11241-11246.

Baneyx, F., & Mujacic, M. (2004). Recombinant protein folding and misfolding in *Escherichia coli*. *Nature Biotechnology, 22*(11), 1399-1408.

Benning, M. M., Shim, H., Raushel, F. M., & Holden, H. M. (2001). High Resolution x-ray structures of diffrerent metal-substituted forms of phosphotriesterase from *Pseudomonas diminuta*. *Biochemistry, 40*(9), 2712-2722.

Bird, S. B., Sutherland, T. D., Gresham, C., Oakeshott, J., Scott, C., & Eddleston, M. (2008). OpdA, a bacterial organophosphorus hydrolase, prevents lethality in rats after poisoning with highly toxic organophosphorus pesticides. *Toxicology, 247*(2-3), 88-92.

Blatchford, P. A., Scott, C., French, N., & Rehm, B. H. (2012). Immobilization of organophosphohydrolase OpdA from *Agrobacterium radiobacter* by overproduction at the surface of polyester inclusions inside engineered *Escherichia coli*. *Biotechnology and Bioengineering, 109*(5), 1101-1108.

Bradford, M. M. (1976). A rapid and sensitive method for the quantification of microgram quantities of protein utilising the principle of protein-dye binding. *Analytical Biochemistry, 72*, 248-254.

Brady, D., & Jordaan, J. (2009). Advances in enzyme immobilisation. *Biotechnology Letters, 31*(11), 1639-1650.

Brady, D., Jordaan, J., Simpson, C., Chetty, A., Arumugam, C., & Moolman, F. S. (2008). Spherezymes: a novel structured self-immobilisation enzyme technology. *BMC Biotechnology, 8*(8).

Carrio, M., Gonzalez-Montalban, N., Vera, A., Villaverde, A., & Ventura, S. (2005). Amyloid-like properties of bacterial inclusion bodies. *Journal of Molecular Biology, 347*(5), 1025-1037.

Carrio, M. M., & Villaverde, A. (2002). Construction and deconstruction of bacterial inclusion bodies. *Journal of Biotechnology, 96*(1), 3-12.

Carrio, M. M., & Villaverde, A. (2005). Localization of chaperones DnaK and GroEL in bacterial inclusion bodies. *Journal of Bacteriology, 187*(10), 3599-3601.

Chalfie, M., Tu, Y., Euskirchen, G., Ward, W. W., & Prasher, D. C. (1994). Green fluorescent protein as a marker for gene expression. *Science, 263*, 802-805.

Chen, K., & Arnold, F. H. (1993). Tuning the activity of an enzyme for unusual environments: Sequential random mutagenesis of subtilisin E for catalysis in dimethylformamide. *Proceedings of the National Academy of Sciences USA, 90*(12), 5618-5622.

Chung, C. T., Niemela, S. L., & Miller, R. H. (1989). One-step preparation of competent *Escherichia coli*: Transformation and storage of bacterial cells in the same solution. *Proceedings of the National Academy of Sciences USA, 86*(7), 2172-2175.

Cody, C. W., Prasher, D. C., Westler, W. M., Pendergast, F. G., & Ward, W. W. (1993). Chemical structure of the hexapeptide chromophore of the *Aequorea* green fluorescent protein. *Biochemistry, 32*(5), 1212-1218.

De, M., Rana, S., Akpinar, H., Miranda, O. R., Arvizo, R. R., Bunz, U. H., & Rotello, V. M. (2009). Sensing of proteins in human serum using conjugates of nanoparticles and green fluorescent protein. *Nature Chemistry, 1*(6), 461-465.

Doglia, S. M., Ami, D., Natalello, A., Gatti-Lafranconi, P., & Lotti, M. (2008). Fourier transform infrared spectroscopy analysis of the conformational quality of recombinant proteins within inclusion bodies. *Biotechnology Journal, 3*, 193-201.

Dopf, J., & Horiagon, T. M. (1996). Deletion mapping of the *Aequorea victoria* green fluorescent protein. *Gene, 173*, 39-44.

Dumas, D. P., Caldwell, S. R., Wild, J. R., & Raushel, F. M. (1989). Purification and properties of the phosphotriesterase from *Pseudomonas diminuta*. *The Journal of Biological Chemistry, 264*(33), 19659-19665.

Erhmann, M. A., Scheyhing, C. H., & Vogel, R. F. (2001). In vitro stability and expression of green fluorescent protein under high pressure conditions. *Letters in Applied Microbiology, 32*(4), 230-234.

Garcia-Fruitos, E. (2010). Inclusion bodies: a new concept. *Microbial Cell Factories, 9*(80), 1-3.

Garcia-Fruitos, E., Aris, A., & Villaverde, A. (2007). Localization of functional polypeptides in bacterial inclusion bodies. *Applied and Environmental Microbiology, 73*(1), 289-294.

Garcia-Fruitos, E., Gonzalez-Montalban, N., Morell, M., Vera, A., Ferraz, R. M., Aris, A., Ventura, S., & Villaverde, A. (2005). Aggregation as bacterial inclusion bodies does not imply inactivation of enzymes and fluorescent proteins. *Microbial Cell Factories, 4*(27).

García-Fruitós, E., Martínez-Alonso, M., Gonzàlez-Montalbán, N., Valli, M., Mattanovich, D., & Villaverde, A. (2007). Divergent genetic control of protein solubility and conformational quality in *Escherichia coli*. *Journal of Molecular Biology, 374*(1), 195-205.

Garcia-Fruitos, E., Rodriguez-Carmona, E., Diez-Gil, C., Ferraz, R. M., Vazquez, E., Corchero, J. L., Cano-Sarabia, M., Ratera, I., Ventosa, N., Veciana, J., & Villaverde, A. (2009). Surface cell growth engineering assisted by a novel bacterial nanomaterial. *Advanced Materials, 21*(42), 4249-4253.

Garcia-Fruitos, E., Sabate, R., de Groot, N. S., Villaverde, A., & Ventura, S. (2011). Biological role of bacterial inclusion bodies: a model for amyloid aggregation. *The FEBS journal, 278*(14), 2419-2427.

Garcia-Fruitos, E., Vazquez, E., Diez-Gil, C., Corchero, J. L., Seras-Franzoso, J., Ratera, I., Veciana, J., & Villaverde, A. (2012). Bacterial inclusion bodies: making gold from waste. *Trends in Biotechnology, 30*(2), 65-70.

Georgiou, G., & Valax, P. (1999). Isolating inclusion bodies from bacteria. *Methods in Enzymology, 309*, 48-58.

Glasgow, L. R., & Hill, R. L. (1980). Interaction of *Mycoplasma gallisepticum* with sialyl glycoproteins. *Infection and Immunity, 30*(2), 353-361.

Grage, K., Jahns, A. C., Parlane, N., Palanisamy, R., Rasiah, I. A., Atwood, J. A., & Rehm, B. H. A. (2009). Bacterial polyhydroxyalkanoate granules: biogenesis, structure, and potential use as nano-/ micro-beads in biotechnological and biomedical applications. *Biomacromolcules, 10*(4), 660-669.

Grage, K., & Rehm, B. H. A. (2008). In vivo production of scFv-displaying bioploymer beads using a self-assembly promoting fusion partner. *Bioconjugate Chemistry, 19*(1), 254-262.

Gresham, C., Rosenbaum, C., Gaspari, R. J., Jackson, C. J., & Bird, S. B. (2010). Kinetics and efficacy of an organophosphorus hydrolase in a rodent model of methyl-parathion poisoning. *Academic Emergency Medicine : Official Journal of the Society for Academic Emergency Medicine, 17*(7), 736-740.

Guglielmi, F., Monti, D. M., Arciello, A., Torrassa, S., Cozzolino, F., Pucci, P., Relini, A., & Piccoli, R. (2009). Enzymatically active fibrils generated by the self-assembly of the ApoA-I fibrillogenic domain functionalized with a catalytic moiety. *Biomaterials, 30*(5), 829-835.

Gupta, R., Gigras, P., Mohapatra, H., Goswami, V. K., & Chauhan, B. (2003). Microbial α-amylases: a biotechnological perspective. *Process Biochemistry, 38*(11), 1599-1616.

Hanahan, D. (1983). Studies on transformation of *Escherichia coli* with plasmids. *Journal of Molecular Biology, 166*, 557-580.

Hanefeld, U., Gardossi, L., & Magner, E. (2009). Understanding enzyme immobilisation. *Chemical Society Reviews, 38*(2), 453-468.

Heim, R., Cubitt, A. B., & Tsien, R. Y. (1995). Improved green fluorescence. *Nature, 373*, 663-664.

Heim, R., Prasher, D. C., & Tsien, R. Y. (1994). Wavelength mutations and posttranslational autoxidation of green fluorescent protein. *Proceedings of the National Academy of Sciences USA, 91*, 12501-12504.

Heyman, A., Levy, I., Altman, A., & Shoseyov, O. (2007). SP1 as a novel scaffold buidling block for self-assembly nanofabrication of submicron enzymatic structures. *Nano Letters, 7*(6), 1575-1579.

Hooks, D. O., Blatchford, P. A., & Rehm, B. H. A. (2013). Bioengineering of bacterial polymer inclusions catalyzing the synthesis of *N*-acetyl neuraminic acid. *Applied and Environmental Microbiology, 79*(9), 3116-3121.

Hsieh, B. H., Deng, J. F., Ger, J., & Tsai, W. J. (2001). Acetylcholinesterase inhibition and the extrapyramidal syndrome: A review of the neurotoxicity of organophosphate. *NeuroToxicology, 22*(4), 423-427.

Hwang, K. Y., Song, H. K., Chang, C., Lee, J., Lee, S. Y., Kim, K. K., Choe, S., Sweet, R.M., & Suh, S. W. (1997). Crystal structure of thermostable alpha-amylase from *Bacillus licheniformis* refined at 1.7 A resolution. *Molecules and Cells, 7*(2), 251-258.

Ivanova, V. N., Dobreva, E. P., & Emanuilova, E. I. (1993). Purification and characterization of a thermostable alpha-amylase from *Bacillus licheniformis. Journal of Biotechnology, 28*, 277-289.

Izard, T., Lawrence, M. C., Malby, R. L., Lilley, G. G., & Colman, P. M. (1994). The three-dimensional structure of *N*-acetylneuraminate lyase from *Escherichia coli*. *Structure, 2*(5), 361-369.

Jahns, A. C., Haverkamp, R. G., & Rehm, B. H. A. (2008). Multifunctional inorganic-binding beads self-assembled inside engineered bacteria. *Bioconjugate Chemistry, 19*(10), 2072-2080.

Jahns, A. C., Maspolim, Y., Chen, S., Guthrie, J. M., Blackwell, L. F., & Rehm, B. H. A. (2013). *In vivo* self-assembly of fluorescent protein microparticles displaying specific binding domains. *Bioconjugate Chemistry,* (In press).

Jeyaratnam, J. (1990). Acute pesticide poisoning: a major global health problem. *World Health Statistics Quarterly, 43*(3), 139-144.

Kepp, O., Galluzzi, L., Lipinski, M., Yuan, J., & Kroemer, G. (2011). Cell death assays for drug discovery. *Nature Reviews: Drug Discovery, 10*(3), 221-237.

Kragl, U., Gygax, D., Ghisalba, O., & Wandrey, C. (1991). Enzymatic two-step synthesis of *N*-acetyl-D-neuraminic acid in the enzyme membrance reactor. *Angewandte Chemie- International Edition in English, 30*(7), 827-828.

Laemmli, U. K. (1970). Cleavage of structural proteins during the assembly of the head of bacteriophage T4. *Nature, 227*(5259), 680-685.

Lee, S., Oneda, H., Minoda, M., Tanaka, A., & Inouye, K. (2006). Comparison of starch hydrolysis activity and thermal stability of two *Bacillus licheniformis* alpha-amylases and insights into engineering alpha-amylase variants active under acidic conditions. *Journal of Biochemistry, 139*(6), 997-1005.

Li, Q., Wei, D., Wang, L., Jia, Z., Le, X., Gao, Y., Huang, S., & Xie, K. (2010). Modeling liver metastasis using a tumor cell line derived from an enhanced green fluorescent protein transgenic mouse. *Clinical & Experimental Metastasis, 27*(1), 11-18.

Liu, Y.H., Liu, Y., Chen, Z.S., Lian, J., Huang, X., & Chung, Y.C. (2004). Purification and characterization of a novel organophosphorus pesticide hydrolase from *Penicillium lilacinum* BP303. *Enzyme and Microbial Technology, 34*(3-4), 297-303.

Lumjiaktase, P., Aguilar, C., Battin, T., Riedel, K., & Eberl, L. (2010). Construction of self-transmissible green fluorescent protein-based biosensor plasmids and their use for identification of *N*-acyl homoserine-producing bacteria in lake sediments. *Applied and Environmental Microbiology, 76*(18), 6119-6127.

Lutz, S. (2010). Beyond directed evolution--semi-rational protein engineering and design. *Current Opinion in Biotechnology, 21*(6), 734-743.

Luxananil, P., Promchai, R., Wanasen, S., Kamdee, S., Thepkasikul, P., Plengvidhya, V., Visessanguan, W., & Valyasevi, R. (2009). Monitoring *Lactobacillus plantarum* BCC 9546 starter culture during fermentation of Nham, a traditional Thai pork sausage. *International Journal of Food Microbiology, 129*(3), 312-315.

Machius, M., Declerck, N., Huber, R., & Wiegand, G. (2003). Kinetic stabilization of *Bacillus licheniformis* alpha-amylase through introduction of hydrophobic residues at the surface. *The Journal of Biological Chemistry, 278*(13), 11546-11553.

Martinez-Alonso, M., Garcia-Fruitos, E., & Villaverde, A. (2008). Yield, solubility and conformational quality of soluble proteins are not simultaneously favored in recombinant *Escherichia coli*. *Biotechnology and Bioengineering, 101*(6), 1353-1358.

Maru, I., Ohnishi, J., Ohta, Y., & Tsukada, Y. (2002). Why is sialic acid attracting interest now? Complete enzymatic synthesis of sialic acid with *N*-acylglucosamine 2-epimerase. *Journal of Bioscience and Bioengineering, 93*(3), 258-265.

Morell, M., Bravo, R., Espargaro, A., Sisquella, X., Aviles, F. X., Fernandez-Busquets, X., & Ventura, S. (2008). Inclusion bodies: specificity in their aggregation process and amyloid-like structure. *Biochimica et Biophysica Acta, 1783*(10), 1815-1825.

Morise, H., Shimomura, O., Johnson, F. H., & Winant, J. (1974). Intermolecular energy transfer in the bioluminescent system of *Aequorea*. *Biochemistry, 13*(12), 2656-2662.

Mulbry, W. (2000). Characterization of a novel organophosphorus hydrolase from *Nocardiodes simplex* NRRL B-24074. *Microbiological Research, 154*(4), 285-288.

Nahalka, J., Mislovicova, D., & Kavcova, H. (2009). Targeting lectin activity into inclusion bodies for the characterisation of glycoproteins. *Molecular BioSystems, 5*(8), 819-821.

Parlane, N. A., Grage, K., Lee, J. W., Buddle, B. M., Denis, M., & Rehm, B. H. (2011). Production of a particulate hepatitis C vaccine candidate by an engineered *Lactococcus lactis* strain. *Applied and Environmental Microbiology, 77*(24), 8516-8522.

Pessela, B. C. C., Mateo, C., Carrascosa, A. V., Vian, A., Garcia, J. L., Rivas, G., Alfonso, C., Guisan, J.M., & Fernandez-Lafuente, R. (2003). One-step purification, covalent immobilization, and additional stabilization of a thermophilic poly-his-tagged β-galactosidase from *Thermus* sp. strain T2 by using novel heterofunctional chelate-epoxy sepabeads. *Biomacromolecules, 4*(1), 107-113.

Peternel, S., & Komel, R. (2011). Active protein aggregates produced in *Escherichia coli*. *International Journal of Molecular Sciences, 12*(11), 8275-8287.

Peters, V., & Rehm, B. H. (2005). *In vivo* monitoring of PHA granule formation using GFP-labeled PHA synthases. *FEMS Microbiology Letters, 248*(1), 93-100.

Peters, V., & Rehm, B. H. (2006). *In vivo* enzyme immobilization by use of engineered polyhydroxyalkanoate synthase. *Applied and Environmental Microbiology, 72*(3), 1777-1783.

Price, N. C., & Stevens, L. (1999). *Fundamentals of Enzymology: The Cell and Molecular Biology of Catalytic Proteins* (3rd ed.). New York: Oxford University Press Inc.

Promega. (2010). pGEM-T and pGEM-T Easy Vector Systems: Instructions for use of products A1360, A1380, A3600, and A3610. Madison, WI, USA: Promega Corporation.

Raja, C. E., & Selvam, G. S. (2011). Construction of green fluorescent protein based bacterial biosensor for heavy metal remediation. *International Journal of Environmental Science and Technology, 8*(4), 793-798.

Rasiah, I. A., & Rehm, B. H. (2009). One-step production of immobilized alpha-amylase in recombinant *Escherichia coli*. *Applied and Environmental Microbiology, 75*(7), 2012-2016.

Ringenberg, M., Lichtensteiger, C., & Vimr, E. (2001). Redirection of sialic acid metabolism in genetically engineered *Escherichia coli*. *Glycobiology, 11*(7), 533-539.

Rodriguez, V. B., Alameda, E. J., Gallegos, J. F. M., Requena, A. R., & Lopez, A. I. (2006). Enzymatic hydrolysis of soluble starch with an alpha-Amylase from *Bacillus licheniformis*. *Biotechnology Progress, 22*(3), 718-722.

Rowland, S. S., Speedie, M. K., & Pogell, B. M. (1991). Purification and characterization of a secreted recombinant phosphotriesterase (parathion hydrolase) from *Streptomyces lividans*. *Applied and Environmental Microbiology, 57*(2), 440-444.

Sanchez, S., & Demain, A. L. (2011). Enzymes and bioconversions of industrial, pharmaceutical, and biotechnological significance. *Organic Process Research & Development, 15*, 224-230.

Savile, C. K., Janey, J. M., Mundorff, E. C., Moore, J. C., Tam, S., Jarvis, W. R., Colbeck, J. C., Krebber, A., Fleitz, F. J., Brands, J., Devine, P. N., Huisman, G. W., & Hughes, G. J. (2010). Biocatalytic asymmetric synthesis of chiral amines from ketones applied to sitagliptin manufacture. *Science, 329*(5989), 305-309.

Scott, C., Pandey, G., Hartley, C. J., Jackson, C. J., Cheesman, M. J., Taylor, M. C., Pandey, R., Khurana, J.L., Teese, M., Coppin, C.W., Weir, K.M., Jain, R.K., Lal, R., Russell, R.J., & Oakeshott, J. G. (2008). The enzymatic basis for pesticide bioremediation. *Indian Journal of Microbiology, 48*(1), 65-79.

Sheldon, R. A. (2007). Enzyme immobilization: The quest for optimum performance. *Advanced Synthesis & Catalysis, 349*(8-9), 1289-1307.

Sheldon, R. A., Schoevaart, R., & Van Langen, L. M. (2005). Cross-linked enzyme aggregates (CLEAs): A novel and versatile method for enzyme immobilization (a review). *Biocatalysis and Biotransformation, 23*(3-4), 141-147.

Shevchenko, A., Jensen, O. N., Podtelejnikov, A. V., Sagliocco, F., Wilm, M., Vorm, O., Mortensen, P., Shevchenko, A., Boucherie, H., & Mann, M. (1996). Linking genome and proteome by mass-spectrometry: Large scale identification of yeast proteins from two dimensional gels. *Proceedings of the National Academy of Sciences USA, 93*(25), 14440-14445.

Shewale, S. D., & Pandit, A. B. (2007). Hydrolysis of soluble starch using *Bacillus licheniformis* alpha-amylase immobilized on superporous CELBEADS. *Carbohydrate Research, 342*(8), 997-1008.

Siegel, J. B., Zanghellini, A., Lovick, H. M., Kiss, G., Lambert, A. R., St Clair, J. L., Gallaher, J.L., Hilvert, D., Gelb, M.H., Stoddard, B.L., Houk, K.N., Michael, F.E., & Baker, D. (2010). Computational design of an enzyme catalyst for a stereoselective bimolecular Diels-Alder reaction. *Science, 329*(5989), 309-313.

Sigma-Aldrich. Enzymatic Assay of a-amylase (EC 3.2.1.1). Retrieved 26 Oct, 2012, from http://www.sigmaaldrich.com/technical-documents/protocols/biology/enzymatic-assay-of-a-amylase.html

Soetan, K. O., Aiyelaagbe, O. O., & Olaiya, C. O. (2010). A review of the biochemical, biotechnological, and other applications of enzymes. *African Journal of Biotechnology, 9*(4), 382-393.

Speed, M. A., Wang, D. I. C., & King, J. (1996). Specific aggregation of partially folded polypeptide chains: The molecular basis of inclusion body composition. *Nature Biotechnology, 14*(10), 1283-1287.

Spiekermann, P., Rehm, B. H. A., Kalscheuer, R., Baumeister, D., & Steinbuchel, A. (1999). A sensitive viable-colony staining method using Nile red for direct screening of bacteria that accumulate polyhydroxyalkanoic acids and other lipid storage compounds. *Archives of Microbiology, 171*(2), 73-80.

St. Clair, N. L., & Navia, M. A. (1992). Cross-linked enzyme crystals as robust biocatalysts. *Journal of the American Chemical Society, 114*(18), 7314-7316.

Steinmann, B., Christmann, A., Heiseler, T., Fritz, J., & Kolmar, H. (2010). *In vivo* enzyme immobilization by inclusion body display. *Applied and Environmental Microbiology, 76*(16), 5563-5569.

Suzuki, Y., Nagao, Y., Kato, H., Matsumoto, M., Nerome, K., Nakajima, K., & Nobusawa, E. (1986). Human influenza A virus hemagglutinin distinguishes sialyloligosaccharides in membrance-associated gangliosides as its receptor which mediates the adsorption and fusion processes of virus infection: Specificity for oligosaccharides and sialic acids and the sequence to which sialic acid is attached. *Journal of Biological Chemistry, 261*(36), 17057-17061.

Tokatlidis, K., Dhurjati, P., Millet, J., Beguin, P., & J.P., A. (1991). High activity of inclusion bodies formed in *Escherichia coli* overproducing *Clostridium thermocellum* endoglucanase D. *FEBS Letters, 282*(1), 205-208.

Tsuji, F. I. (2010). Early history, discovery, and expression of *Aequorea* green fluorescent protein, with a note on an unfinished experiment. *Microscopy Research and Technique, 73*(8), 785-796.

Vihinen, M., & Mantsala, P. (1989). Microbial amylolytic enzymes. *Critical Reviews in Biochemistry and Molecular Biology, 24*(4), 329-418.

Vimr, E., Steenbergen, S., & Cieslewicz, M. (1995). Biosynthesis of the polysialic acid capsule by *Escherichia coli* K1. *Journal of Industrial Microbiology, 15*(4), 352-360.

Wachter, R. M., King, B. A., Heim, R., Kallio, K., Tsien, R. Y., Boxer, S. G., & Remington, S. J. (1997). Crystal structure and photodynamic behavior of the blue emission variant Y66H/Y145F of green fluorescent protein. *Biochemistry, 36*(32), 9759-9765.

Worrall, D. M., & Goss, N. H. (1989). The formation of biologically active beta-galactosidase inclusion bodies in *Escherichia coli*. *Australian Journal of Biotechnology, 3*(1), 28-32.

Xu, P., Qiu, J. H., Zhang, Y. N., Chen, J., Wang, P. G., Yan, B., Song, J., Xi, R. M., Deng, Z. X., & Ma, C. Q. (2007). Efficient whole-cell biocatalytic synthesis of *N*-acetyl-D-neuraminic acid. *Advanced Synthesis & Catalysis, 349*(10), 1614-1618.

Xu, X., Gao, C., Zhang, X., Che, B., Ma, C., Qiu, J., Tao, F., & Xu, P. (2011). Production of *N*-acetyl-D-neuraminic acid by use of an efficient spore surface display system. *Applied and Environmental Microbiology, 77*(10), 3197-3201.

Yamabhai, M., Emrat, S., Sukasem, S., Pesatcha, P., Jaruseranee, N., & Buranabanyat, B. (2008). Secretion of recombinant *Bacillus* hydrolytic enzymes using *Escherichia coli* expression systems. *Journal of Biotechnology, 133*(1), 50-57.

Yang, F., Moss, L. G., & Phillips, G. N. (1996). The molecular structure of green fluorescent protein. *Nature Biotechnology, 14*(10), 1246-1251.

Zimmer, M. (2002). Green fluorescent protein (GFP)- applications, structure, and related photophysical behaviour. *Chemical Reviews, 102*(3), 759-781.